IDŐJÁRÁS

QUARTERLY JOURNAL
OF THE HUNGARIAN METEOROLOGICAL SERVICE

CONTENTS

****

http://omsz.met.hu/irodalom/firat_ido/ido_hu.html

VOL. 107 * NO. 1 * JANUARY–MARCH 2003

IDŐJÁRÁS

Quarterly Journal of the Hungarian Meteorological Service

Editorial Office: P.O. Box 39, H-1675 Budapest, Hungary or
Gilice tér 39, H-1181 Budapest, Hungary
E-mail: prager.t@met.hu or *antal.e@met.hu*
Fax: (36-1) 346-4809

Subscription by

mail: IDŐJÁRÁS, P.O. Box 39, H-1675 Budapest, Hungary
E-mail: prager.t@met.hu or *antal.e@met.hu*; *Fax: (36-1) 346-4809*

IDŐJÁRÁS

Quarterly Journal of the Hungarian Meteorological Service
Vol. 107, No. 1, January–March 2003, pp. 1–29

High-latitude environmental dynamics in the context of global change

Kirill Ya. Kondratyev

Research Centre for Ecological Safety, St. Petersburg Centre, RAS
Nansen Fund on Environment and Remote Sensing, St. Petersburg
Korpusnaya St., 18, 197110 St. Petersburg, Russia
E-mail: kondratyev@KK10221.spb.edu

(Manuscript received May 8, 2002; in final form November 21, 2002)

Abstract—Key problems of high-latitude environmental dynamics are discussed including present-day and paleo environmental changes. We review a range of international and national programs aimed at informing of knowledge and understanding of these changes through further development of observation systems, multivariate multidisciplinary analysis, and numerical simulation modeling approaches.

Key-words: global change, global climate change, Arctic system, Arctic ocean, thermohaline circulation, sea ice extent, permafrost, stratospheric ozone, Arctic shelf, paleoclimate, atmospheric pollution, Arctic haze, extended cloudiness, Siberian rivers, ice sheets.

1. Introduction

Recent growing attention to the Arctic environmental problems is motivated by a number of circumstances, including (*Arctic Climate System Assessment (ACIA)*, 2000; *Arctic Science...*, 1999; *CAFF...*, 2001; *Everett* and *Fitzharris*, 2001; *Johannessen et al.*, 2000; *Kalabin*, 2000; *Kondratyev et al.*, 1996; *Rapley*, 1999; *Toward an Arctic...*, 1998; *Toward Prediction...*, 1998; *Vörösmarty et al.*, 2001; *Wadhams et al.*, 1997; *Weller* and *Lange*, 1999; *White et al.*, 2000; *Yudakhine*, 2000; *Zakharov* and *Malinin*, 2000): a stronger sensitivity of high latitude environment to various external forcings; increasing understanding of the importance of numerous interactions and feedbacks between components of the Earth's system; growing necessity to use natural resources located at high latitudes (Arctic shelf especially). It is fair to say

(*Vörösmarty et al.,* 2001), that "the Arctic system constitutes a unique and important environment with a central role in the dynamics and evolution of the earth system".

Some of the recent scientific results have been pointed out in the *ACIA* Implementation Plan (2000):

- There has been increased coastal erosion in the Bering Sea from storm surges resulting from reduced sea ice.
- Sea ice extent in the Arctic has decreased Arctic-wide by 0.35% per year since 1979. During summer of 1998, record reduction of sea ice coverage was observed in the Beaufort and Chukchi Seas.
- Sea ice thickness has also been reduced by between 1–2 meters in many parts of the Arctic Ocean and the sub-Arctic seas.
- Streamflow discharge of major Siberian rivers into the Arctic Ocean has increased in recent years and is associated with a warmer climate and enhanced precipitation in the river basins.
- Since 1970, the Arctic Oscillation, which is a measure of the strength of the circumpolar vortex, has strengthened. This has been found to be consistent with temperature and sea ice coverage changes in the Arctic.
- There has been an increased warming of the Arctic Ocean's Atlantic layer and an approximate 20% greater coverage of Atlantic water types.
- Record low levels of ozone were measured in 2000 in the Arctic with increasing evidence that these levels are likely to continue for at least the next 20 years.
- Ongoing studies indicate that the current UV levels can have a significant effect of fish larvae survival rates.
- General warming of soils in regions with permafrost, derived primarily from Alaskan data, has been observed over recent year.

It has been emphasized in *ACIA* (2000), that past assessments indicated that the Arctic is important to global-scale processes in at least four important ways:

- Thermohaline circulation dominated by the Arctic Ocean and Nordic Seas is responsible for a considerable part of the Earth's poleward heat transport, and may also serve as a sink as well as a source for CO_2. Alterations of this circulation, as have been observed during climatic changes of the past, can affect global climate and in particular the climate of Europe and North America.
- Melting of the Arctic land ice sheets can cause sea level rise around the world. A compilation of studies suggests that a global warming of 1°C will lead to ~1 mm per year of sea-level rise from small ice caps and

glaciers. The Arctic will supply over half of this total, with an additional 0.3–0.4 mm per year contributed from Greenland although uncertainties remain about the mass balance of the Greenland ice sheet.

- Arctic soils can act as either sinks or sources of greenhouse gases depending on temperature and moisture changes within the Arctic. Moisture has opposing effects on the concentrations of the two major trace gases: CH flux declines with soil drying, while CO_2 flux initially increases. These changes can influence greenhouse gas warming globally.
- Our current understanding of the Arctic climate system suggests that positive feedbacks in high-latitude systems, including the snow and ice albedo effect, amplify anthropogenically-induced atmospheric changes, and that disturbances in the circumpolar Arctic climate may substantially influence global climate.

In the context of the health of the Arctic marine environment, from the viewpoint of proper functioning of economically important ecosystems, D. Drewry and O. Orheim (*Arctic Science...,* 1999) have formulated a number of key questions:

- How was the polar basin formed, where are the plate boundaries?
- What has been the detailed paleo-climatic history of the high Arctic Ocean during the last 1 million years?
- Do decreases in ice extent and upper stratification of the ocean signal a different sea ice regime?
- What is the stability of the sea ice cover, what are the effects of radiative feedback in the Arctic, and how do they modulate global ocean circulation?
- What is the role of continental shelves in the cycling of C, N, Si, and other chemicals?
- What is the productivity of the Arctic Ocean, and what is the structure and diversity of higher trophic levels?
- What are the effects of environmental change, both of climate and of pollutants and contaminants such as the introduction of POPs (persistent organic pollutants) into the food chain?

High-latitude climate dynamics is of particular interest. According to *Weller* and *Lange* (1999), "While considerable uncertainty still exists about the exact nature of the future impacts of global climate change, there can no longer be any doubt that major changes in the climate have occurred in recent decades in the Arctic, with visible and measurable impacts following the

climatic changes. Greater impacts are likely in the future and while some of them will be positive, others will be detrimental to human activities".

Recent analysis of ice cores from the Arctic (*Everett* and *Fitzharris,* 2001) has revealed large-scale and rapid paleo-climate changes. Rapid warming took place ~11,500 years ago, at the end of the last glacial period. The coldest parts of ice cores had been as much as 21°C colder than the present temperature in Central Greenland; and the temperatures increased by more than 10°C in a few decades. There is evidence of even more rapid change in the precipitation pattern, rapid reorganizations of atmospheric circulation, and periods of rapid warming during the previous 20,000 years. Rapid warmings of ~10°C in a few decades during the last glacial period in Central Greenland had been followed by periods of slower cooling over a few centuries, and then a generally rapid return to glacial conditions. About 20 such intervals, each lasting between 500 and 2,000 years, occurred during the last glacial period.

It has been emphasized *(Everett* and *Fitzharris,* 2001), that the polar systems are extremely sensitive to the variability of temperature, and several aspects of these systems will be affected by any further climate change. Primary impacts will be on the physical environment, including ice, permafrost, and hydrology; on biota and ecosystems, including fisheries and terrestrial systems; and on human activities, including social and economic impacts on settlements, resource extraction and transportation, and existing infrastructure. Scenario predictions of potential future global warming indicate a necessity to particularly take into account various phenomena, such as thermocarst erosion in lowland areas, thawing of permafrost accompanied by hydrological and climatic changes. Climate change will affect terrestrial ecological systems through changes in permafrost as well as direct climatic changes, including changes in precipitation, snow cover, and temperature. Terrestrial ecosystems are likely to change from tundra to boreal forests, although vegetative changes are likely to lag behind climatic change. Major shifts in biomass will be associated with changes in microbiological (bacteria, algae, etc.) and insect communities (some of them may diminish while others prosper).

It has been pointed out (*Everett* and *Fitzharris,* 2001), that in the recent geologic past, tundra was a carbon sink, but recent climatic warming in the Arctic, coupled with the concomitant drying of the active layer and lowering of the water table, has shifted areas of the Arctic from sinks to sources of CO_2 (this problem is, however, far from being solved). An important potential consequence of permafrost thawing is emission of methane – a greenhouse gas. Changes in an other greenhouse gas, the tropospheric ozone, might happen due to warming of the troposphere (*Kondratyev* and *Varotsos,* 2000).

An interesting illustration of potential future surprises due to interactions and feedbacks has been discussed by *Stevenson et al.* (2000), who obtained future estimates of tropospheric ozone radiative forcing and methane turnover in the context of the impact of climate change. (It should be pointed out, that studies of the contribution of tropospheric ozone, O_{3T}, as a greenhouse gas, as well as assessments of potential impact of global warming on permafrost melting and methane emissions are still at the preliminary stage of development.) Interactive simulations of climate dynamics and O_{3T} changes during the time period 1990–2100 for scenarios of "high" (A2) or "central" (B2) cases of CO_2 emissions resulted in tropospheric ozone radiative forcing (RF) equal to +0.27(A2) or +0.09(B2) W/m^2. If climate-ozone coupling was neglected, relevant RF values would be equal to +0.43 (+0.22) W/m^2. When climate change was included, CH_4 lifetime fell by 0–5%. Hence, climate warming exerts a negative feedback on itself by enhancing O_{3T} and CH_4 destruction.

Three principal achievements have stimulated recent progress in studying the Arctic environment (*Dickson,* 1999): (1) further development of observation programs with the use of various observation means (including satellites and submarines); (2) declassification of the military Soviet-American archive of ocean "climatology" data; (3) discovery of the fact that the climatic forcing in the region of Arctic and northern seas in the 1990s has increased in comparison with that observed during the previous century (similar situation also took place with respect to climate dynamics indicators (such as Arctic Oscillation (AO) and North Atlantic Oscillation (NAO)).

Overland and *Adams* (2001) have pointed out that "decadal differences between the 1990s and 1980s in winter (JFM) sea-level pressure and 300 hPa zonal winds have an Arctic-centered character with nearly equal contributions from the Atlantic and Pacific sectors. In contrast, the differences between positive and negative AO composites defined from monthly values of Principal Components from the same period have similar magnitudes in the Pacific and Arctic, but have additional large NAO signature in the Atlantic sector. Thus Arctic changes of decadal scales are more symmetric with the pole than suggested by the standard AO index definition. Change point analysis of the AO shows that a shift in value near 1989 is an alternative hypothesis to a linear trend. Analysis of zonal and meridional winds by longitudinal sectors shows the importance of the standing wave pattern in interpreting the AO, which supplements the view of the AO as a simple zonal average (annular) mode". Thus, the Arctic Oscillation should be considered as a physical phenomenon connected with the enhancement of circumpolar vortex and relevant mass and temperature changes in the troposphere and stratosphere.

By the end of the 1980s – beginning of the 1990s, a very strong NAO enhancement resulted in powerful transport of warmer and fresher Norwegian Atlantic waters to the north of the Fram Strait and the Barents Sea. Entering the Arctic, the sub-layer of Atlantic waters was becoming thinner, warming (by about 2°C) and increasing its horizontal extent (~20%). At smaller depths, the cold haloclyne (which thermally isolates the sea ice cover from the warm Atlantic layer located below) shifted towards the euroasiatic basin, which resulted in substantial changes of mass and energy balances of the ice cover surface. This and other phenomena have been studied within a number of recent programs (*Aagard et al.,* 1998; *Allison et al.,* 2001; *Arctic Science...,* 2000; Barry, 1998; *Climate Change...,* 2001; *Toward an Arctic...,* 1998; *Toward Predictiion...,* 1998; *Wadhams et al.,* 1997). Climatic impact of polynyas is of particular interest (*Holland,* 2001; *Lemke,* 2001).

Alekseev (1998) has emphasized that the Arctic is in many respects a key part of the global climatic system, where the strongest natural fluctuations of climatic characteristics develop. The global impact of the Arctic is primarily accomplished through the Arctic Ocean, which is capable of changing the structure of its circulation regime under the influence of changes in fresh water, salt, and heat exchange with the non-polar parts of the global system. The freshened upper layer and sea ice located above it turn out to be most active components, with fresh water, heat, and salt transport being the major processes responsible for coupling between the high-latitude environment and its lower-latitude parts.

Specific features of the arctic atmosphere, such as phenomena of arctic haze as well as extended cloudiness and radiation, have been studied during the period of the First GARP (Global Atmospheric Research Programme) Global Experiment – FGGE (*Kondratyev et al.,* 1992; *Kondratyev,* 1999).

Important progress has been achieved in the field of arctic climate diagnostics (*Adamenko* and *Kondratyev,* 1999; *Nagurny* and *Maistrova,* 2002). Basic features of arctic climate dynamics have been demonstrated, such as strong space and time variability of various scales. *Nagurny* and *Maistrova* (2002) have shown, for instance, that as far as interannual lower troposphere temperature variations are concerned, before the 1980s negative anomalies had prevailed, while later on, for the whole troposphere, positive temperature anomalies were typical. Total polar atmosphere energy (potential plus internal) during the previous 40 years has not changed, however.

A much more difficult situation exists in the field of numerical modeling of high-latitude climate change. It has been mentioned in the *Report...* (2001), that current estimates of future changes to the Arctic vary significantly. The model results disagree as to both the magnitude of changes and regional aspects of these changes.

2. Climate and cryosphere

An important step forward in studying the Arctic environment is the Climate and Cryosphere (CliC) Project (*Allison et al.,* 2001). The term "cryosphere" describes those portions of the earth's surface, where water is in solid form. This includes all kinds of ice, snow, and frozen ground such as permafrost. The cryosphere is an important part of the global climate system. It is strongly influenced by temperature, solar radiation, and precipitation, and, in turn, influences each of these properties. It also has an effect on the exchange of heat and moisture between the Earth's surface (land or sea) and the atmosphere, clouds, river flow (hydrology), and atmospheric and oceanic circulation. Parts of the cryosphere are strongly influenced by changes in climate. The cryosphere may therefore act as an early indicator of both natural and human-induced climate changes.

As a core project of the World Climate Research Programme, the "Climate and Cryosphere" (CliC) project encourages and promotes research into the cryosphere and its interactions as part of the global climate system. It seeks to focus attention on the most important issues, encourage communication between researchers with common interests in cryospheric and climate science, promote international co-operation, and highlight the importance of this field of science to policy makers, funding agencies, and the general public. CliC also publicizes significant findings regarding the role of the cryosphere in climate, and recommends directions for future study.

CliC aims to improve understanding of the cryosphere and its interactions with the global climate system, and to enhance the ability to use parts of the cryosphere for detection of climate change. To attain scientific goals, CliC seeks to develop and coordinate national and international activities aimed at increasing the understanding of four main scientific themes:

- Interactions between the atmosphere and snow and ice on the land surface.
- Interactions between glaciers and ice sheets and sea level.
- Interactions between sea ice, oceans, and the atmosphere.
- Interactions of the cryosphere with the atmosphere and oceans on a global scale.

CliC encourages the use of observations, process studies, and numerical modeling within each of the above topic areas. In addition, CliC promotes the establishment of new cryospheric monitoring programs.

The cryosphere is also considered as an indicator of climate variability and change. It has been pointed out in (*Allison et al.,* 2001):

"Atmosphere-snow/ice-land interactions are concerned with the role of the terrestrial cryosphere within the climate system and with improved understanding of the processes, and of observational and predictive capabilities

applicable over a range of time and space scales. Better understanding of the interactions and feedback of the land/cryosphere system and their adequate parameterization within climate and hydrological models are still needed. Specific issues include the interactions and feedback of terrestrial snow and ice in the current climate and their variability; in land surface processes; and in the hydrological cycle. Improved knowledge is required of the amount, distribution, and variability of solid precipitation on a regional and global scale, and its response to a changing climate. Seasonally-frozen ground and permafrost modulate water and energy fluxes, and the exchange of carbon, between the land and the atmosphere. How do changes of the seasonal thaw depth alter the land-atmosphere interaction, and what will be the response and feedback of permafrost to changes in the climate system? These issues require improved understanding of the processes and improved observational and modeling capabilities that describe the terrestrial cryosphere in the entire coupled atmosphere-land-ice-ocean climate system.

Over a considerable fraction of the high-latitude global ocean, sea ice forms a boundary between the atmosphere and the ocean, and considerably influences their interaction. The details and consequences of the role of sea ice in the global climate system are still poorly known. Improved knowledge is needed of the broad-scale time-varying distributions of the physical characteristics of sea ice, particularly ice thickness and the overlying snow-cover thickness, in both hemispheres, and the dominant processes of ice formation, modification, decay, and transport which influence and determine ice thickness, composition, and distribution. We do not know how accurate present model predictions of the sea ice responses to climate change are, since the representation of much of the physics is incomplete in many models, and it will be necessary to improve coupled models considerably to provide this predictive capability.

Key issues on the global scale are: understanding the direct interactions between the cryosphere and atmosphere, correctly parameterizing the processes involved in models, and providing improved data sets to support these activities. In particular, improved interactive modeling of the atmosphere-cryosphere surface energy budget and surface hydrology, including fresh-water runoff, is required.

The scientific strategy for a CliC project is similar in each of the areas of interaction: a combination of measurement, observation, monitoring, and analysis, field process studies and modeling at a range of time and space scales. A CliC modeling strategy must address improved parameterization in models of the direct interactions between all components of the cryosphere, atmosphere, and ocean. It will need to do this at a variety of scales from the regional to global; and with a hierarchy of models ranging from those of

individual processes to fully coupled climate models. It will also be essential to provide the improved data sets needed for validation of models and parameterization schemes."

Data presented in *Table 1* characterize major components of the cryosphere (*Allison et al.,* 2001). It has been mentioned (*Allison et al.,* 2001), that the processes operating in the coupled cryosphere-climate system involve three time scales – intraseasonal-interannual, decadal-centennial, and millennial or longer. The longest time scale is addressed through the IGBP PAGES program, although abrupt climate shifts evidenced in ice core and ocean sediment records (Heinrich events, involving extensive deposition of ice-rafted detritus in the North Atlantic) are also highly relevant to CliC. The other two time scales are commensurate with WCRP interests, as it is manifest in ACSYS, GEWEX, and CLIVAR. In the space domain, cryospheric processes and phenomena need to be investigated over a wide range of scales from meters to thousands of kilometers.

Table 1. Areal and volumetric extent of major components of the cryosphere

Component	**Area (10^6 km^2)**	**Ice volume (10^6 km^3)**	**Sea level equivalent (m)** (a)
LAND SNOW COVER (b)			
Northern Hemisphere Late January	46.5	0.002	
Late August	3.9		
Southern Hemisphere Late July	0.85		
Early May	0.07		
SEA ICE			
Northern Hemisphere Late March	14.0 (c)	0.05	
Early September	6.0 (c)	0.02	
Southern Hemisphere Late September	15.0 (d)	0.02	
Late February	2.0 (d)	0.002	
PERMAFROST (underlying the exposed land surface, excluding Antarctica and Southern Hemisphere high mountains)			
Continuous (e)	10.69	0.0097–0.0250	0.024–0.063
Discontinuous and Sporadic	12.10	0.0017–0.0115	0.004–0.028
CONTINENTAL ICE AND ICE SHELVES			
East Antarctica (f)	10.1	22.7	56.8
West Antarctica and Antarctic Peninsula (f)	2.3	3.0	7.5
Greenland	1.8	2.6	6.6
Small ice caps and Mountain glaciers	0.68	0.18	0.5
Ice shelves (f)	1.5	0.66	–

(a) Sea level equivalent does not equate directly with potential sea-level rise, as a correction is required for the volume of the Antarctic and Greenland ice sheets that are presently below sea level. 400,000 km^3 of ice is equivalent to 1 m of global sea level.

(b) Snow cover includes that on land ice, but excludes snow-covered sea ice.

(c) Actual ice areas, excluding open water. Ice extent ranges between approximately 7.0 and 15.4 $\times$ 10^6 km^2.

(d) Actual ice area excluding open water. Ice extent ranges between approximately 3.8 and 18.8 $\times$ 10^6 km^2. Southern Hemisphere sea ice is mostly seasonal and generally much thinner than Arctic sea ice.

(e) Data calculated using the Digital Circum-Arctic Map of Permafrost and Ground-Ice Conditions, and the GLOBE-1 km Elevation Data Set.

(f) Ice sheet data include only grounded ice. Floating ice shelves, which do not affect sea level, are considered separately.

2.1 Cryosphere dynamics

Studying the cryosphere dynamics has a great importance for many applications. Data of *Table 2* illustrate some of the applications (*Allison et al.*, 2001).

Four overarching goals, that address major concerns for the WCRP, can be identified (*Allison et al.*, 2001). These are:

- To improve understanding of the physical processes and feedbacks through which the cryosphere interacts within the climate system.
- To improve the representation of cryospheric processes in models to reduce uncertainties in simulations of climate and predictions of climate change.
- To assess and quantify the impacts of past and future climatic variability and change on components of the cryosphere and their consequences, particularly for global energy and water budgets, frozen ground conditions, sea level change, and the maintenance of polar sea-ice covers.
- To enhance the observation and monitoring of the cryosphere in support of process studies, model evaluation, and change detection.

Table 2. Examples of socio-economic sectors affected by changes in the cryosphere

SOCIO-ECONOMIC COMPONENT	CRYOSPHERE FACTOR
A. Direct effects	
Loss of coastal land and population displacement:	• Land ice melt contribution to sea level
Transportation	
• Shipping	• Iceberg hazard; sea-ice extent, thickness
• Barge traffic	• Fresh-water ice season
• Tundra roads	• Fresh-water ice thaw; frozen ground thaw
• Road/rail traffic	• Freeze events; snowfall
Water Resources	
• Consumption	
• Irrigation	• Snow/glacier melt runoff
• Hydropower	• Glacier melt runoff
• Agriculture	• Moisture recharge extremes
Hydrocarbon and mineral resource development	• Icebergs and sea ice; frozen ground duration and thickness
Wildlife population	• Snow cover; frozen ground and sea ice
Recreation/safety	• Snow cover; avalanches
B. Indirect effects	
Enhanced greenhouse effect	• Thaw of clathrates
Traditional lifestyles (Arctic, sub-arctic and high mountains)	• Changes in sea ice and fresh-water ice, snow cover, and frozen ground
Tourism/local economies	• Loss of glaciers; shorter snow season
Insurance sector	• Changes in risk factor

Specific questions that help define the primary tasks of CliC are:

- How stable is the global cryosphere?
  - How well do we understand and model the key processes involved in each cryospheric component of the climate system?
  - How do we best determine the rates of change in the cryospheric components?
- What is the contribution of glaciers, ice caps, and ice sheets to changes in global sea level on decadal-to-century time scales?
  - How can we reduce the current uncertainties in these estimates?
- What changes in frozen ground regimes can be anticipated on decadal-to-century time scales that would have major socio-economic consequences, either directly or through feedback on the climate system?

- What will be the annual magnitudes, rates of change, and patterns of seasonal redistribution in water supplies from snow- and ice-fed rivers under climate changes?
- What will be the nature of changes in sea-ice mass balance in both polar regions in response to climate change?
- What is the likelihood of abrupt climate changes resulting from regime changes in ice shelf – ocean and sea ice – ocean interactions that impact the ocean thermohaline circulation?
- How do we monitor cryospheric components as indicators of change in the climate system?

Monitoring cryosphere dynamics is a key aspect of high-latitude environmental studies (*Kondratyev et al.,* 1996; *Kondratyev* and *Cracknell,* 1998), especially because of rather controversial information concerning ice cover dynamics. It is true, for instance, for ice thickness observations. *Holloway* and *Sou* (2001) have pointed out that "while submarine records had indicated a stunningly rapid thinning, model results show that the position of submarine observations was exceptionally biased towards regions of thinning. A conclusion is that observations to date, along as with much physics as models represent, imply little or no overall thinning".

2.2 Arctic environmental pollution

The Arctic region exploration strategy in a broad context of biospheric studies has been discussed in details by *Matishov* (1998, 2000) as well as *Matishov* and *Matishov* (2001), where a necessity of an ecosystem approach in studying land and marine biota, as well as conditions of socio-economic development in high-latitude regions have been particularly emphasized. *Aibulatov* (2000) and *Matishov* and *Matishov* (2001) have discussed general problems of high-latitude environmental dynamics with special emphasis on radioactive pollution as an echo of the cold war. *Aibulatov* (2000) has analyzed principal sources of artificial radioisotopes in the Russian Arctic seas such as atomic explosions on Novaya Zemlya, the global radionuclide background as a result of the overall nuclear tests conducted on the planet, Russian chemical and mining plants, Chernobyl accident, West-European radiochemical plants, solid and liquid radioactive waste dumping in the Barents and Kara Seas, the Northern Military Marine and its bases, atomic submarine construction and maintenance facilities, and Atomflot (atomic fleet) of the Murmansk Shipping Company.

Studying of the distribution of ^{137}Cs, ^{90}Sr, and $^{239,240}Pu$ in the water masses of the North, Norwegian, Barents, Kara, White, and Laptev Seas has resulted in the following conclusions (*Aibulatov,* 2000):

- The general level of radioactive contamination of the waters of Arctic seas, except for several local areas, is characterized at the present time by little difference in comparison with background level (~ 6 Bq/kg).
- The radioactive pollution of the waters of the North and Norwegian Seas is entirely due to the emissions from radiochemical plants located in Western Europe.
- The contamination of waters of the Barents, White, Kara, and Laptev Seas is due to both local (Russian) sources and West-European plants.
- The field observations in the Kara Sea in 1992–1995 have resulted in the conclusion, that there have been no substantial radioactive emissions from the burial sites in the area.
- The contribution of the Ob and Yenisei river runoff to the overall radioactive transport is not significant at the present time, except cases of extremely heavy floods which happen very rarely.
- Compared to open waters of the Arctic Ocean, shelf seas of the Russian Arctic are more heavily contaminated.

Aibulatov (2000) has pointed out that judging from the ^{137}Cs-distribution patterns in the Kara Sea, it becomes evident that the Yenisei and Ob rivers (less evident, however, in the latter case) should be considered as transport channels for inputs of technogenic radionuclides to the Arctic Ocean waters. There are radioactive sources in the ocean as well. The ^{137}Cs activity level reached its maximum in 1984 and was equal to 245 Bq/kg in open sea; during the 1990s (1993) this level was found to be equal to 100 Bq/kg in the Yenisei estuary.

Arctic fjords have been classified into categories of comparatively clean, contaminated, heavily contaminated, and potentially contaminated. Contaminated areas include, for instance, Kola Gulf and, probably, all the fjords of the northern Kola Peninsula, west of Murmansk. The content of radionuclides in phytobenthos, in the coastal zone east of Murmansk, is low. Evidently, there has not been recently any serious radionuclide penetration into this area. A rather low gamma-nuclide level (1–3 Bq/kg) is typical for the zoobenthos of the Barents Sea. This is also true for the Kara Sea.

Impact of all the sources of radioactivity in the zone of the Arctic coast on the local population has not been assessed reliably enough. It was particularly difficult to separately identify natural and anthropogenic components of such

an impact. *Aibulatov* (2000) has discussed future research on the Russian Arctic radioactive pollution, including:

- Development of a coordinated Russian Arctic Sea Radioactivity Ecological Monitoring Programme.
- Assessments of impacts of different radioactive sources on the contamination of the Arctic marine environment including water basins, land, and atmosphere.
- Studies of detailed space and time variability of various long-lived technogenic radionuclides in bottom sediments.
- A detailed examination of all Novaya Zemlya fjords in connection with dumping radioactive waste.
- Research of the impact of radioactive pollution on the Arctic marine ecosystem dynamics.
- Studying medical aspects of environmental pollution in the Arctic.

2.3 High-latitude ecodynamics

The fundamental study of radioactivity of the Arctic and sub-Arctic marine ecosystems has been undertaken by *Matishov* and *Matishov* (2001), which resulted in the substantiation of a new branch of science – radiational ecological oceanology. Investigations have been conducted of the level of artificial radionuclide concentration in both environment and biota of the bays and inlets (the Kola, the Chernaya, the West Litsa), where radioactively dangerous objects are located. In this context, a classification has been suggested for coastal areas (bays, gulfs, fjords) in accordance with contamination levels for bottom sediments. Important role of a biofilter of pelagic zone and coastal zone has been discovered during the processes of self-purification of water reservoirs and transport of radionuclides from water to bottom sediments. For the first time, the levels of ^{137}Cs, ^{90}Sr, $^{239,240}Pu$ concentrations for different types and populations of sea organisms were measured. Migrations of radioisotopes along the trophic chains (from macrophytes and plankton to zoobenthos, fish, birds, seals, and whales) were studied as well. The assessments of comparative contributions of global, regional, and local sources of radioactive environmental contamination during the time-period from nuclear tests till recent time have been analyzed and used as a source of information for environmental predictions. An important optimistic conclusion concerning consequences of potential accidents is that for all prescribed scenarios of radioactive emissions, it is highly improbable that large-scale contamination of the Arctic Ocean will take place with ruinous

impacts on marine bioresources. High biological assimilation capacity in combination with specific features of hydrodynamic and other processes is supposed to serve as a barrier against dangerous pollution of the Arctic Ocean.

Kalabin (2000) has accomplished a study of the environmental dynamics and industrial potential of the Murmansk region, the most urbanized and industrially developed trans-polar region of the planet. Under these conditions, specific features of environmental dynamics result in the enhancement of anthropogenic impacts. In this context, *Kalabin* (2000) has analyzed critical environmental loads for some of the northern ecosystems, and emphasized a necessity to investigate their assimilation (buffer) capacity as a principal aspect of sustainably functioning natural systems. The solution of regional problems of sustainable development requires a careful analysis of the interaction between ecodynamics and socio-economic development.

3. Scientific field programs

The progress achieved in studying the Arctic environment variability is due to the accomplishment of a number of international research programs. The Arctic Climate System Study (ACSYS) project is of particular importance, developed in 1991 as the WCRP initiative, and a practicable program for the next decade to assess the role of the Arctic in global climate (*Arctic Climate...*, 1994; *Kondratyev et al.*, 1996). Five areas are emphasized: ocean circulation; sea ice climatology; Arctic atmosphere; hydrological cycle; and modeling. The scientific goals of ACSYS, which started its main observational phase in January 1994 and will continue for a ten-year period, includes the three main objectives (*Arctic Climate...*, 1994):

- understanding the interaction between the Arctic Ocean circulation, ice cover, and hydrological cycle;
- initiating long-term climate research and monitoring programs for the Arctic;
- providing a scientific basis for an accurate representation of Arctic processes in global climate models.

The Arctic Ocean Circulation Programme of ACSYS consists of four components:

- the Arctic Ocean Hydrographic Survey to collect a high-quality hydrographic data-base representative of the Arctic Ocean;
- the Arctic Ocean Shelf Studies, which are aimed at understanding how the shelf processes partition salt- and fresh-water components; at defining the

dynamics and thermodynamics of the shelf waters as well as other processes;

- the Arctic Ocean Variability Project designed to assess the variability of the circulation and density structure of the Arctic Ocean;
- the Historical Arctic Ocean Climate Database Project aimed to establish a universally available digital hydrographic database for the Arctic Ocean for analysis of climate-related processes and variability, and to provide a data set suitable for initialization and verification of arctic climate and circulation models.

The ACSYS sea ice program includes three main components:

- establishing an Arctic basin-wide sea ice climatology database;
- monitoring the export of sea ice through the Fram Strait;
- arctic sea ice processes studies.

One of the main tasks of the ACSYS arctic sea ice program is to establish a climatology of ice thickness and ice velocity. Such data will be supplied by the WCRP Arctic Ice Thickness Project, the International Arctic Buoy Programme, sonar profiling from naval submarines and unmanned vehicles, airborne oceanographic lidars, and polar satellites carrying appropriate instruments.

The arctic atmosphere provides the dynamic and thermodynamic forcing of the Arctic Ocean circulation and sea ice. Key directions of research include problems such as cloud-radiation interaction, air-sea interaction in the presence of ice cover (impacts of polynyas and leads are of special interest), arctic haze, etc.

Primary ACSYS efforts within the project of the Hydrological Cycle in the arctic region are aimed at:

- documentation and intercomparison of solid precipitation measurement procedures used in high latitudes and
- development of methodologies for determining areal (regional) distributions of precipitation from station data.

There are two relevant data-archiving efforts: Arctic Precipitation Data Archive (APDA) and Arctic Run-off Data Base (ARDB).

The principal purpose of the ACSYS modeling program is simulations of climate variations in polar regions, which arise from the interaction between atmosphere, sea ice, and ocean.

Apart from the ACSYS project described above, a number of new research programs have been developed, such as the Study of Environmental Arctic Change (SEARCH), which is an interdisciplinary, multi-scale program dedicated to understanding the complex interrelated changes that have been observed in the Arctic environment in the past few decades (*SEARCH...*, 2000,

2001). SEARCH is envisioned as a long-term effort of observations, modeling, process studies, and applications with emphasis on five major thematic areas:

- human society;
- marine/terrestrial biosphere;
- atmosphere and cryosphere;
- ocean, and
- integrated projects/models/assessment.

The Arctic System Science (ARCSS) Programme (*Toward Prediction...*, 1998) is an interdisciplinary program with the principal goals to (1) understand the physical, geological, chemical, biological, and sociocultural processes of the arctic system that interact with the total Earth's system, and thus contribute to or are influenced by global change, in order to (2) advance the scientific basis for predicting environmental change on a seasonal-to-centuries time scale, and for formulating policy options in response to the anticipated impacts of global change on humans and societal support systems. The following four scientific thrusts include central aims of ARCSS:

- to understand the global and regional impacts of the arctic climate system and its variability;
- to determine the role of the Arctic in global biogeochemical cycling;
- to identify global change impacts on the structure and stability of arctic ecosystems;
- to establish the links between environmental change and human activity.

ARCSS has four linked ongoing components: Ocean/Atmosphere/Ice Interactions (OAII); Land/Atmosphere/Ice Interactions (LAII); Paleoenvironmental Studies (including GISP2, Greenland Ice Sheet Project Two, and PALE, Paleoclimates of Arctic Lakes and Estuaries); Synthesis, Integration, and Modeling Studies (SIMS), and Human Dimensions of the Arctic System (HARC). K. Aagard (*Toward an Arctic...*, 1998) discussed basic problems with a multidisciplinary look at the Arctic Ocean, including: physical and chemical studies; biological studies; contaminant studies; measurements of the properties, and variability of the ice cover and surface radiation budget; studies of atmospheric chemistry; geological observations.

LAII research has three main goals (*Witness...*, 1994):

- to estimate important fluxes in the region, including the amount of carbon dioxide, and methane reaching the atmosphere, the amount of river water reaching the Arctic Ocean, and the radiative flux back to the atmosphere;
- to predict how possible changes in the arctic energy balance, temperature, and precipitation will lead to feedback affecting large areas; this

incorporates changes in water budget, duration of snow cover, extent of permafrost, and soil warming, wetting, and drying; and

- to predict how the land and fresh-water biotic communities of the Arctic will change, and how this change will affect future ecosystem structure and function.

A major LAII research project is the Flux Study; its principal purpose is a regional estimate of the present and future movement of materials between the land, atmosphere, and ocean in the Kuparuk river basin in northern Alaska.

Three of the nineteen LAII projects are part of the International Tundra Experiment (ITEX), which looks at the response of plant communities to climate change. Three others are concerned with atmosphere processes, including weather patterns affecting snowmelt, arctic-wide temperature trends, and water vapor over the Arctic, and its relationship to the atmospheric circulation and surface conditions. One project deals with response of large birds to climate and sea-level change at river deltas, and one studies the balance and recent volume changes of McCall Glacier in the Brooks Range.

Synthesis, integration, and modeling studies are intended to discover linkages and strengthen system-level understanding. Research on the past and contemporary relationship of humans to global climate change is thought to be critical to understanding the consequences of global change in the Arctic.

There are a number of ARCSS data projects, including: LAII Flux Study Alaska North Slope data sampler CD-ROM; OAII Northeast Water (NEW) polynya project CD-ROM; Arctic solar and terrestrial radiation CD-ROM, etc.

The list of the OAII components includes the joint US/Japan cruise, the Western Arctic Mooring project, and the Northeast Water Polynya project. Among other OAII projects, the most notable are the US/Canada Arctic Ocean Section and the Surface Heat Budget of the Arctic Ocean (SHEBA) projects.

An outstanding effort has been accomplished in 1994 within the Canada/US 1994 Arctic Ocean Section, when two icebreakers entered the ice in the northern Chukchi Sea on July 26, 1994, reached the North Pole on August 22, and left the ice northwest of Spitsbergen on August 30, thereby completing the first crossing of the Arctic Ocean by surface vessels. This voyage will greatly alter our understanding of biological productivity, the food web, ocean circulation and thermal structure, and the role of clouds in the summer radiation balance, as well as the extent of contamination and spreading pathways (especially related to radionuclides and chlorinated organics), and the extent and effects of sediment transport by sea ice (*Witness...*, 1994).

In connection with the SHEBA project, the US Department of Energy's Atmosphere Radiation Measurement (ARM) program indicated its intention to develop a Cloud and Radiation Testbed (CART) facility on the North Slope of

Alaska. The principal focus of this program will be on atmospheric radiative transport, especially as modified by clouds (which impacts the growth and decay of sea ice), as well as testing, validation, and comparison of radiation transfer models in both ice pack and arctic coastal environment.

A special place is occupied by the Russian-American Initiative on Shelf-Land Environments in the Arctic (RAISE) with the principal goal of facilitating ship-based research in the Russian Arctic (*RAISE...*, 2001). Earlier relevant land-based research projects under the RAISE umbrella included studies of:

- organic material and nutrient fluxes from Russian rivers;
- seasonal flooding dynamics along rivers, and
- reconstruction of late Pleistocene glacial and sea-level history on Wrangel Island.

New scientific topics in the near-shore waters of the Russian continental shelf will include a broad range of studies: from the biogeochemical fate of organic materials contributed to the Arctic Ocean by shoreline erosion and river runoff to the social and biological impacts of changes in sea-ice distributions.

The Western Arctic Shelf-Basin Interactions (SBI) project, sponsored by ARCSS Programme and the U.S. Office of Naval Research, is investigating the arctic marine ecosystem to improve our capacity to predict environmental change. The SBI Phase II Field Implementation Plan (2002–2006) focuses on three research topics in the core study area:

- northward fluxes of water and bioactive elements through the Bering Strait input region;
- seasonal and spatial variability in the prediction and recycling of biogenic matter on the shelf-slope area; and
- temporal and spatial variability of exchanges across the shelf-slope region into the Canada Basin.

4. Priorities and perspectives

The recent meeting of the International Arctic Science Committee (IASC) has identified the following four science priorities (*Witness...*, 1994):

- arctic processes relevant to global systems;
- effects of global change on the Arctic and its peoples;
- natural processes within the Arctic; and
- sustainable development in the Arctic.

The following areas in arctic global change research have been considered the most significant:

- terrestrial ecosystem;
- mass balance of glaciers and ice sheets;
- regional cumulative impacts; and
- human dimensions.

An important aspect of studying high-latitude environmental dynamics is an assessment of the impact of potential anthropogenic climate warming. In this context *Frederick* (1994) has formulated key issues of integrated assessments of the impact of climate change on natural resources. Specific project objectives include: (1) characterizing the current state of natural science and socioeconomic modeling of the impacts of climate change and current climate variability on forests, grasslands, and water; (2) identifying what can be done currently with impact assessments and how to undertake such assessments; (3) identifying impediments linking biophysical and socioeconomic models into integrated assessments for policy purposes; (4) recommending research activities that will improve the state of the art and remove impediments model integration.

The following questions are supposed to be answered:

- How will the overall system (physical-biological-economic) respond to various imposed stresses?
- How do the uncertainties in the component models add up to give an overall system response uncertainty?
- Is society made more vulnerable to extreme natural events either by changing those events or by reducing human ability to respond with corrective actions?
- How likely is it that the consequences of climate change will be severe or catastrophic?
- What is at risk and when is it a risk?
- What are the likely impacts on the landscape and hydrological system?
- How might the boundary conditions and overall productivity of the forests, grasslands, and other rangelands be affected?
- How might increasing carbon dioxide levels affect crops and food supplies for humans, livestock, and wildlife?
- What are the socioeconomic consequences of these physical and biological changes?
- What are the likely consequences of mitigation actions for ecosystems?

- Can the costs associated with climate change be reduced through natural adaptation of ecosystems or policy-initiated adaptation?

Frederick (1994) has emphasized, that the accumulated results of many regional and local climate impact assessments may help provide informed answers to these questions. Nevertheless, the uncertainties surrounding both the nature and impacts of any future climate change are likely to remain very large, precluding precise estimates of the net benefits associated with alternative policy responses. Even if the range of uncertainty were diminished, it might still be difficult to justify specific measures on narrow economic grounds, because (as noted above) the impacts on natural resource systems are apt to be poorly reflected in standard benefit-cost analysis.

Mendelsohn and *Rosenberg* (1994) have formulated the following questions relevant to global warming effects in the area of ecological and water resources:

- Do changes in ecosystems provide important feedbacks to the natural carbon, nitrogen, and methane cycles? For example, will the natural sinks or emitters be affected by changing precipitation, temperature, and CO_2 levels?
- What are the appropriate output measures of ecosystem component models? What are the ecological effects of climate change that policy analysts should use to determinate the importance of an ecosystem change?
- What climate change-driven shifts in ecosystem boundaries can be predicted?
- Will these effects be subtle and small or large and dramatic, and over what time frame and spatial dimensions?
- Will climate change cause a change in the productivity of valuable market or non-market species? For example, to what extent will some forests grow more quickly or more slowly? Will desired non-market species, such as bear, elk, and bald eagles, be more or less plentiful?
- What species could be lost with rapid climate changes? How do the vulnerable species break down by type and geographic distribution? How should conservation policies adapt to a world requiring change?
- How are ecosystems likely to change as the climate evolves over time: will there be a large increase in early succession species and where?
- How will average flows in rivers change with greenhouse warming? How will these flows change over seasons? Will the probabilities of catastrophic events change?

- What values do people assign to the changes in ecosystems by climate change? Which changes are important and which are minor? Can a value be assigned to non-use?
- How much should the society be willing to pay to reduce the probability of losing specific species? If different scenarios favour different species, how should the society trade between these outcomes?
- What impact do ecosystem changes have upon the economy? For example, how will climate change affect grazing, commercial fishing, timber, or commercial tourism?

It has been suggested (*Proceedings...*, 1999) that priority program areas and relevant projects are as follows:

- Impacts of global changes on the arctic region and its peoples:
  - regional cumulative impacts,
  - effects of increased UV radiation.
- Arctic processes of relevance to global systems:
  - mass balance of glaciers and ice sheets,
  - terrestrial ecosystems and feedback on climate change.
- Natural processes within the Arctic:
  - arctic marine/coastal/riverine systems,
  - disturbance and recovery of terrestrial ecosystems.
- Sustainable development in the Arctic:
  - sustainable use of living resources,
  - dynamics of arctic populations and ecosystems,
  - environmental and social impacts of industrial development.

Future priorities of the ARCSS include the following research questions (*Toward Prediction...*, 1998): How will the arctic climate change over the next 50 to 100 years? How will human activities interact with future global change to affect the sustainability of natural ecosystems and human societies? How will changes in arctic biogeochemical cycles and feedbacks affect arctic and global systems? How will changes in arctic hydrological cycles and feedbacks affect arctic and global systems? Are predicted changes in the Arctic detectable?

Important perspectives are connected with paleoenvironmental studies by the Paleoenvironmental Arctic Sciences (PARCS) community (*PARCS...*, 2000), which have a principal aim of answering the question: how much do recent observations of climate change in the Arctic reflect natural climate cycles? Relevant major topics include:

- the medieval warm period (apparently, AD 1000–1400) and Little Ice Age (approximately AD 1400–1850);
- high-amplitude Holocene climate cycles, and
- the possible connection of the onset of the neoglacial (a mid-Holocene cooling, particularly evident at high northern latitudes) with shifts in the frequency and amplitude of such climate cycles.

According to the PARCS, there are very warm past scenarios, that can serve as analogues for future climate warming:

- the early Holocene, when the Arctic had experienced high summer insolation anomalies, and
- the last interglacial period (marine isotope stage 5), which appears as a very strong warming in the paleorecord approximately 125,000 years ago.

Key topics to investigate in relation to these periods are:

- feedbacks and nonlinear changes (surprises) as consequences of strong warming - particularly the role of sea ice, ice sheets, and land surface cover;
- implications of strong warming for arctic and global carbon budgets.

To summarize what has been mentioned in connection with recent Arctic environmental programs, it must be emphasized, that the relevant information was not at all exhaustive (see also *IASC...*, 2001). An obvious conclusion is that the number of programs is too great. A clear necessity exists of better coordination of all on-going efforts and their "regularization".

Vörösmarty et al. (2001) are right in their conclusion that "understanding the full dimension of arctic change is a fundamental challenge to the scientific community over the coming decades, and will require a major new effort at interdisciplinary synthesis. It also requires an unprecedented degree of international cooperation".

Undoubtedly, the Second International Polar Year is an urgent necessity.

References

Aagard, K. and *Carmack, E.C.*, 1994: The Arctic Ocean and climate: A perspective. *Geophysical Monograph 85. AGU, Washington, D.C.*, 5-20.

Aagard, K. et al. (eds.), 1998: *Proc. of the ACSYS Conference on Polar Processes and Global Climate* (Rosario, USA, 3-6 November 1997). WCRP-106 (WMO/TD No. 908). Geneva.

ACD: Arctic Coastal Dynamics. Science and Implementation Plan, 2001: Int. Arctic Science Committee. Oslo, 20 pp.

ACIA (Arctic Climate Impact Assessment), 2000: Prepared by the Assessment Steering Committee. Fairbanks, Alaska, September 2000, 35 pp.

Adamenko, V.N. and *Kondratyev, K.Ya.*, 1999: Global climate change and its empirical diagnostics. In *Anthropogenic Impact on Northern Nature and Its Consequences* (in Russian). Kola Centre of the Russian Acad. Sci., Apatity, 17-35.

Aibulatov, N.A., 2000: *Cold War Echo in the Russian Arctic Seas* (in Russian). Moscow, GEOS, 307 pp.

Alekseev, G.V., 1998: Arctic climate dynamics in the global environment. *World Clim. Res. Progr./World Meteorol. Org.*, Geneva, No. 908, 11-14.

Alekseev, G.V., Aleksandrov, E.I., Svyaschennikov, P.N., and *Kharlanenkova, N.E.*, 2000: On interaction of climate oscillations in the Arctic and in mid- and low latitudes (in Russian). *Meteorol. and Hydrol.*, No. 6, 5-17.

Allison, I., Barry, R.G., and *Goodison, B.E.* (eds.), 2001: *Climate and Cryosphere (CliC) Project Science and Co-Ordination Plan.* Version 1. WCRP-114 (WMO/TD No. 1053). Geneva, 73 pp, Appendices.

Arctic Climate System Study (ACSYS). Initial Implementation Plan, 1994: WCRP-85 (WMO/TD No. 627), Geneva, Switzerland, 66 pp.

Arctic Pollution, 1997: Arctic Monitoring and Assessment Program. AMAP, Oslo, Norway, 188 pp.

Arctic Science Summit Week. 25-29 April 1999. Tromsø, Norway. *Joint-Science Day: Marine Climate of the Arctic* , 2000. Norsk Polarinstitutt. INTERNRAPPORT. Tromsø, No. 3, 32 pp.

Arfeuille, G., Mysak, L.A., and *Tremblay, L.B.*, 2000: Simulation of the interannual variability of the wind-driven Arctic sea-ice cover during 1958-1998. *Clim. Dynamics 16*, No.2-3, 107-122.

Atkinson, D.E., Alt, B., and *Gajewski, K.*, 2000: A new database of high Arctic climate data from the polar continental shelf project archives. *Bull. Amer. Meteorol. Soc. 81*, 2621-2630.

Baldwin, M.P. and *Dunkerton, T.J.*, 1999: Propagation of the Arctic Oscillation from the stratosphere to the troposphere. *J. Geophys. Res. 104*, ND24, 30,937-30,946.

Barry, R.G. (ed.), 1998: *Organization of Internationally Co-ordinated Research Into Cryosphere and Climate.* WCRP-102 (WMO/TD No. 867). WMO, Geneva, 10 pp. Appendices.

Benner, T.C., Curry, J.A., and *Pinto, J.O.*, 2001: Radiative transfer in the summertime Arctic. *J. Geophys. Res. 106*, N14, 15,173-15,184.

Brebbia, C.A., Villacampa, Y., and *Uso, J.-L.* (eds.), 2001: *Ecosystems and Sustainable Development.* Adv. In Ecol. Sci., 10, 800 pp.

CAFF (Conservation of Arctic Flora and Fauna) 2001. Arctic Flora and Fauna: Status and Conservation. Edita, Helsinki. 272 pp.

Casleden, J., 200: Bridging scientific and traditional knowledge of climate change in the Canadian Arctic. *Global Change Newsletter,* No. 47, 5-8.

Changes in Climate and Environment at High Latitudes, 2001: Abstracts and Proceedings of the Norwegian Geological Society. Tapir Academie Press, Trondheim. 102 pp.

Chao, S.-Y., 1999: Ocean feedback to wind-driven coastal polynyas. *J. Geophys. Res. 104*, NC8, 18,073-18,086.

Chýlek, P. and *Lesins, G.*, 2001: Recent temperature changes in Greenland. In *First Int. Conf. On Global Warming and the Next Ice Age.* Dalhousie Univ., 19-24 Aug. 2001, 71-84.

Climate Change 2001: The Scientific Basis. Contribution of WG1 to the Third Assessment Report of the IPCC (J. T. Houghton et al.), 2001: Cambridge University Press, 881 pp.

Curry, J.A., 2001: Introduction to special section: FIRE Arctic Clouds Experiment. *J. Geophys. Res. 106*, ND14, 14,985-14,989.

Curry, J.A., Schramm, J.L., Perovich, D. K., and *Pinto, J.C.*, 2001: Applications of SHEBA/FIRE data to evaluation of snow/ice albedo parameterizations. *J. Geophys. Res. 106*, N14, 15,345-15,356.

Dare, R.A. and *Atkinson, B.W.*, 1999: Numerical modeling of atmospheric response to polynyas in the Southern Ocean sea ice zone. *J. Geophys. Res. 104*, ND14, 16,691-16,708.

Dickson, R., 1999: All change in the Arctic. *Nature 397*, 389-391.

Doelling, D.R., Minnis, P., Spangenberg, D.A., Chakrapani, V., Mahesh, A., Pope, S.K., and *Valero, P.J.*, 2001: Cloud radiative forcing at the top of the atmosphere during FIRE ACE derived from AVHRR data. *J. Geophys. Res. 106*, N14, 15,279-15,296.

Doiban, V.A., Backich, Yu. M., and *Luzin, G.P.*, 1995: *Northern Sea Route and Market Economics: New Possibilities for Development* (in Russian). Kola Sci. Centre of the Russian Acad. Sci., Apatity, 140 pp.

Dong, X., Mace, G.G., Minnis, P., and *Young, D.F.*, 2001: Arctic stratus cloud properties and their effect on the surface radiation budget: Selected cases from FIRE ACE. *J. Geophys. Res. 106*, N14, 15,297-15,312.

Dorn, W., Dethloff, K., Rinke, A., and *Botzet, M.*, 2000: Distinct circulation states of the Arctic atmosphere induced by natural climate variability. *J. Geophys. Res. 105*, ND24, 29,659-29,668.

Duynkerke, P.G. and *Roode, S.R.*, 2001: Surface energy balance and turbulence characteristics observed at the SHEBA Ice Camp during FIRE III. *J. Geophys. Res. 106*, N14, 15,313-15,322.

Edwards, M., Anderson, R., Chayes, D., Coakley, B., Cochran, J., Jacobsson, M., Kurras, G., Polyak, L., and *Rognstad, M.*, 2001: SCICEX sonars chart new topographies, new theories. *Witness the Arctic 9*, N1, 1-2.

Edwards, M.H., Kurras, G.J., Tolstoy, M., Bohnenstiehl, D.R., Coakley, B.J., and *Cochran, J.R.*, 2001: Evidence of recent volcanic activity on the ultra-slow spreading Gakkel Ridge. *Nature 409*, 808-812.

Ekwurzel, B., Schlosser, P., Mortlock, R. A., Fairbanks, R.G., and *Swift, J.H.*, 2001: River runoff, sea ice meltwater, and Pacific water distribution and mean residence times in the Arctic Ocean. *J. Geophys. Res. 106*, NC5, 9075-9092.

Everett, J.T. and *Fitzharris, B.B.* (eds.), 2001: *The Regional Impacts of Climate Change. Chapter 3: The Arctic and Antarctic.* The IPCC Working Group 2 Report – 2001 (http://www.grida.no/climate/ipcc/regional/042.htm).

First GARP Global Experiment. Vol. 2. Polar aerosols, extended cloudiness and radiation, 1981, (eds.: *K.Ya. Kondratyev* and *V.F. Zhvalev*). Gidrometeoizdat, Leningrad, 150 pp.

Forland, E.J. and *Hanssen-Bauer, I.*, 2000: Increased precipitation in the Norwegian Arctic: True or false? *Clim. Change 46*, N4, 485-509.

Frederick, K.D., 1994: Integrated assessment of the impacts of climate change on natural resources. An Introductory essay. *Clim. Change 28*, N102, 1-14.

French, H.M., 1999: Past and present permafrost as an indicator of climate change. *Polar Research 18*, 269-274.

Garrett, T.J., Hobbs, P.V., and *Gerber, H.*, 2001: Shortwave, single-scattering properties of arctic ice clouds. *J. Geophys. Res. 106*, 15,155-15,172.

Girard, E. and *Curry, J.A.*, 2001: Simulation of arctic low-level clouds observed during the FIRE Arctic Experiment using a new bulk microphysics scheme. *J. Geophys. Res. 106*, 15,139-15,154.

Gloersen, P., Parkinson, C.L., Cavalieri, D.J., Comiso, J.C., and *Zwally, H.J.*, 1999: Spatial distribution of trends and seasonality in the hemispheric sea ice covers: 1978-1996. *J. Geophys. Res. 104*, NC9, 20,827-20,836.

Goldner, D.R., 1999: On the uncertainty of the mass, heat, and salt budgets of the Arctic Ocean. *J. Geophys. Res. 104,* NC12, 29,757-29,770.

Goody, R., 1980: Polar processes and world climate (a brief review). *Mon. Weather Rev. 108*, N12, 1935-1942.

Gordon, C., Cooper, C., Senior, C.A., Banks, H., Gregory, J.M., Johns, T.C., Mitchell, J.F.B., and *Wood, R.A.*, 2000: The simulation of SST, sea ice extents and ocean heat transports in a version of the Hadley Centre coupled model without flux adjustments. *Clim. Dynamics 16*, N2-3, 147-168.

Gramberg, I.S. et al. (eds.) (2000). *Arctic at the Threshold of the Third Millennium* (in Russian). NAUKA, St. Petersburg, 204 pp.

Grassl, H., 1999: The cryosphere: An early indicator and global player. *Polar Research 18*, N2, 119-125.

Grotefendt, K., Lagemann, K., Quadfasel, D., and *Ronski, S.*, 1998: Is the Arctic warming? *J. Geophys. Res. 103*, NC12, 27,679-27,688.

Haas, C. and *Eicken, H.*, 2001: Interannual variability of summer sea ice thickness in the Siberian and central Arctic under different atmospheric circulation regimes. *J. Geophys. Res. 106*, NC3, 4449-4462.

Haggerry, J.A. and *Curry, J.A.*, 2001: Variability of sea ice emissivity estimated from airborne passive microwave measurements during FIRE SHEBA. *J. Geophys. Res. 106*, N14, 15,265-15,278.

Hanesiak, J.M., Barber, D.G., De Abreu, R.A., and *Yackel, J.J.*, 2001: Local and regional albedo observations of arctic first-year sea ice during melt ponding. *J. Geophys. Res. 106*, NC1, 1005-1016.

Hobbs, P.V., Rangno, A.L., Shupe, M., and *Uttal, T.*, 2001: Airborne studies of cloud structures over the Arctic Ocean and comparisons with retrievals from shipbased remote sensing measurements. *J. Geophys. Res. 106*, N14, 15,029-15,044.

Hoerling, M.P., Hurrell, J.W., and *Xu, T.*, 2001: Tropical origins for recent North Atlantic climate change. *Science 292*, No. 5514, 90-92.

Holland, D.M., 2001: Explaining the Weddell Polynya – a large ocean eddy shed at Maud Rise. *Science 292*, 1697-1700.

Holloway, G. and *Sou, T.*, 2001: Is Arctic sea ice rapidly thinning? *Ice and Climate News*, No. 1, 2-5.

Hoskins, B.J. and *Yang, G.-Y.*, 2000: The equatorial response to higher-latitude forcing. *J. Atmos. Sci. 57*, 1197-1213.

Hunke, E.C. and *Ackley, S.F.*, 2001: A numerical investigation of the 1997-1998 Ronne Polynya. *J. Geophys. Res. 106*, N15, 22,373-22,382.

IASC Project Catalogue, 2001: The International Arctic Science Committee. Oslo, Norway, 57 pp.

Impacts of Global Climate Change in the Arctic Region, 1999: IASC, Fairbanks, Alaska, 59 pp.

Interactions Between the Cryosphere, Climate, and Greenhouse Gases, 1999. Eds.: *M. Trauter et al.* IAHS Press, 281 pp.

Iversen, T., 1996: Atmospheric transport pathways for the Arctic. *Chem. Exchange between the Atmos. and Polar Snow: Proc. NATO Adv. Res. Workshop "Process. Chem. Exchange Between Atmos. and Polar Snow"*, Ciocco, March 19-23, 1995. Berlin e.a., 71-92.

Izrael, Y.A., Kalabin, G.V., and *Nikonov, V.V.* (eds.), 1999: *Anthropogenic Impact on Northern Nature and Its Ecological Consequences* (in Russian). Kola Sci. Centre, Russian Acad. Sci., Apatity, 314 pp.

Jaworowski, Z., 1989: *Pollution of the Norwegian Arctic: A review*. Rapportserie Nr. 55. Norsk Polarinstitutt, Oslo. 93 pp.

Jaworowski, Z., Segalstad, T.V., and *Hisdal, V.*, 1990: *Atmospheric CO_2 and global warming: A critical review*. Norsk Polarinstitutt, Rapportserie Nr. 39, 75 pp.

Jiang, H., Feingold, G., Cotton, W.R., and *Duynkerke, P.G.*, 2001: Large-eddy simulations of entrainment of cloud condensation nuclei into the Arctic boundary layer: May 18, 1998, FIRE/SHEBA case study. *J. Geophys. Res. 106*, ND14, 15,113-15,122.

Johannessen, O.M., Muench, R.D., and *Overland, J.E.* (eds.), 2000: *The Polar Oceans and Their Role in Shaping the Global Environment*. Amer. Geophys. Union. Geophys. Monogr. 85. Washington, D.C., 525 pp.

Kalabin, G.V., 2000: *Ecodynamics of Anthropogenic Environment Province of the North* (in Russian). Kola Sci. Centre, Russian Acad. Sci., Apatity, 294 pp.

Khvorostyanov, V.I., Curry, J.A., Pinto, J.O., Shupe, M., Baker, M., and *Sassen, K.*, 2001: Modeling with explicit spectral water and ice microphysics of two-layer cloud system of altostratus and cirrus observed during the FIRE Arctic Clouds Experiment. *J. Geophys. Res. 106*, N14, 15,099-15,112.

Kienast, S.S. and *McKay, J.L.*, 2001: Sea surface temperatures in the subarctic Northeast Pacific reflect millenial scale climate oscillations during the last 16 kyrs. *Geophys. Res. Lett. 28*, N8, 1563-1566.

Kondratyev, K.Ya., Bondarenko, V.G., and *Khvorostyanov, V.I.*, 1992: A three-dimensional numerical model of cloud formation and aerosol transport in the orographically inhomogeneous atmospheric boundary layer. *Boundary-Layer Meteorol. 61*, N3, 265-285.

Kondratyev, K.Ya., Johannessen, O.M., and *Melentyev, V.V.*, 1996: *High-Latitude Climate and Remote Sensing*. Wiley/PRAXIS, Chichester, U. K., 200 pp.

Kondratyev, K.Ya. and *Cracknell, A.P.*, 1998: *Observing Global Climate Change*. London e.a., Taylor & Francis, 761 pp.

Kondratyev, K.Ya., 1999: *Climatic Effects of Aerosols and Clouds*. Springer/PRAXIS, Chichester, U. K., 264 pp.

Kondratyev, K.Ya. and *Varotsos, C.A.*, 2000: *Atmospheric Ozone Variability: Implications for Climate Change, Human Health, and Ecosystems*. Springer/PRAXIS, Chichester, U. K., 614 pp.

Krapivin, V.F. and *Kondratyev, K.Ya.*, 2002: *Global Environmental Change: Ecoinformatics* (in Russian). St. Petersburg State Univ., 721 pp.

Lawson, R.P., Baker, B.A., Schmitt, C.G., and *Jensen, T.L.*, 2001: An overview of microphysical properties of Arctic clouds observed in May and July 1998 during FIRE ACE. *J. Geophys. Res. 106,* N14, 14,989-15,014.

Lemke, P., Harder, M., and *Hilmer, M.*, 2000: The response of Arctic sea ice to global change. *Clim. Change 46,* N3, 277-287.

Lemke, P., 2001: Open windows to the polar oceans. *Science 292*, 1670-1671.

Lohmann, U., Humble, J., Leaitch, W.R., Isaac, G.A., and *Gultepe, I.*, 2001: Simulations of ice clouds during FIRE ACE using the CCCMA single-column model. *J. Geophys. Res. 106,* N14, 15,123-15,138.

Losev, K.S., 2001: *Ecological Issues and Sustainable Development Perspectives of Russia in the XXI Century*. Cosmoinform Publ., Moscow, 400 pp.

Marchand, R.T., Ackerman, T.P., King, M.D., Moroney, C., Davies, R., Muller, J.-P.A.L., and *Gerber, H.*, 2001: Multiangle observations of Arctic clouds from FIRE ACE: June 3, 1998, case study. *J. Geophys. Res. 106,* N14, 15,201-15,214.

Matishov, G.G., 1998: Strategy of Arctic studies (in Russian). *Herald of the Russian Acad. Sci. 68*, N6, 515-520.

Matishov, G.G., 2000: Contemporary problems of oceanology and geography of the World Ocean (in Russian). *Herald of the Russian Acad. Sci. 70,* N8, 682-687.

Matishov, D.G. and *Matishov, G.G.*, 2001: *Radiational Ecological Oceanology* (in Russian). Kola Science Centre, Russian Acad. Sci., Apatity, 419 pp.

May, B.D. and *Lley, D.E.*, 2001: Growth and steady state stages of thermohaline intrusion in the Arctic Ocean. *J. Geophys. Res. 106*, NC8, 16,783-16,794.

Mendelsohn, R. and *Rosenberg, N.J.*, 1994: Framework for integrated assessment of global warming impacts. *Clim. Change 28*, N1-2, 15-44.

Minnis, P., Chakrapani, V., Doelling, D.R., Nguyen, L., Palikonda, R., Spangenberg, D.A., Uttal, T., Arduini, R.F., and *Shupe, M.*, 2001: *J. Geophys. Res. 106*, N14, 15,215-15,232.

Mysak, L.A. and *Venegas, S.A.*, 1998: Decadal climate oscillations in the Arctic: A new feedback loop for atmosphere-ice-ocean interactions. *Geophys. Res. Lett. 25,* N19, 3607-3610.

Nagurny, A. P. and *Maistrova, V.V.*, 2002: Long-term temperature trends for the free atmosphere in the Arctic (in Russian). *Doklady RAS,* (in press).

Newman, P.A., Nash, E.R., and *Rosenfeld, J.E.*, 2001: What controls the temperature of the Arctic stratosphere during the spring? *J. Geophys. Res. 106,* ND17, 19,999-20,010.

Overland, J.E. and *Adams, J.M.*, 2001: On the temporal character and regionality of the Arctic Oscillation. *Geophys. Res. Lett. 28,* N14, 2811-2814.

PARCS develops two updated research goals, 2000: *Witness the Arctic 9*, N1, p.8.

Parkinson, C.L., Cavalieri, D.J., Gloersen, P., Zwally, H.J., and *Comiso, J.C.*, 1999: Arctic sea ice extents, areas, and trends, 1978-1996. *J. Geophys. Res. 104*, NC9, 20,837-20,856.

Polyakov, I.V., Proshutinsky, A.Y., and *Johnson, M.A.,* 1999: Seasonal cycles in two regimes of Arctic climate. *J. Geophys. Res. 104*, NC11, 25,761-25,788.

Proceedings of the International Symposium on Polar Aspects of Global Change, 1999. Tromsø, Norway, 24-28 August 1998. Polar Research, 18, N2, 404 pp.

Proshutinsky, A., 2000: Arctic climate variability during 20th century. *Int. WOCE Newsletter,* N40, 9-12.

Przybylak, R., 2000: Diurnal temperature range in the Arctic and its relation to hemispheric and Arctic circulation patterns. *Int. J. of Climatol. 20*, N3, 231-254.

RAISE Plan focuses on ship-based research in Russia, 2001: *Witness the Arctic 9*, N1, p.7.

Rangno, A.L. and *Hobbs, P.V.,* 2001: Ice particles in stratiform clouds in the Arctic and possible mechanisms for the production of high ice concentrations. *J. Geophys. Res. 106*, N14, 15,065-15,076.

Rapley, C., 1999: Global change and the polar regions. *Polar Research 18,* N2, 117-118.

Report from the Arctic Climate Impact Assessment Modeling and Scenarios Workshop. Stockholm, Sweden, January 29-31, 2001. The ACIA Secretariat, Fairbanks, 28 pp.

Riedlinger, D. and *Berkes, F.,* 2001: Contributions of traditional knowledge to understanding climate change in the Canadian Arctic. *Polar Research 37*, N203, 315-328.

Rimbu, N., Lohmann, G., Felis, T., and *Pätzold, J.,* 2001: Arctic Oscillation signature in a Red Sea coral. *Geophys. Res. Lett. 28*, N15, 2959-2962.

Rind, D., Chandler, M., Lerner, J., Martinson, D.G., and *Yuan, X.,* 2001: Climate response to basin-specific changes in latitudinal temperature gradients and implications for sea ice variability. *J. Geophys. Res. 106*, ND17, 20,161-20,174.

Rinke, A., Lynch, A.H., and *Dethloff, K.,* 2000: Intercomparison of Arctic regional climate simulations: Case studies of January and June 1990. *J. Geophys. Res. 105*, ND24, 29,669-29,684.

Rogachev, K.A. and *Carmack, E.C.,* 2002: Eddies in the western Subarctic Pacific: Their internal structure and linkages to the regime shift phenomena. *Int. WOCE Newsletter,* N42, 25-28.

Rybak, E. and *Rybak, O.,* 2001: Changes of the ice cover in the Barents Sea: Links with the large-scale processes in the atmosphere. In *First Int. Conf. On Global Warming and the Next Ice Age*. Dalhousie Univ., 19-24 Aug., 2001, 155-159.

Sandven, S., Johannessen, O.M., Miles, M.W., Pettersson, L.H., and *Kloster, K.,* 1999: Barents Sea seasonal ice zone features and processes from ERS-1 synthetic aperture radar: Seasonal Ice Zone Experiment 1992. *J. Geophys. Res. 104*, NC7, 15,843-15,857.

SEARCH research opportunities emerging, Winter 2000/2001. *Witness the Arctic 8*, N2, p.8.

SEARCH develops implementation framework, 2001. *Witness the Arctic 9*, N1, p.3.

Semiletov, I.P., 1999: Aquatic sources and sinks of CO_2 and CH_4 in the polar regions. *J. Atmos. Sci. 56*, N2, 286-306.

Serreze, M.C., Walsh, J.E., Chapin, F.S. III, Ostercamp, T., Dyurgerov, M., Romanovsky, V., Oechel, W.C., Morison, J., Zhang, T., and *Barry, R.G.,* 2000: Observational evidence of recent change in the northern high-latitude environment. *Clim. Change 46,* N1-2, 159-307.

Shupe, M.D., Uttal, T., Matronson, S.Y., and *Frisch, A.S.,* 2001: Cloud water contents and hydrometeor sizes during FIRE Arctic Clouds Experiment. *J. Geophys. Res. 106*, N14, 15,015-15,028.

Stevens, T., 2001: Climate change in the Arctic and the 107th Congress. *Witness the Arctic 9*, N1, p. 21.

Stevenson, D.S., Johnson, C.E., Collins, W.J., Derwent, R.G., and *Edwards, J.M.,* 2000: Future estimates of tropospheric ozone radiative forcing and methane turnover – the impact of climate change. *Geophys. Res. Lett. 27*, N14, 2073-2076.

Sumner, A.L. and *Shepson, P.B.,* 1999: Snowpack production of formaldehyde and its effect on the Arctic troposphere. *Nature 398*, N6724, 230-233.

Suortti, T., Karhu, J., Kivi, R., Kyro, E., Rosen, J., Kjome, N., Larsen, N., Neuber, R., Khattatov, V., Rudakov, V., and *Nakane, H.,* 2001: Evolution of the Arctic stratospheric aerosol mixing

ratio measured with balloon-borne aerosol backscatter sounders for years 1988-2000. *J. Geophys. Res. 106*, ND18, 20,759-20,766.

Toward An Arctic System Synthesis: Results and Recommendations, 1998: The Arctic Research Consortium of the United States (ARCUS). Fairbanks, Alaska, 165 pp.

Toward Prediction of the Arctic System: predicting future states of the arctic system on seasonal-to-century time scales by interacting observations, process research, modeling, and assessment, 1998: The Arctic Research Consortium of the United States (ARCUS). Fairbanks, Alaska, 54 pp.

Tschudi, M.A., Curry, J.A., and *Maslanik, J.A.,* 2001: Airborne observations of summertime surface features and their effect on surface albedo during FIRE/SHEBA. *J. Geophys. Res. 106*, N14, 15,335-15,344.

Volkov, V.A., Johannessen, O.M., Borodachev, V.E., Voinov, G.M., Pettersen, L.H., Bobylev, L.P., and *Kouraev, A.V.*, 2002: *Polar Seas Oceanography. An integrated case study of the Kara Sea.* Springer/PRAXIS, Chichester, UK., 450 pp.

Vörösmarty, C.J., Hinzman, L.D., Peterson, B.J., Bromwich, D.H., Hamilton, L.C., Morison, J., Romanovsky, V.E., Sturm, M., and *Webb, R.S.*, 2001: *The Hydrological Cycle and Its Role in Arctic and Global Environmental Change: A Rationale and Strategy for Synthesis Study.* Arctic Research Consortium of the U. S., Fairbanks, Alaska, 84 pp.

Wadhams, P., Dowdeswell, J.A., and *Schofield, A.N.* (eds.), 1997: *The Arctic and Environmental Change.* Gordon & Breach, Newark, NJ, e.a., 208 pp.

Wang, M., 2001: Temperature decadal change over Arctic as seen from TOVS and NCEP analysis. In *First Int. Conf. On Global Warming and the Next Ice Age*, Dalhousie Univ., 19-224 Aug. 2001. p.177.

Wang, S., Wang, Q., Jordan, R.E., and *Persson, P.O.G.,* 2001: Interactions among longwave radiation of clouds, turbulence, and snow surface temperature in the Arctic: A model sensitivity study. *J. Geophys. Res. 106*, N14, 15,323-15,334

Warren, S.G., Rigor, I.G., Untersteiner, N., Radionov, V.F., Bryazgin, N.N., Aleksandrov, Y.I., and *Colony, R.*, 1999: Snow depth on Arctic sea ice. *J. Climate 12*, N6, 1814-1829.

Weatherly, J.W., Briegleb, B.P., Large, W.G., and *Maslanik, J.A.*, 1998: Sea ice and polar climate in the NCAR CSM. *J. Climate 11*, 1472-1486.

Weller, G., 1999: The aim of the symposium. *Polar Research 18*, N2, 115-116.

Weller, G. and *Lange, M.*, (eds.), 1999: *Impacts of Global Climate Change in the Arctic Region.* Intern. Arctic Science Com., Fairbanks, Alaska, 59 pp.

Wetzel, P.J., 2001: Ice house effect: A selective Arctic cooling trend current models are missing. In *First Int. Conf. On Global Warming and the Next Ice Age,* Dalhousie Univ., 19-24 Aug., 2001, 178-181.

White, A., Cannell, M.G.R., and *Friend, A.D.*, 2000: The high-latitude terrestrial carbon sink: a model analysis. *Global Change Biology 6*, 227-245.

Winsor, P. and *Bjork, G.*, 2000: Polynya activity in the Arctic Ocean from 1958 to 1997. *J. Geophys. Res. 105,* NC4, 8789-8804.

Young, O.R., 1999: The interplay of global and polar regimes. *Polar Research 18*, N2, 397-402.

Yudakhine, F.N., (ed.), 2000: *The North: Ecology* (in Russian). Ural Section of the Russian Acad. Sci., Ekaterinburg, 415 pp.

Zakharov, V.F. and *Malinin, V.N.*, 2000: *Sea Ice and Climate* (in Russian). Gidrometeoizdat, St. Petersburg, 92 pp.

Zhang, Y. and *Hunke, E.C.*, 2001: Recent Arctic change simulated with a coupled ice-ocean model. *J. Geophys. Res. 106*, NC3, 4369-4390.

Zhou, X., Seine, H.J., Honrath, R.E., Fuentes, J.D., Simpson, W., Shepson, P.B., and *Bottenheim, J.W.*, 2001: Snowpack photochemical production of HONO: a major source of OH in the Arctic boundary layer in springtime. *Geophys. Res. Lett. 28*, N21, 4087-4090.

IDŐJÁRÁS

Quarterly Journal of the Hungarian Meteorological Service
Vol. 107, No. 1, January–March 2003, pp. 31–48

Homogeneity analysis of climatological time series – experiments and problems

Margarita Syrakova

Department of Meteorology and Geophysics, Faculty of Physics, University of Sofia
5, J. Bourchier blvd., Sofia 1164, Bulgaria; E-mail: marsyr@phys.uni-sofia.bg

(Manuscript received 27 August 2001; in final form 19 February, 2002)

Abstract—Experiments with different tests for homogeneity are performed. Sensitivity of the tests to different modifications of the time series is examined. Experiments were made with artificially generated normally distributed random series, on which different modifications were imposed: trends (constant and changing), simple periodicity (sine wave), jump, and various combinations of jump plus another change. Experiments with the combined models aimed to examine whether the jump can be detected in the presence of other modifications (with a presumption that the most probable form of inhomogeneity is an abrupt change). To obtain reliable results, each experiment was repeated with 100 different random series, and the results for individual series were averaged.

The experiments show that graphical tests can give an indication about the form of the change. Serious problems are the cases when two or more modifications interfere in such a way that the tests fail to indicate the change.

An example with the annual precipitation series of Sofia (Bulgaria) is presented.

Key-words: homogeneity tests, precipitation series.

1. Introduction

In recent years much attention has been directed at climate variability and climate change. Empirical investigations of the problem are based on long-term climate time series. This, in turn, has enhanced the concern about the quality of the series – first of all the homogeneity of the series should be tested. In the first place, the homogeneity tests are aimed at detecting abrupt changes in the series, which cause slippage of the mean. The presumption is that in many cases such changes are "artificial" – a consequence of change of

measuring instrument, location, averaging method, etc. In other cases the series may be "contaminated" by anthropogenic trend, e.g., an increasing trend in temperature series at a station located in an enlarging urban area.

Many tests exist and are used in climate series homogeneity analysis. Results, however, should be interpreted very carefully, because the detected changes may not be "artificial". Natural climate changes may also have effect on the statistics, i.e., one should distinguish between statistical and climatic (in)homogeneity, where climatic inhomogeneity means the influence of the mentioned nonclimatic factors. One way to distinguish between these two possibilities is to take into account metadata, i.e., information about the measurement and station history. This information is very valuable in time series homogeneity analysis, but unfortunately is not always available, or is not of good quality. Another way to overcome the problem is to compare the tested series to reference series placed in very similar climate conditions. Since various forms of natural climate variation (trends, periodicities, abrupt changes, etc.) are almost coherent in tested and reference series, they will not dominate the resultant series (the series of differences or ratios between tested and reference series), and the inhomogeneity will be revealed as a systematic change in the difference/ratio series. This relative approach in homogeneity analysis is very fruitful and widely and successfully used (*Alisov et al.*, 1952; *Potter*, 1981; *Alexandersson*, 1986; *Karl* and *Williams*, 1987; *Rhoades* and *Salinger*, 1993; *Hanssen-Bauer* and *Forland*, 1994; *Peterson* and *Easterling*, 1994; *Easterling* and *Peterson*, 1995; *Alexandersson* and *Moberg*, 1997; *Moberg* and *Alexandersson*, 1997; *Szentimrey*, 1998). Reference series are defined in different ways by different authors.

There are, however, situations when it is not possible to find appropriate reference series. This is valid, for example, for the initial part of a long series – up to certain year one cannot find any series well correlated with it, because the observations in the surrounding stations (with large enough correlation coefficients) have started much later. This problem is especially valid for the precipitation due to its high spatial variability.

The aim of this investigation was to examine the sensitivity of different tests to different modifications of the time series. For this purpose, artificial but realistic time series were generated and tested for inhomogeneity.

2. Series and method

Normally distributed random numbers were generated to form time series reproducing the mean and variance of annual precipitation on the territory of Bulgaria. Each series has a length of $n=100$, i.e., simulated series cover 100-

year periods. Random series were modified in various ways and tested for homogeneity using several statistical techniques. The procedure (modification and testing) was repeated with 100 different random series and the results for the individual series were averaged.

Modifications imposed on the random series can be divided into two groups: simple and combined models. They represent imitations of possible climate variability and abrupt change. The magnitude of a modification is expressed by the standard deviation of the random series (σ). Experiments include the following models (1 to 4 – simple, 5 to 9 – combined):

(1) *Linear trend* from 0 to Δ_t, i.e., with a slope $\Delta_t / n = \Delta_t / 100$, Δ_t is from $\pm 0.25\sigma$ to $\pm 2\sigma$ ("+" means an increase, "–" means a decrease from the beginning to the end of the series).

(2) *Linear trend with changing slope* (*changing trend*). This model may have various modifications. We have chosen the modification with an increase/decrease from 0 to Δ_c at a certain point n_c, followed by a returning to the initial "zero" level at the last point, i.e., the two slopes are Δ_c / n_c and $\Delta_c / (100 - n_c)$. The magnitude of Δ_c is from $\pm 0.25\sigma$ to $\pm 2\sigma$ ("+" means an increasing initial trend, "–" means a decreasing initial trend). This model may roughly be considered as a part of a long-term oscillation.

(3) *Long-term oscillation* (periodicity) in the form of one *sine wave* with amplitude Δ_s. The experiments include amplitudes from $\pm 0.25\sigma$ to $\pm 2\sigma$, the minus sign means opposite phase. Very big amplitudes, however, are not realistic.

(4) *Abrupt change* (*jump*) at point n_j, with a magnitude Δ_j from $\pm 0.25\sigma$ to $\pm 2\sigma$.

(5) *Jump+trend* with different combinations of the magnitudes Δ_j and Δ_t, each one is from $\pm 0.5\sigma$ to $\pm 1.5\sigma$, and two different points of the jump: $n_{j1} = 30$ or $n_{j2} = 60$.

(6) *Jump+sine wave* with Δ_j from $\pm 0.5\sigma$ to $\pm 1.5\sigma$, and Δ_s from $\pm 0.25\sigma$ to $\pm \sigma$. The jump is located at different points of the sine wave.

(7) *Jump+sine+trend* with Δ_j, Δ_t from $\pm 0.5\sigma$ to $\pm 1.5\sigma$, and $\Delta_s = \pm 0.3\sigma$, jump located at $n_j = 30$, i.e., not far from the extremum of the sine wave.

(8) *Jump+changing trend* with Δ_j and Δ_c from $\pm 0.5\sigma$ to $\pm 1.5\sigma$, change of the slope at $n_c = 40$, and jump at $n_{j1} = 30$ or $n_{j2} = 70$ (at different distances from the break of the slope).

(9) *Jump+jump* with different magnitudes and signs from $\pm 0.5\sigma$ to $\pm 1.5\sigma$ at points $n_{j1} = 30$ and $n_{j2} = 60$. This combination (more than one change point) has been examined by many authors (*Lanzante*, 1996; *Mestre*, 1998; *Sneyers et al.*, 1998).

Several statistical techniques for homogeneity analysis were used in the experiments. Critical values of the test statistics for the acceptance of null hypotheses were chosen according to a significance level $\alpha = 5\%$.

First, the series were tested for randomness using several techniques. One of them is the comparison of lag-1 serial correlation coefficient, r_1, with its critical value (*Mitchell*, 1966; *Zhukovskii et al.*, 1976; *Sneyers*, 1990, 1992). The critical value is $|r_1|_c = t_c \sqrt{(1 - r_1^2)/(n-2)}$ with t_c taken from the table of Student (or normal – for long series) probability distribution at the level of significance desired.

Similar techniques include Abbe and von Neumann tests (*Mitchell*, 1966; *Rozhdestvenskii* and *Chebotarev*, 1974; *Brownlee*, 1977) based on the ratio $q = d^2/2\sigma^2$ (Abbe) or $V = d^2/\sigma^2$ (von Neumann), where σ^2 is the variance and d^2 is the mean square successive difference $[\sum_{1}^{n-1}(x_{i+1} - x_i)^2]/(n-1)$. Because of the relationship between q (or V) and r_1 (in fact $q = 1 - r_1$), these three tests give identical results, and only the results for r_1 will be discussed.

As a non-parametric alternative to the lag-1 correlation coefficient, the Spearman rank correlation coefficient, r_s, is recommended (*Mitchell*, 1966; *Sneyers*, 1990; *Lanzante*, 1996),

$$r_s = 1 - \frac{6}{n(n^2-1)} \sum_{i=1}^{n} [r(x_i) - i]^2 , \qquad (1)$$

where $r(x_i)$ are the ranks of the elements x_i of the series, arranged in increasing order. Under the hypothesis of randomness, the test statistic $u_s = u(r_s) = r_s \sqrt{n-1}$ has a standard normal distribution and the critical values are ± 1.96.

Another test of randomness is the run-test (*Thom*, 1966; *Davis*, 1973; *Rozhdestvenskii* and *Chebotarev*, 1974; *Brownlee*, 1977; *Sneyers*, 1990). This is a non-parametric test, which counts the number of the runs U_r above and below the median of the series. The counted number U_r is compared with the tabulated critical values for a certain significance level (*Bol'shev* and *Smirnov*,

1983). Too many runs indicate high frequency oscillations, while too few runs suggest a trend or abrupt changes.

A test used to detect inconstancy of the mean is based on the statistic (*Mitchell*, 1966; *Rozhdestvenskii* and *Chebotarev*, 1974; *Zhukovskii et al.*, 1976; *Kobisheva* and *Narovlianskii*, 1978; *Isaev*, 1988; *Zwiers* and *von Storch*, 1995)

$$t = \frac{\bar{x}_2 - \bar{x}_1}{\sqrt{n_1\sigma_1^2 + n_2\sigma_2^2}} \sqrt{\frac{n_1 n_2 (n_1 + n_2 - 2)}{n_1 + n_2}}, \tag{2}$$

where $n_1 + n_2 = n$, $\bar{x}_1$ and $\bar{x}_2$, ${\sigma_1}^2$ and ${\sigma_2}^2$ are the means and variances over n_1 and n_2 terms of the series, respectively. If the observations, x_i, are independent and normally distributed, the expectations (represented by the sample means) are not significantly different, and the *t*-statistic has a Student's distribution with $(n_1 + n_2 - 2)$ degrees of freedom. When the stability of the mean is tested, the series is divided into two subseries with lengths $n_1 = 3,4,...,n-3$, and $n_2 = n-3,...,3$, and after calculating the values of $|t|$ for each combination of n_1 and n_2, the maximum value $|t|_{\max}$ is found. If $|t|_{\max}$ is less than the critical value, the series may be considered homogeneous with probability $(1-\alpha)$. If $|t|_{\max}$ exceeds the critical value and if the cause is an abrupt change, its location can be identified with the place of $|t|_{\max}$.

A statistic, similar to the Student's *t*-statistic, is (*Kobisheva* and *Narovlianskii*, 1978; *Isaev*, 1988; *Zwiers* and *von Storch*, 1995)

$$z = (\bar{x}_2 - \bar{x}_1) \Big/ \sqrt{\frac{\sigma_1^2}{n_1} + \frac{\sigma_2^2}{n_2}}, \tag{3}$$

which has a standard normal distribution for large *n*.

Both statistics assume independence of the observations. Methods to overcome this restriction are suggested by *Zwiers* and *von Storch* (1995), where one can find tables with critical values of $|z|$, for $|r_1| > |r_1|_c$.

In our experiments, instead of determining one single value $|t|_{\max}$ or $|z|_{\max}$, sequential versions of both tests were realized, and the values of $|t|$ or $|z|$ were represented graphically along the time axis. This representation is more informative on the peculiarities of the analyzed series than only the magnitude

of $|t|_{\max}$ or $|z|_{\max}$. Results from the *t*-test and *z*-test turned out to be almost identical, that is why only results of the *t*-test will be discussed.

Another test, the widely used non-parametric Mann-Kendall test, is applied in a sequential forward and backward way (*Goossens* and *Berger*, 1986; *Sneyers*, 1990, 1992). The method consists of calculating the test statistic $u(d_n) = [d_n - E(d_n)] / \sigma(d_n)$, where $d_n = \sum_{i=1}^{n} m_i$, m_i is the number of inequalities $x_j < x_i$ with $j < i$. For long series, under the hypothesis of randomness, d_n is normally distributed with expected value $E(d_n) = n(n-1)/4$ and variance $\sigma^2(d_n) = n(n-1)(2n+5)/72$, i.e., $u(d_n)$ has a standard normal distribution. The sequential version is based on computation of all $u(d_i)$, $i = 1,...,n$, which form a curve $u(t)$ along the time axis. The same principle is applied to the backward series to calculate the values $u'(d_i)$ and construct the backward curve $u'(t)$. In the absence of any systematic change in the series, the curves $u(t)$ and $u'(t)$ remain within the critical limits (± 1.96 for $\alpha = 5\%$). In case of significant trend or abrupt change, they exceed the critical levels. Intersection of $u(t)$ and $u'(t)$ is expected to localize the point of the change.

Another method for detecting changes in the mean is based on the cumulative sums (cusums) (*Alisov et al.*, 1952; *Craddock*, 1979; *Rubinshtein*, 1979; *Rhoades* and *Salinger*, 1993). These may be the sums of successive terms of the series (*CS*), sums of successive deviations from the general mean (*CS*1), or sums of successive deviations from the current means (*CS*2), i.e., the means, which are calculated over the terms included in the current sum. (It should be noticed that the first value of *CS*2 and the last value of *CS*1 are equal to zero.) In our experiments the cusums were calculated not for the "original" series but for the series of rank expectations $F(x_i) = r(x_i)/(n+1)$ (*Sneyers*, 1997; *Sneyers et al.*, 1998), where $r(x_i)$ are the ranks of the elements x_i of the series, arranged in increasing order. In this way, these tests as well as the Mann-Kendall test take into account only the arrangement of the terms in the series but not their magnitudes.

The method is graphical. When the terms of the series are arranged randomly, i.e., when small (big) values are not concentrated in one or another part of the series, the mean values are statistically stable. In such case, the cusums *CS* will lie along a straight line with a constant slope, and the cumulative deviations *CS*1 and *CS*2 will fluctuate around the zero level (the *x*-axis). In case of a systematic change in the series, the slope of the *CS*-curve is not constant, and the curves *CS*1 and *CS*2 do not fluctuate around the *x*-axis. An abrupt change results in a sharp change of the slope of the curves *CS* and *CS*2. The place of the jump can be identified by a sharp extreme value of *CS*1 plot.

Buishand (1982) has suggested several statistics based on the cusums $(CS1)_i = \sum_{j=1}^{i} (x_j - \bar{x})$, $i = 1,...,n$, and more exactly, on the rescaled cusums $S_i = (CS1)_i / \sigma_x$, where σ_x is the standard deviation of the examined series. These statistics are as follows:

$$Q = \max |S_i| , \tag{4}$$

$$R = (S_i)_{\max} - (S_i)_{\min} , \tag{5}$$

$$U = \frac{1}{n(n+1)} \sum_{i=1}^{n-1} S_i^2 , \tag{6}$$

$$A = \sum_{i=1}^{n-1} \frac{S_i^2}{i(n-i)} . \tag{7}$$

Critical values of these statistics are given in *Buishand* (1982).

Pettitt test (*Pettitt*, 1979) was also used in our experiments. It is a non-parametric technique for detecting a change point. However, we will not discuss it here, because the graphical representation of the Pettitt's test statistic is identical with the graphical representation of the cusums *CS*1 applied to rank expectations.

3. Results and discussion

First, the results for nongraphical tests are discussed. *Table 1* shows the sensitivity of the tests to different systematic changes, i.e., the influence of the magnitude of certain modification on the test statistic. Results of the tests for both the randomness and stability of the mean (the Buishand statistics) are included in the table. These results are valid for the simple modes (models (1)–(4) described in the previous section) with $\Delta > 0$. Two stars (**) indicate that the test statistic exceeds the critical value, empty places mean that the test statistic is below the critical value, and one star (*) corresponds to almost critical value of the test statistic.

The most sensitive one turned out to be the Buishand test, i.e., modifications have greater influence on the mean values than on the randomness. The least sensitive one is the run-test. All tests are most sensitive to an abrupt change, but a jump $\Delta_j < 0.5\sigma$ is not detected by any of the tests. The tests are sensitive to periodicity, but periodicities with rather high

amplitudes are included in the table. (Quasi)periodicities can be visualized in climate time series by means of low-pass filters (see *Fig. 6*). Almost all tests detect the changing trend at higher Δ than in case of other modifications, so such variations may remain undetected unless they are quite big.

Table 1. Influence of the magnitude Δ of certain modification on the test statistics. An empty place shows that the respective statistic is below the critical value, one star (*) shows that it is about the critical value, two stars (**) mean that the critical value is exceeded at 5% significance level. r_1 is lag-1 correlation coefficient, u_s is the Spearman test statistic, U_r is run test statistic, *Q, R, U, A* are Buishand statistics.

Δ	**0.25σ**	**0.5σ**	**0.75σ**	**σ**	**1.25σ**	**1.5σ**	**1.75σ**	**2σ**
				Linear trend				
r_1						*	**	**
u_s			*	**	**	**	**	**
U_r								
Q			*	**	**	**	**	**
R				*	**	**	**	**
U			**	**	**	**	**	**
A			**	**	**	**	**	**
				Linear trend with changing slope (at n_c = 40)				
r_1							**	**
u_s								
U_r								
Q					*	**	**	**
R			*	**	**	**	**	**
U					*	**	**	**
A				*	**	**	**	**
				Sine wave				
r_1						**	**	**
u_s			*	**	**	**	**	**
U_r							**	**
Q			**	**	**	**	**	**
R			**	**	**	**	**	**
U			**	**	**	**	**	**
A			**	**	**	**	**	**
				Jump (at n_j = 30)				
r_1				*	**	**	**	**
u_s			**	**	**	**	**	**
U_r						**	**	**
Q		*	**	**	**	**	**	**
R			**	**	**	**	**	**
U		**	**	**	**	**	**	**
A		**	**	**	**	**	**	**

Experiments with models of changing trends and jump are made for different locations of the change. The results (not included in the table) show that the closer the change of the slope is to the midpoint, the less sensitive the tests are to this modification. On the contrary, when the jump is closer to the midpoint, it can be detected for smaller Δ.

As it was mentioned, these results are averages obtained from 100 experiments for each magnitude Δ of every modification. Dispersion of individual results around the mean value of the respective statistic shows that the probability for the test statistic exceeding the critical level increases with the increase of Δ. For example, in the case of a linear trend, this probability for r_1 is 6% for $\Delta_t = 0.25\sigma$, about 45% for $\Delta_t = 1.5\sigma$, and becomes 100% only for $\Delta_t > 3\sigma$. The results show that tests may fail to detect even a big systematic change. The risk is the least in case of an abrupt change (jump), and "the least risky" ones are the Buishand statistics.

The combined models are more interesting than the "pure" changes. It is not possible to represent results from the numerous combinations of "jump + another change" which were tested, but the main conclusion is that in some cases the effect is enhanced, while in others, due to compensation, the test statistics remain below the critical levels. In the model "jump + trend", one can easily suppose that a positive jump may be compensated by a negative trend and vice versa. This is confirmed even by the most sensitive Buishand statistics (hereafter we will discuss these statistics because of their higher sensitivity). When Δ_j is about 0.5σ, the jump is compensated by a trend with magnitude $|\Delta_t| \geq |\Delta_j|$; however, when $|\Delta_t| >> |\Delta_j|$, the test statistic exceeds the critical value because of the effect of the trend. For larger jumps, some of the Buishand statistics remain below the critical levels for $|\Delta_t| > |\Delta_j|$, but not for $|\Delta_t| \approx |\Delta_j|$.

In the combination "jump + sine", the effect of the jump Δ_j is compensated when Δ_s is of the same sign, i.e., the effect depends on the phase of the oscillation and direction of the jump. The compensation is most probable when the jump is near the point of inflection and with $\Delta_s \approx \Delta_j$.

The model "jump+sine+trend" is more complicated. With the assumed parameters of the model (jump near the extremum of a sine wave with an amplitude 0.3σ), the Buishand test statistics are below the critical levels for the following combinations: Δ_j and Δ_s of the same sign, Δ_t of the opposite sign, with $|\Delta_t| \approx |\Delta_j|$, or opposite signs of Δ_j and Δ_s, compensated by a trend in the direction opposite to the jump with magnitude $|\Delta_t| > |\Delta_j|$. With the chosen amplitude of the oscillation, the compensation is most probable for $\Delta_j < \sigma$.

In the model "jump + changing trend", a compensation is possible when the jump is relatively small ($\approx 0.5\sigma$) and occurs far from the point of change of the slope. Under these conditions, the Buishand statistics are under critical values when positive jump is located in the decreasing branch, or negative jump is located in the increasing branch.

The combination "jump+jump" is a matter of discussion in many works. Compensation may be expected in the case of opposite signs of jumps with almost equal magnitudes. Some tests confirm this, even for $\Delta_j > \sigma$, but for the Buishand statistics this is valid only for $\Delta_j < \sigma$.

Results from the graphical tests were plotted for each model with chosen magnitudes of modifications (each plot was an average over 100 results). In this way we have obtained a set of "ideal" patterns for the models considered here.

In *Figs. 1–3* examples of these results are given for four simple models. These include plots of the Student's *t*-test in the sequential version used here (*Fig. 1*), Mann-Kendall test (*Fig. 2*), and cusums *CS*1 and *CS*2 (*Fig. 3*). Plots of the cusums *CS* are not represented and not discussed, because they give worse visualization of the changes in the series compared to the other tests. Interpretation of the results obtained by the Student's and Mann-Kendall tests is based not only on the form of the curves (which is important for all tests) but on the critical values of the test statistics as well. Examples in *Figs. 1* and *2* include patterns in which test statistics remain within the critical limits, and patterns in which they exceed the critical levels, depending on the magnitude Δ of the respective modification. All curves are quite smooth and easy for interpretation (the slight disturbance around the beginning is common for all curves and will not be taken into account).

We shall notice that the indication given by the magnitudes of the Student's and Mann-Kendall test statistics is identical with the indication given by the Buishand statistics: t, $u(t)$, $u'(t)$, and the Buishand statistics exceed the critical values for almost one and the same magnitude of certain change ($\Delta_t \approx \sigma$, $\Delta_c \approx 1.25\sigma$, $\Delta_s \approx 0.75\sigma$, $\Delta_j \approx 0.75\sigma$).

In *Figs. 1–3*, the differences between the specific patterns of the curves, corresponding to different forms of modifications can be seen quite clearly. The jump can be easily indicated by the sharp peak (*t*-test and *CS*1), or the sharp change of the slope ($u(t)$, $u'(t)$, and *CS*2) at the place of its occurrence. In the case of a linear trend, t and *CS*1 curves are flat (the patterns resemble a plateau, not a peak), and the slopes of $u(t)$, $u'(t)$, and *CS*2 do not change significantly. The curves for the model of a changing trend are more complicated – each curve consists of two parts, indicating the two opposite trends. Patterns for the model of a sine wave can result in a wrong interpretation, either as an indication of a jump, or as an indication of a trend.

For this model, the peak of the curve (t, *CS*1) or the change of the slope ($u(t)$, $u'(t)$, *CS*2) is located at the point of inflection, i.e., at the place of the transition from values above/below the average to values below/above the average, which seems like a jump (trend) from one level to another.

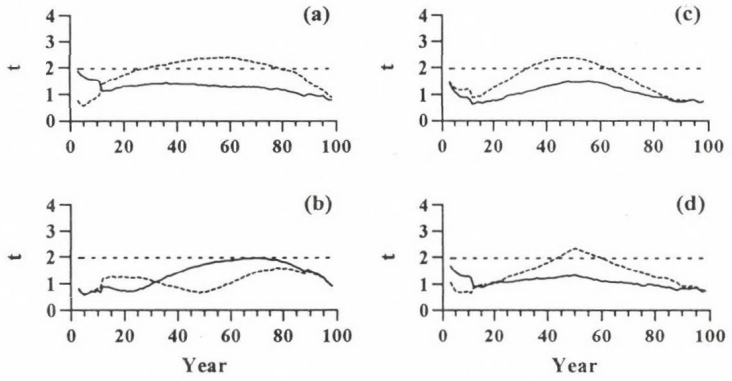

Fig. 1. Plots of the Student's t-test for models of linear trend, changing trend, sine wave, and jump. The 5% significance value is denoted. (*a*) linear trend, $\Delta_t = 0.5\sigma$ (solid line) and $\Delta_t = -\sigma$ (dashed line); (*b*) changing trend, $\Delta_c = -\sigma$, $n_c = 25$ (solid line) and $\Delta_c = -\sigma$, $n_c = 50$ (dashed line); (*c*) sine wave, $\Delta_s = 0.5\sigma$ (solid line) and $\Delta_s = -0.75\sigma$ (dashed line); (*d*) jump, $\Delta_j = 0.25\sigma$, $n_j = 50$ (solid line) and $\Delta_j = 0.5\sigma$, $n_j = 50$ (dashed line).

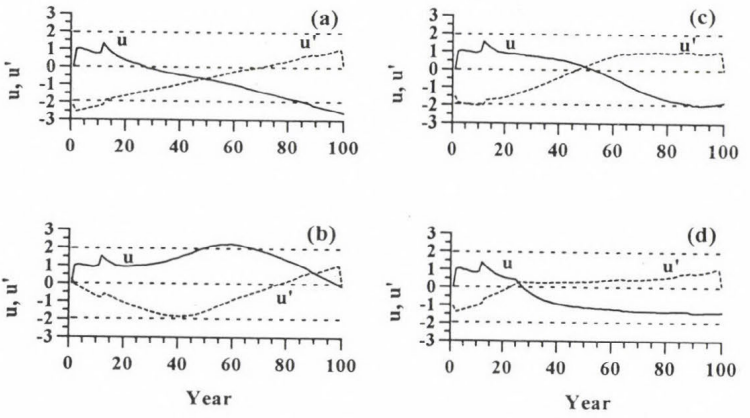

Fig. 2. Plots of the Mann-Kendall test for models of linear trend, changing trend, sine wave, and jump (u is the forward sequential statistic, u' is the backward sequential statistic). The 5% significance values are denoted. (*a*) linear trend, $\Delta_t = -\sigma$; (*b*) changing trend, $\Delta_c = \sigma$, $n_c = 50$; (*c*) sine wave, $\Delta_s = 0.75\sigma$; (*d*) jump, $\Delta_j = -0.5\sigma$ $n_j = 25$.

Graphical tests (except the t-test, which is based on $|t|$) indicate also the direction of the systematic change. A positive trend or jump ($\Delta_t, \Delta_j > 0$) results in negative values of $CS1$ and monotonic increase of $CS2$ and $u(t)$; the effect is the same for negative amplitude of the sine wave ($\Delta_s < 0$ means a decrease followed by an increase). An opposite (negative) direction of the change results in an opposite evolution of the test curves.

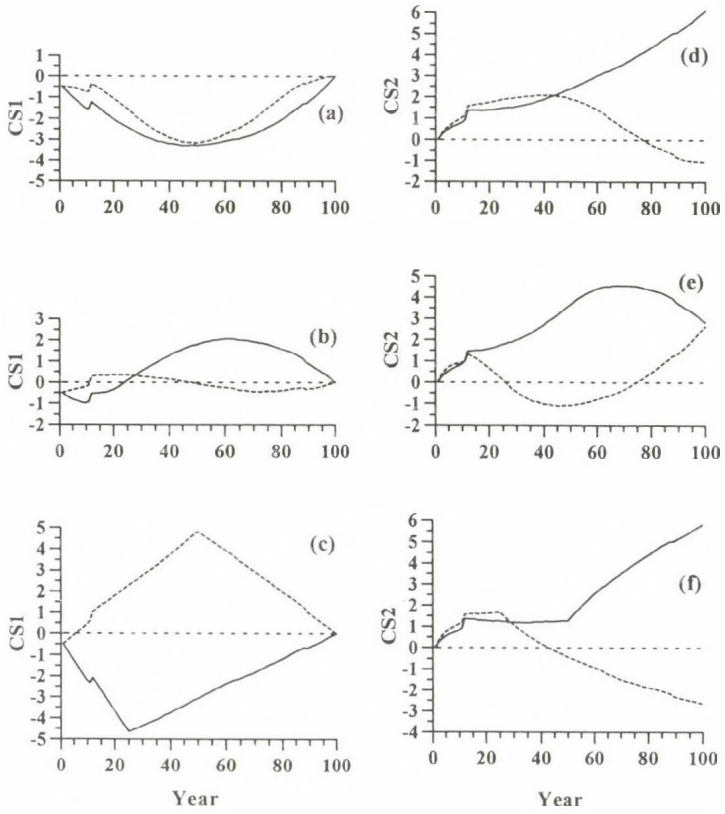

Fig. 3. Plots of cumulative deviations from the general mean ($CS1$) and from the current mean ($CS2$) for models of linear trend, changing trend, sine wave, and jump. (*a*) linear trend, $\Delta_t = \sigma$ (solid line) and sine wave, $\Delta_s = -0.75\sigma$ (dashed line); (*b*) changing trend, $\Delta_c = 0.75\sigma$, $n_c = 25$ (solid line) and $\Delta_c = -0.25\sigma$, $n_c = 50$ (dashed line); (*c*) jump, $\Delta_j = \sigma$, $n_j = 25$ (solid line) and $\Delta_j = -0.75\sigma$, $n_j = 50$ (dashed line); (*d*) linear trend, $\Delta_t = 0.75\sigma$ (solid line) and sine wave, $\Delta_s = 0.25\sigma$ (dashed line); (*e*) changing trend, $\Delta_c = 0.75\sigma$, $n_c = 50$ (solid line) and $\Delta_c = -\sigma$, $n_c = 25$ (dashed line); (*f*) jump, $\Delta_j = 0.5\sigma$, $n_j = 50$ (solid line) and $\Delta_j = -0.5\sigma$, $n_j = 25$ (dashed line).

The graphical tests applied to the combined models confirm the effects of mutual compensation or enhancement of certain systematic changes in the series. In *Fig. 4*, examples of the effect of compensation are given - in spite of the systematic changes, imposed on the series, the tests give indication of randomness. Yet it seems possible to detect the jump in some of these ideal smooth curves, this is not the case with the individual curves.

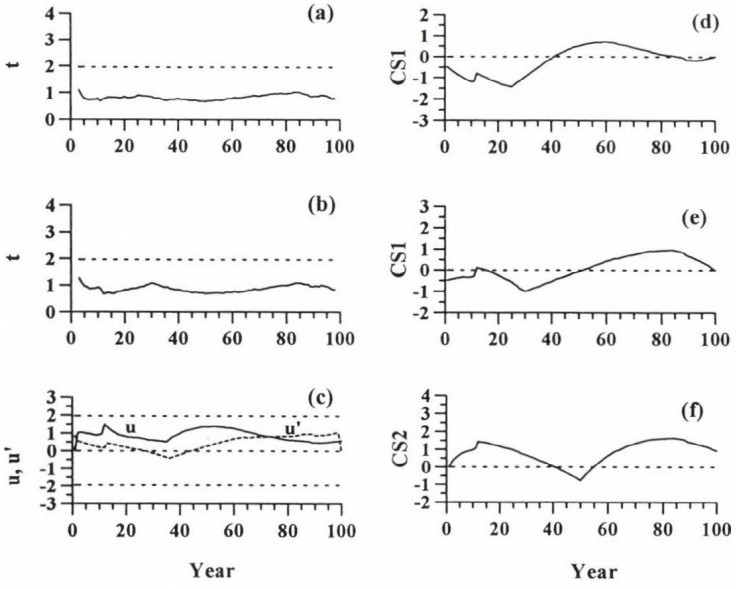

Fig. 4. Examples of the effect of compensation of different systematic changes imposed on the random series. (*a*) Student's *t*-test for the combination "jump+trend" with $\Delta_j = 0.5\sigma$ ($n_j = 50$), $\Delta_t = -\sigma$; (*b*) Student's *t*-test for the combination "jump+sine+trend" with $\Delta_j = 0.5\sigma$ ($n_j = 30$), $\Delta_s = -0.3\sigma$, $\Delta_t = -\sigma$; (*c*) Mann-Kendall test for the combination "jump+sine" with $\Delta_j = 0.5\sigma$ ($n_j = 35$), $\Delta_s = 0.5\sigma$; (*d*) *CS*1 for the combination "jump+sine" with $\Delta_j = 0.5\sigma$ ($n_j = 25$), $\Delta_s = 0.5\sigma$; (*e*) *CS*1 for the combination "jump+sine+trend" with $\Delta_j = 0.5\sigma$ ($n_j = 30$), $\Delta_s = -0.3\sigma$, $\Delta_t = -\sigma$; (*f*) CS2 for the combination "jump+trend" with $\Delta_j = \sigma$ ($n_j = 50$), $\Delta_t = -1.5\sigma$.

Although the results from different tests are similar, they are not completely identical. Here the results for the combination "jump+trend" with $\Delta_j = 0.5\sigma$ and $\Delta_t = -0.5\sigma$ are presented. All Buishand test statistics are below the critical values. Student's and Mann-Kendall test statistics (*Fig. 5*) are also within the critical limits. The curve *CS*1 also may be interpreted as an indication

of randomness (relatively small values around zero level). The plot of *CS*2-curve, however, indicates that the hypothesis of randomness cannot be accepted.

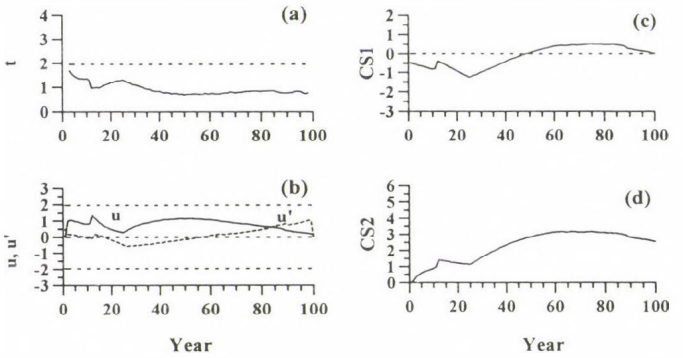

Fig. 5. Plots of the Student's *t*-test (*a*), Mann-Kendall test (*b*) and the cumulative deviations *CS*1 (*c*) and *CS*2 (*d*) for the combined modification "jump+trend" with $\Delta_j = 0.5\sigma$ ($n_j = 25$), $\Delta_t = -0.5\sigma$.

4. Example

As an example, an analysis of the time series of annual precipitation at Sofia (Bulgaria) is presented. Data are shown in *Fig. 6* and a smooth curve is added obtained by a 9-point Gaussian filter applied twice. The horizontal dashed line corresponds to the mean calculated from the reference period 1961–1990.

The selected station has longest regular observations in Bulgaria. It was set up on February 1, 1887 in the centre of the city in an area where a year

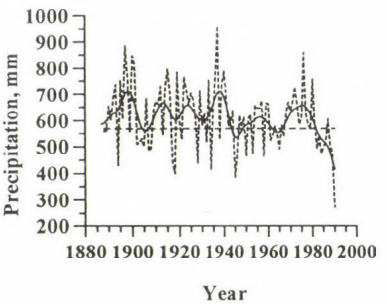

Fig. 6. Time series of annual precipitation at Sofia (Bulgaria). The smooth curve is obtained by 9-point Gaussian filter applied twice, the horizontal line corresponds to the mean value for the reference period 1961–1990.

later the Botanical Garden was established and was closed in 1992. The site and the type of the rain-gauge have not been changed. The period considered here is 1888–1990.

In *Fig. 6*, a definite tendency to a decrease can be noticed and a jump about 1940 may be suspected. The values of the test statistics are: $r_1 = 0.140$, $u_s = -1.76$, $U_r = 48$, $Q = 1.35$, $R = 1.44$, $U = 0.52$, $A = 3.25$. The corresponding critical values are $|r_1|_c = 0.193$, $|u_s|_c = 1.96$, $U_r = [41,62]$, $Q_c = 1.29$, $R_c = 1.62$, $U_c = 0.457$, $A_c = 2.48$, meaning that Buishand statistics Q, U, and A give an indication for some systematic changes.

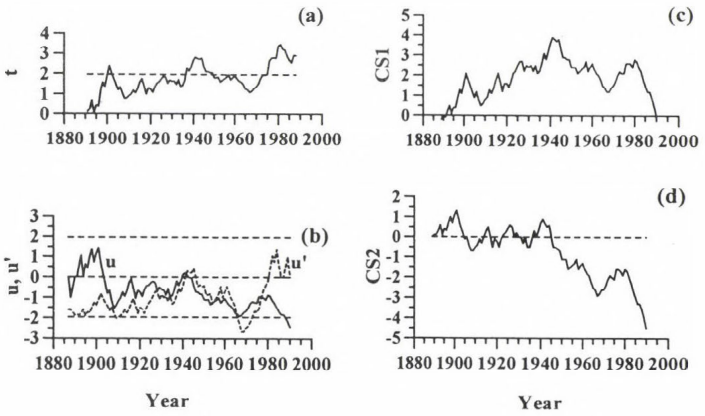

Fig. 7. Plots of the Student's *t*-test (*a*), Mann-Kendall test (*b*), and cumulative deviations *CS*1 (*c*) and *CS*2 (*d*) for the time series of annual precipitation at Sofia.

Graphical tests are presented in *Fig. 7*. The Student's *t*-statistic exceeds the critical value in three periods, maximums occur in 1900, 1940, and 1980. Each of them is localized about the midpoint of a period with sharp decrease in the series. The first and second periods may be regarded as transitions from a maximum to a minimum of a quasi-periodic oscillation. Maximums of the curve *CS*1 are localized at the same points, but the main one in this plot is in 1940. The curve *CS*2 also indicates a sharp change in 1940, after a period of random oscillations. In the plot representing Mann-Kendall test, the two curves intersect in 1940, but without exceeding the critical level as a result of the downward march of $u(t)$ (to the right) and $u'(t)$ (to the left). More "suspicious" is the intersection of the curves about 1980 indicating a new sharp decrease of precipitation. Comparing the results of these tests, one can see that the *t*-test and the Mann-Kendall test give priority to the change occurring in 1980, while the cumulative deviations give priority to the change in 1940.

Analyzing all the results, one may conclude that the series contains abrupt systematic changes. Considering, however, the station history, we may suppose that they are rather manifestations of climate instability than of inhomogeneities of observations. In order to check this assumption we should take into account some other available information. For instance, we can examine seasonal precipitation series and compare the results of different seasons to each other and to the results of the annual series. In case of inhomogeneity, the change of the level should occur at the same moment in all series, while in case of a climatic change, such coincidence may not be excluded but is not likely. Downward shifts around 1940 and 1980 in the annual series are detected in spring and summer series dominating the annual precipitation. The autumn and winter series, however, show different features. Downward shift in the autumn series takes place about 15 years earlier (in 1925), and the decrease after 1980 is followed by an increase after a short period. Winter precipitation exhibits an upward shift after 1925, the higher level is still persisting around and after 1940, and an upward trend can be seen around 1980. Therefore, it is reasonable to conclude that detected changes represent climate variability and are not a manifestation of inhomogeneity.

5. Summary and conclusions

Experiments with different tests for detecting inhomogeneity in climate time series are performed. In these experiments modifications with different forms and magnitudes are imposed on artificial normally distributed random series: trends (constant and changing), simple periodicity (sine wave), jump, and various combinations of jump plus another change. Results from following tests are discussed: the lag-1 serial correlation coefficient r_1, the Spearman rank correlation coefficient r_s, the run test U_r, the Buishand statistics Q, R, U, A, the Student's t-test in a serial version, the serial version of the Mann-Kendall test based on the evolution of the curves $u(t)$ and $u'(t)$, the cumulative deviations from the general mean (*CS*1) and current mean (*CS*2). The last two are applied to the rank expectations of the elements of the series. Conclusions are based on 100 times repeated experiments for each model and each magnitude of respective modifications, and are the following.

Buishand, Student, and Mann-Kendall statistics show almost equal sensitivity. The correlation coefficients and run test are less sensitive, i.e., they reach the critical values for greater magnitudes of the respective modification. This diminishes the risk of failure of the requirement for simple randomness of the series, which has to be satisfied for some tests for stability of the mean. If the magnitude of the change is not big enough, even the most

sensitive test statistics may fail to detect it, remaining within the critical limits (e.g., the "critical magnitude" in the case of a jump is about 0.5σ).

Identification of the form of the change may be obtained by means of the graphical tests. The jump causes a sharp change in the curve evolution – well manifested peak (t, $CS1$) or change of the slope ($u(t)$, $u'(t)$, $CS2$). In the case of a trend, the curve is flat (t, $CS1$) or monotonically increasing/decreasing with a smooth (gradual) change of the slope ($u(t)$, $u'(t)$, $CS2$). A (quasi)-periodicity may obtain a wrong interpretation, mostly as a jump indicated at the place of transition from the period of higher/lower than the average to the period of lower/higher than the average values.

Problems arise also in the cases of realistic combined modifications in the series, e.g., "jump + trend", "jump + periodicity", etc. In these cases, when the effect of the jump is enhanced by other changes, the jump can be easily detected. In such combinations the problem is when the effect of the jump is obscured by other modifications, and the tests give an indication of randomness. The most "promising" in these cases are the plots of the cumulative deviations of the type $CS2$.

When it is not possible to find suitable reference series (the situation considered here), as many tests should be used in the analysis as possible, and all reliable information should be taken into account. This information is also necessary to make a conclusion about the nature of certain modification revealed by the tests and minimize the risk to interpret a natural climate change as an artificial contamination of the series.

As an example, the tests are applied to annual precipitation series in Sofia (Bulgaria), and the results are discussed.

Acknowledgements—This work is supported by the Sofia University Science Foundation, Grant 3300/2000. The author wishes to thank the National Institute of Meteorology and Hydrology, Bulgaria, for providing the precipitation data, and *Prof. D. Syrakov* for the computer programs used in the work.

References

Alexandersson, H., 1986: A homogeneity test applied to precipitation data. *J. Climatol. 6*, 661-675.

Alexandersson, H. and *Moberg, A.*, 1997: Homogenization of Swedish temperature data. Part I: Homogeneity test for linear trends. *Int. J. Climatol. 17*, 25-34.

Alisov, B.P., *Drozdov, O.A.*, and *Rubinshtein, E.S.*, 1952: *Course on Climatology*. Part I, II (in Russian). Gidrometeoizdat, Leningrad, 487 pp.

Bol'shev, L.N. and *Smirnov, N.V.*, 1983: *Tables of Mathematical Statistics* (in Russian). Nauka, Moscow, 416 pp.

Brownlee, K.A., 1977: *Statistical Theory and Methodology in Science and Engineering* (Translated in Russian). Nauka, Moscow, 407 pp.

Buishand, T.A., 1982: Some methods for testing the homogeneity of rainfall records. *J. Hydrology 58*, 11-27.

Craddock, J.M., 1979: Methods of comparing annual rainfall records for climatic purposes. *Weather 34*, 332-346.

Davis, J.C., 1973. *Statistics and Data Analysis in Geology* (Translated in Russian, 1977). Mir, Moscow, 572 pp.

Easterling, D.R. and *Peterson, T.C.*, 1995: A new method for detecting undocumented discontinuities in climatological time series. *Int. J. Climatol. 15*, 369-377.

Goossens, Ch. and *Berger, A.*, 1986: Annual and seasonal climatic variations over the Northern Hemisphere and Europe during the last century. *Ann. Geophys. 4B (4)*, 385-400.

Hanssen-Bauer, I. and *Forland, E.J.*, 1994: Homogenizing long Norwegian precipitation series. *J. Climate 7*, 1001-1013.

Isaev, A.A., 1988: *Statistics in Meteorology and Climatology* (in Russian). Moscow University Press, 245 pp.

Karl, T.R. and *Williams, C.N. Jr.*, 1987: An approach to adjusting climatological time series for discontinuous inhomogeneity. *J. Climate Appl. Meteorol. 26*, 1744-1763.

Kobisheva, N.V. and *Narovlianskii, G.Ya.*, 1978: *Climatological Treatment of Meteorological Information* (in Russian). Gidrometeoizdat, Leningrad, 295 pp.

Lanzante, J.R., 1996: Resistant, robust and non-parametric techniques for the analysis of climate data: Theory and examples, including applications to historical radiosonde station data. *Int. J. Climatol. 16*, 1197-1226.

Mestre, O., 1998: Step-by-step procedures for choosing a model with change-points. *Proc. of the Second Seminar for Homogenization of Surface Climatological Data.* Budapest, Hungary, 9-13 Nov. 1998, 15-25.

Mitchell, J.M., 1966: Climatic Change. *WMO Technical Note 79*, WMO, Geneva, 79 pp.

Moberg, A. and *Alexandersson, H.*, 1997: Homogenization of Swedish temperature data. Part II: Homogenized gridded air temperature compared with a subset of global gridded air temperature since 1861. *Int. J. Climatol. 17*, 35-54.

Peterson, T.C. and *Easterling, D.R.*, 1994: Creating of homogeneous composite climatological reference series. *Int. J. Climatol. 14*, 671-679.

Pettitt, A.N., 1979: A non-parametric approach to the change-point problem. *Appl. Statistics 28*, 126-135.

Potter, K.W., 1981: Illustration of a new test for detecting a shift in mean in precipitation series. *Mon. Wea. Rev. 109*, 2040-2045.

Rhoades, D.A. and *Salinger, M.J.*, 1993: Adjustment of temperature and rainfall records for site changes. *Int. J. Climatol. 13*, 899-913.

Rozhdestvenskii, A.V. and *Chebotarev, A.I.*, 1974: *Statistical Methods in Hydrology* (in Russian). Gidrometeoizdat, Leningrad, 433 pp.

Rubinshtein, E.S., 1979: *Homogeneity of Meteorological Series in Time and Space in Connection with Climate Change Research* (in Russian). Gidrometeoizdat, Leningrad, 80 pp.

Sneyers, R., 1990: On the Statistical Analysis of Series of Observations. *WMO Technical Note 143*, 190 pp.

Sneyers, R., 1992: On the use of statistical analysis for the objective determination of climate change. *Meteorol. Zeitschrift, N.F. 1*, 247-256.

Sneyers, R., 1997: Climate chaotic instability: statistical determination and theoretical background. *Environmetrics 8*, 517-532.

Sneyers, R., Tuomenvirta, H., and *Heino, R.*, 1998: Observations inhomogeneities and detection of climate change. *Geophysica 34(3)*, 159-178.

Szentimrey, T., 1998: Multiple analysis of series for homogenization (MASH). *Proc. of the Second Seminar for Homogenization of Surface Climatological Data.* Budapest, Hungary, 9-13 Nov. 1998, 27-46.

Thom, H.C.S., 1966: Some Methods of Climatological Analysis. *WMO Technical Note 81*, 53 p.

Zhukovskii, E.E., Kiseleva, T.L., and *Mandel'shtam, S.M.*, 1976: *Statistical Analysis of Random Processes* (in Russian). Gidrometeoizdat, Leningrad, 407 pp.

Zwiers, F.W. and *von Storch, H.*, 1995: Taking serial correlation into account in tests of the mean. *J. Climate 8*, 336-351.

IDŐJÁRÁS

Quarterly Journal of the Hungarian Meteorological Service
Vol. 107, No. 1, January–March 2003, pp. 49–65

Preliminary results of high resolution sensitivity studies using the adjoint of the ALADIN mesoscale numerical weather prediction model

Cornel Soci[1], **András Horányi**[2], and **Claude Fischer**[3]

[1]*National Institute of Meteorology and Hidrology,*
97, Sos. Bucuresti-Ploiesti, 71552 Bucharest, Romania
E-mail: cornel.soci@meteo.inmh.ro
[2]*Hungarian Meteorological Service, P.O. Box 38, H-1525 Budapest, Hungary*
E-mail: horanyi.a@met.hu
[3]*Météo France, 42, Av. G. Coriolis, 31057 Toulouse Cedex 1, France*
E-mail: claude.fischer@meteo.fr

(Manuscript received February 6, 2002; in final form October 3, 2002)

Abstract—This paper reviews the theoretical background and practical implementation of adjoint computations in numerical weather prediction. In our study, the limited area model ALADIN has been used. Preliminary results obtained for meso-beta type of resolutions, focusing on a local domain inside Central Europe with an 8 km grid mesh are presented. The purpose is to obtain a closer match of a model forecast with a verifying analysis, as measured by a given cost function. To achieve this goal, gradients with respect to the initial conditions are computed; these gradient fields give the sensitivity of the forecast error cost function with respect to the initial conditions. Additionally, the impact on other features of the forecast, mainly precipitation, is also investigated. Two cases were selected, when the precipitation amounts were overestimated over the Pannonian Plains. Mesoscale sensitivities computed adiabatically or using different parameterization schemes are compared. Results from sensitivity experiments with respect to initial conditions show that the errors in initial data can, at least partially, be made responsible for the misforecast of precipitation quantities.

Key-words: limited area model, adjoint method, sensitivity studies, ALADIN.

1. Introduction

The quality of numerical weather forecasts produced by a limited area model is subject to several possible causes. Besides the weaknesses in the model formulation, the forecast could depend crucially on initial and lateral boundary conditions.

A common problem in numerical weather prediction models is the inaccuracy in the initial data. Experiments with forecast error sensitivity studies have revealed that errors in the initial data are most responsible for the quality of a forecast. As explained in *Le Dimet* and *Talagrand* (1986), the adjoint model allows efficient computation of the gradient of a forecast aspect of a numerical weather prediction model with respect to the initial conditions. Forecast aspect can be any model output. The gradient fields strongly suggest where to look for initial condition errors that may have a big effect in the consecutive forecasts. They also indicate what to expect from any small changes in the initial conditions that might be applied (*Errico*, 1997), provided that a linear type of evolution is sustained. In the last decade, several approaches to diagnose such errors have been proposed (*Errico* and *Vukićević,* 1992; *Rabier et al.*, 1996; *Gustafsson* and *Huang*, 1996). These studies mostly have addressed synoptic scale features predicted by global or large-sized limited area models.

Sensitivity analysis using the adjoint of the high resolution doubly-periodic primitive equation model ALADIN has been initiated by *Horányi* and *Joly* (1996). Using an adiabatic adjoint model, they studied the sensitivity of two idealised frontal waves. They showed that the steady fronts are associated with very strong amplifications of the fastest growing eigenvectors. In this article, features of mesoscale sensitivity for a selected case study are described. Sensitivities of forecast errors with respect to the initial conditions are computed and used as small perturbations added to the model dynamical fields for improving the 6 hours precipitation forecast.

With the present state-of-the-art knowledge, one may consider the adjoint approach not to be so beneficial because small scale meteorology is more dominated by non-linear processes such as saturation or boundary layer fluxes. However, the adjoint framework still remains a candidate for a dynamically consistent assimilation of high-frequency data, even if possibly restricted to time intervals much smaller than those employed for synoptic scale studies. At synoptic scale, 48 hours long windows are usual, in accordance with the typical time scale of baroclinic development. We stress that the developments of the adjoint tools in the ALADIN model give the opportunity to evaluate these ideas.

Although this article only presents preliminary results, for example ignoring moist diabatic processes in the adjoint computation, it shows that the ALADIN adjoint tools can provide answers for the previously raised questions. What is at stake in the long term is the evolution of the benefit of a 4D-VAR data assimilation at small scales.

The paper is organized as follows. Section 2 describes the mathematical basis for using an adjoint operator for sensitivity analysis. Section 3 deals

with the description of the steps needed for performing a sensitivity experiment. Results are presented in section 4 and concluding remarks follow in section 5.

2. *Methodology*

Let **x** define the model state vector. Typically, **x** is a set of three dimensional fields, namely u, v, T, q, which stand for zonal and meridional wind components, temperature, and specific humidity respectively, and a two dimensional field p_s, which is surface pressure. Depending on whether the model is spectral or finite-differences, the components of the state vector are spectral coefficients or values at all model grid points. A non-linear numerical weather prediction model, M, is a set of discretized primitive equations which approximate the processes of the real atmosphere. Hereafter, the non-linear model considered is ALADIN, a limited area spectral model (*Horányi et al.*, 1996). Since the non-linear model is discretized in time, formally, its evolution within a time interval, $[t_0, t]$, can be described by using a discrete equation

$$\mathbf{x}(t_{i+1}) = M\,[\mathbf{x}(t_i)], \tag{1}$$

where $\mathbf{x}(t_i)$ and $\mathbf{x}(t_{i+1})$ are the model vectors at time step i and $i+1$, respectively. Therefore, the final model state, $\mathbf{x}(t)$, is determined from the model initial state, $\mathbf{x}(t_0)$, by n successive steps.

In sensitivity computations, we are concerned about small perturbations, hereafter denoted $\delta\mathbf{x}(t)$. By definition, $\delta\mathbf{x}(t) = \mathbf{x}(t) - \bar{\mathbf{x}}(t)$, where $\bar{\mathbf{x}}(t)$ is an evolving basic state that we will specify as a solution to Eq. (1) given an initial condition $\bar{\mathbf{x}}(t_0)$, while $\mathbf{x}(t)$ is a perturbed non-linear solution that is initially close to $\bar{\mathbf{x}}(t)$. The perturbation of the model state, $\delta\mathbf{x}(t)$, is governed by the tangent linear equation which can be derived from Eq. (1) using first order Taylor expansion. Hence,

$$\delta\mathbf{x}(t_{i+1}) = \mathbf{M}\,\delta\mathbf{x}(t_i), \tag{2}$$

where $\mathbf{M}$ is the derivative of M with respect to $\mathbf{x}$ evaluated at $\bar{\mathbf{x}}(t)$. $\mathbf{M}$ is also called the tangent linear model (a more proper wording would be the propagator, see *Joly,* 1995), and it can be understood as the Jacobian matrix of M evaluated along the non-linear trajectory, $\bar{\mathbf{x}}(t)$. The tangent linear model describes the linearized evolution of errors or perturbations in a forecast model. It is obtained by the differentiation of the code of the direct model, M.

If M includes discontinuous functions, then some values of the Jacobian derivatives will not exist. This is, for instance, the case of some physical parameterization schemes, such as large scale precipitation or deep convection, which involve strong non-linear processes. In such a case, the strategy adopted for the tangent linear model is to simplify the parameterization scheme by neglecting some diabatic terms, while, at the same time remaining as close as possible to the physical parameterization scheme of the non-linear model (*Janisková et al.*, 1999).

Furthermore, we stress that in the ALADIN model, the treatment of lateral boundary conditions is presently done in a very crude way. Consistently, with the full, non-linear model, a Davies-type of coupling is retained (*Davies*, 1983). However, the tangent linear model, and the adjoint model as well, is coupled with zeroed perturbations along the lateral boundaries. This formulation forces to ignore any incoming perturbation (the flow is supposed to coincide with the reference trajectory). It also forces to forget about outgoing sensitivity information. Thus, such a treatment is sub-optimal for sensitivity studies, but it appears as a very convenient framework, especially when the focus is put on narrow time windows, where most of the sensitivity signal is kept inside the model domain, as will be the case here. At the same time, when using a high resolution model, the computational cost often forces to choose a small model domain, therefore the sensitivity study is performed in an experimental framework defined as a compromise between targeted small scale processes technically allowed and the computational cost.

Since $\mathbf{M}$ is a linear operator, it is possible to define its adjoint, denoted $\mathbf{M}^*$. It is defined such as for any two vectors, $\mathbf{y}$ and $\mathbf{z}$, in the phase space of the system, the following equality holds:

$$<\mathbf{y}, \mathbf{M}\,\mathbf{z}> = <\mathbf{M}^*\mathbf{y}, \mathbf{z}>, \tag{3}$$

where $<,>$ stands for the inner product. The adjoint operator is also linear, and for the discretized models it represents the transpose matrix, $\mathbf{M}^T$, of $\mathbf{M}$.

The adjoint model is constructed as the exact adjoint of the tangent linear model with the purpose of computation of phase space gradients. It is developed mainly for data assimilation applications and predictability, but it can be used also as a tool which relates the origin of numerical forecast errors to errors in initial data through sensitivity experiments. If a verifying analysis, denoted $\mathbf{x}^a(t)$, is available at time t, it is possible to compare the forecast with the analysis taken as an estimate of the true state of the atmosphere. The difference between the non-linear model solution, i.e., the forecast, and the verifying analysis is defined as the forecast error. This misfit can be quantified

by a diagnostic function, J, usually called forecast error cost function. Typically, J is a temporally weighted squared function which can be written as

$$J = \frac{1}{2} < \mathbf{x}(t) - \mathbf{x}^a(t), \mathbf{x}(t) - \mathbf{x}^a(t) > . \quad (4)$$

In our study the square norm $<,>$ is the so-called dry total energy. It is defined as

$$< \chi,\chi > = \frac{1}{2} \int_0^1 \int_\Sigma \left(u^2 + v^2 + \frac{C_p}{T_r} T^2 \right) d\Sigma \frac{\partial p}{\partial \eta} d\eta + \frac{1}{2} \int_\Sigma R_d T_r (\ln p_s)^2 d\Sigma . \quad (5)$$

In the definition of the norm, χ is the vector representing a *perturbation* of the atmospheric flow, the inner product being defined in the space of the perturbations. The weights given to its components are functions of the reference temperature, T_r, the specific heat of dry air at constant pressure, C_p, and the gas constant for dry air, R_d. $p(\eta)$ is the pressure at η levels, η being the vertical coordinate, 0 is the surface and 1 is the top of the atmosphere. Σ represents the horizontal integration domain, an area on which the diagnostic function is computed. Hereafter, this is referred as a target area. When using a target area, the input to the forecast error norm is set to zero outside, and only inner values are kept for further computations. This is important for the estimation of the origin of the initial forecast errors, because in such a way the obtained gradients are relevant only to the errors in that target area. The norm is called "dry" since there is no term involving specific humidity, q. Thus, there are no perturbations in the moisture field, which, at the end of the adjoint integration, could be considered as sensitivity of the forecast error cost function to the humidity field. The norm is also called "total" energy, since the first two terms of the right-hand side of Eq. (5) are kinetic energy and the third one is dry static energy. The fourth one is related to the surface pressure with weights chosen such that its dimension becomes energy.

In the adjoint computation, the goal is to determine $\nabla_{\mathbf{x}(t_0)} J$, that is the gradient of J with respect to the initial model state, $\mathbf{x}(t_0)$. To derive $\nabla_{\mathbf{x}(t_0)} J$, we begin by constructing δJ, that is the first order variation of the diagnostic function at the verification time. This is achieved by a given perturbation in the initial conditions, $\delta\mathbf{x}(t_0)$ which will lead to a perturbation $\delta\mathbf{x}(t)$ at the final time. Consequently, a small change, δJ, of the cost function J, can be written

$$\delta J = < \mathbf{M}^* [\mathbf{x}(t) - \mathbf{x}^a(t)], \delta\mathbf{x}(t_0) > . \quad (6)$$

By definition, the gradient of the forecast error cost function at time t_i, $t_0 \leq t_i \leq t$ is such that to first order approximation, $\delta J = < \nabla_{\mathbf{x}(t_i)} J , \delta \mathbf{x}(t_i) >$. Thus, using Eq. (6), the gradient of the forecast error cost function with respect to the initial conditions $\mathbf{x}(t_0)$ reads

$$\nabla_{\mathbf{x}(t_0)} J = \mathbf{M}^* [\mathbf{x}(t) - \mathbf{x}^a(t)], \tag{7}$$

where $\mathbf{M}^*$ is the adjoint of the tangent linear model. This is the basic relation used in sensitivity computations. The right-hand side term is computed by a backward integration of the adjoint model between times t and t_0.

The gradient of the forecast error cost function with respect to the initial conditions is used to generate perturbations to be added to the original initial data. An initial perturbation is a vector of the form $\delta \mathbf{x}_0 = -\alpha \nabla_{\mathbf{x}(t_0)} J$, where α is a scaling factor chosen by experimentation. As explained in *Rabier et al.* (1996), the gradient is dominated by the most unstable components of the analysis errors, because these are the directions along which the forecast error is likely to vary the most. They have shown that for large-scale flows and 48 hours time evolution, these fastest growing components can amplify by a factor of 10 to 15. Thus, the choice of an optimal α is carried out by successive tests such that the forecast errors are substantially reduced. However, the maximum value of the initial perturbation cannot exceed the magnitude of an observation error or that might naturally occur in the real atmosphere. In our experiments the value 1/10 for the scaling factor was chosen.

3. Design of the sensitivity experiments

Generally, a sequence for performing a sensitivity experiment proceeds through the following steps:

- A non-linear forecast is carried out using the full physical parameterization schemes as the operational version (hereafter denoted reference or control run), and started from the same initial model state, $\mathbf{x}(t_0)$. This step is necessary for creating the trajectory containing the model state fields $\mathbf{x}(t_i)$, $t_0 \leq t_i \leq t$, at every time step (in fact this integration is already known at the case selection stage, however, it is needed to be repeated for storing the trajectory). The backward adjoint integration is to be performed around this trajectory.
- At the verification time, t, that is the end of the direct non-linear model integration, the difference between the forecast, denoted by $\mathbf{x}(t)$, and the

valid analysis, $\mathbf{x}^a(t)$, is used for computing the quadratic forecast error cost function (as defined in Eq. (4)) and its gradient. Since for the time when ALADIN model does not have its own operational data assimilation cycle, in our study, the valid analysis refers to the operational ARPEGE analysis. ARPEGE is the global spectral numerical weather prediction model of Météo France (*Courtier et al.,* 1991). The ALADIN model is the high resolution limited-area version of the ARPEGE model.

- A backward integration of the adjoint model is carried out in order to provide an estimate of the gradient of the forecast error cost function with respect to the initial conditions. This integration is performed around the trajectory computed at the first step. Generally, an adjoint model can be either completely adiabatic or it can enfold linearized physical parameterization schemes. In our studies, two schemes simulating the surface drag and vertical transport of momentum due to turbulent exchange were enforced in alternation. The first one, developed by *Buizza* (1993) for a low resolution global model, is a reduced and very simple scheme, because it assumes constant mixing coefficients. A second and more complex one is a package of simplified physical parameterization schemes proposed by *Janisková et al.* (1999), based on the vertical diffusion equation with a first-order closure for the exchange coefficients. Although it contains simplified schemes for radiation and moist processes, this study exclusively concentrates on the use of its dissipative part, namely vertical diffusion and surface drag. This package was developed for a global model too. Thus, a direct comparison between the two schemes is made possible. Hereafter, the simple physics as defined by Buizza will be called "reduced" physics, while the "dissipative part of the physics" will refer to the vertical diffusion and gravity wave drag schemes from Janisková.

- The final stage is the so-called sensitivity forecast. This is carried out starting from modified initial conditions, $\mathbf{x}(t_0)+\delta\mathbf{x}_0$, $(\delta\mathbf{x}_0=-\alpha\ \nabla_{\mathbf{x}(t_0)}J)$, by a new non-linear model integration including exactly the same physical parameterization package as for the control run. In such a way, the vector $\delta\mathbf{x}_0$ is used to diagnose the effect of the errors in the initial data based on forecast errors.

4. Analysis of the results

The integration domain utilized in our sensitivity experiments was the operational ALADIN/HU (ALADIN Hungary) model version, which covers mostly the Central European area. ALADIN/HU is a double nested high reso-

lution model (200 × 144 points horizontally with 31 vertical levels, $\Delta x = 8$ km) embedded into ALADIN/LACE (Limited-Area modelling for Central Europe, 240 × 216 points horizontally with 31 vertical levels, $\Delta x = 12.2$ km), which at its turn is embedded in the global model ARPEGE. Since our intention was to use the dissipative part of the simplified parameterization scheme for the gradients computation, a triple nested model version (80 × 80 horizontal points and 31 vertical levels, $\Delta x = 8$ km) embedded into ALADIN/HU was created as a zoom over Hungary. This appeared as a strong necessity due to computer memory limitations. The problem arrives when a complex parameterization scheme is used, because an additional trajectory at $t-\Delta t$ has to be stored in the computer memory (Δt is the time step of the physics). This extra storage is needed, because the tendencies and fluxes are entirely computed from the variables at previous time step.

As an example of sensitivity analysis, we consider a summer case covering the period between 12–18 UTC, June 22, 2001. From synoptic point of view, at 12 UTC, this case study pertains to a frontal activity linked to a moving low, which at ground level was situated in the western part of Ukraine. This cyclone had a well defined correspondent in the altitude. For instance, at 500 hPa (not shown), it was centered in the western part of Poland (about 800 km to the west). Over Hungary, the low was rapidly advecting cold air originating from the North Sea. Thus, the rapid air flow was found to be associated to a westerly jet stream having a maximum wind speed of about 35 m/s.

This case was selected, because the 6 hours precipitation forecast was overestimated especially in the eastern part of Hungary, over the Great Hungarian Plain. Although, there was an important amount of precipitation forecasted in the western part of the country, we are not concerned with this area due to the proximity of the Alpine region.

The operational numerical precipitation forecast is shown in *Fig. 1a*. A zoom over the region of main interest, i.e., the target area, in the south-eastern part of Hungary is presented in *Fig. 1b*. One can see that 16 mm/6h precipitation have been predicted whereas in that region a maximum of 2 mm/6h was reported by rain-gauge stations (not shown). The problem of such misforecasted precipitation should be seen as a complex one, where errors in initial conditions (e.g., analysis of humidity field, wind shears, or temperature gradients), or in lateral boundary conditions or model errors due to weaknesses in the formulation of the model physics and dynamics play an important role. However, in our study, we concentrate exclusively on the initial condition problem. We try to assess and correct the initial fields with the adjoint method, by focusing mainly on the dynamical processes at mesoscale.

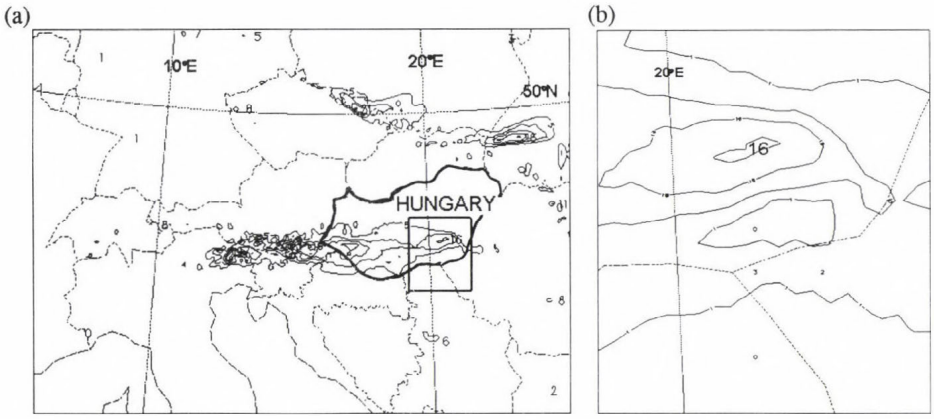

Fig. 1. (*a*) Field of 6 hours reference precipitation forecast over the ALADIN/HU domain. Contour intervals are at every 5 mm/6h. (*b*) Reference 6 hours precipitation field zoomed over the region of interest, i.e., south-eastern part of Hungary. Contour values are 1, 5, 10, and 15, respectively with units mm/6h.

Sensitivity experiments were carried out for 6 hours integration within the period mentioned above. The difference between the 6h forecast and the corresponding verification analysis was used to feed the adjoint model integration with the input gradient of the forecast error cost function. In order to isolate the origin of the forecast error of the misforecasted precipitation field in the eastern part of Hungary, the forecast error norm was computed over a target area inside the model integration domain. This subdomain is shown in *Fig. 1a*. This target area was subjectively chosen after analyzing the forecast error fields at +6h. In *Fig. 2a*, 500 hPa zonal wind speed difference between the control and verifying analysis is illustrated. It is revealed that already after 6 hours, the non-linear model underestimates by about 18 m/s the zonal wind speed in the area of interest. At the same time (as presented in *Fig. 2b*), the temperature difference is about 1.5 K indicating a warmer forecast, than the reality.

At the end of the adjoint integration, the retrieved initial sensitivity includes only the signal of main concern. *Fig. 3* illustrates the evolution of the gradients of the forecast error cost function with respect to zonal wind, $\nabla_U J$, on model level 20 (about 500 hPa), during an adjoint integration performed from +6h to +0h. One may see, how at the beginning of the adjoint integration (*Fig. 3a*) the initial gradient inside the target area is projected onto the integration domain. Further on, the gradient develops and is advected westward, upstream of the winds that tend to advect the perturbation eastward. At +4h (*Fig. 3b*), the sensitivity field was advected westward and located in

the middle of the domain, while at +2h, the gradient has already reached the western boundary of the integration area (*Fig. 3c*). For higher levels, one may anticipate that the gradient passes the border earlier, since its structure is characterized by a typical baroclinic tilt in the vertical. At the end of the adjoint backward integration, the gradient is concentrated near the western border of the domain (*Fig. 3d*).

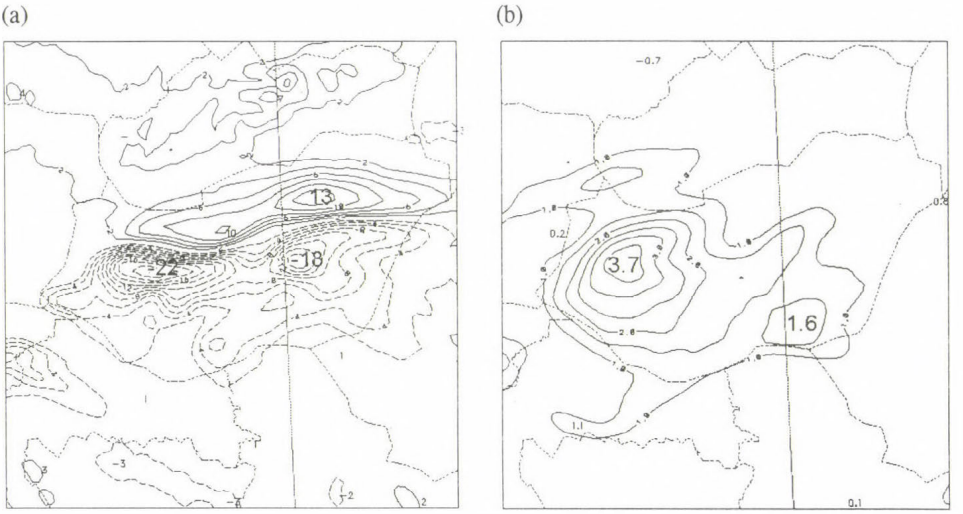

Fig. 2. (*a*) 500 hPa zonal wind difference between the +6 hours reference forecast and the verifying analysis valid at 18 UTC June 22, 2001. Contour intervals are at every 2 m/s. Positive (negative) value contours are continuous (dashed), and zero-valued contours are omitted. (*b*) As in Fig. 2a, except for the temperature. Contour intervals are at every 0.5 K. (Contour for values less than 1 K were omitted.)

In order to study the impact of the dynamics and physics in the sensitivity computation, a set of experiments has been performed using mainly the ALADIN/HU domain. Results from three different adjoint configurations have been compared. In the first run, the gradients have been computed adiabatically, without any physical process simulation, while in the second run, the reduced physics were used. The third run with the dissipative part of the simplified physical parameterization was carried out using the small integration domain.

Let us first analyze the results of the adjoint integration performed with adiabatic and reduced physics. *Figs. 4a–c* illustrate the gradients of the forecast error cost function with respect to the temperature, $\nabla_T J$, on the model level 29 (about 200 m). The figures are zoomed over Hungary

covering the same area as the small domain. The primary qualitative difference between panels (a) and (b) is that in *Fig. 4a* the gradients have larger values and look noisier than in *Fig. 4b*. The difference comes from the fact that the gradients plotted in *Fig. 4a* were computed with an adiabatic adjoint model, whereas in *Fig. 4b* the computation was performed with reduced physics.

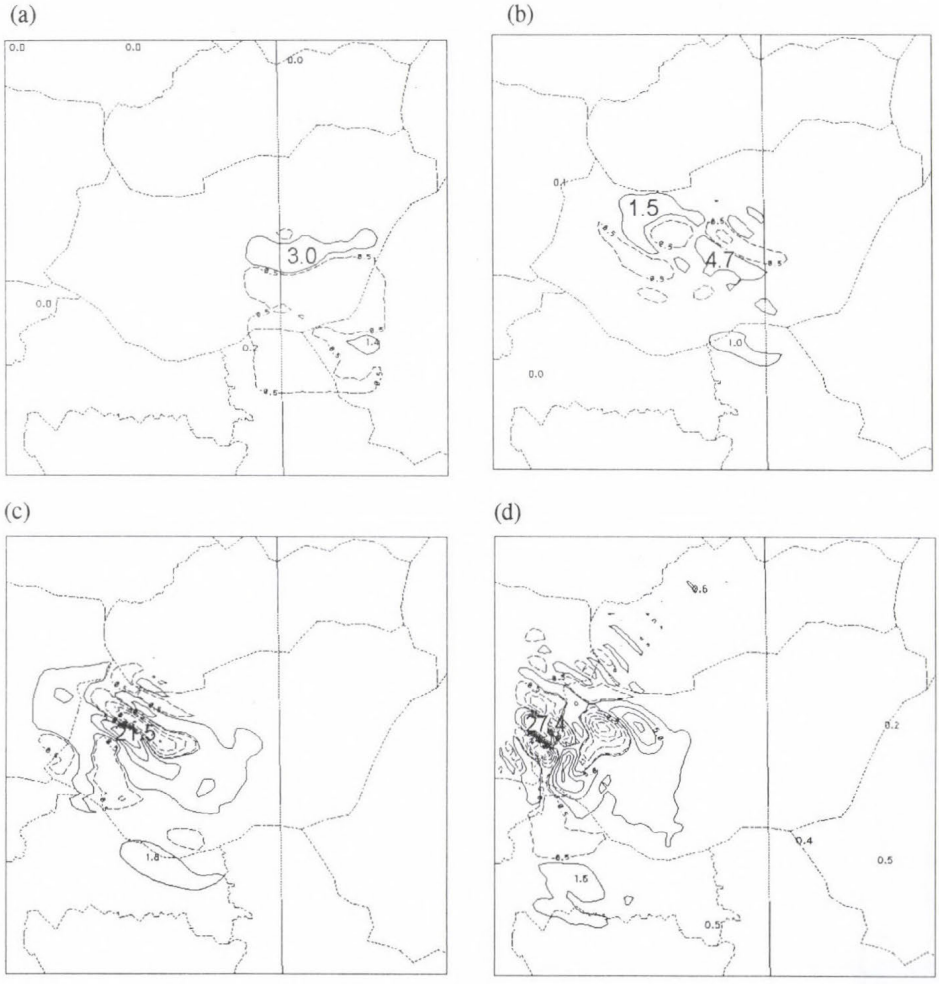

Fig. 3. Evolution of the gradients of the forecast error cost function with respect to zonal wind, $\nabla_U J$, on model level 20: (*a*) at the beginning of the backward adjoint integration, +6 hours; (*b*) +4 hours; (*c*) +2 hours; and (*d*) at +0 hours. Contour intervals are at every 4 Js/m for absolute values greater or equal to 4 Js/m. Contours are shown for absolute values less than 4 with intervals of 0.5 Js/m. Positive (negative) value contours are continuous (dashed), zero-valued contours are omitted.

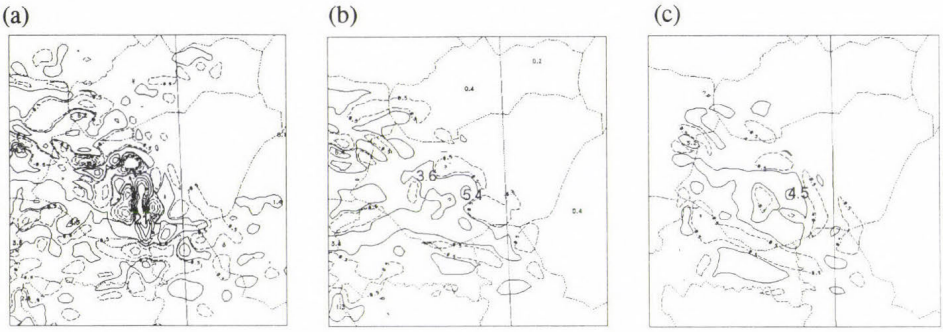

Fig. 4. Gradients of the forecast error cost function with respect to temperature, $\nabla_T J$, on model level 29 computed (*a*) adiabatically, (*b*) with reduced physics and (*c*) with the dissipative part of the simplified physical parameterization. Contour intervals are at every 5 J/K for absolute values greater or equal to 5 J/K except for the first contour plotted for absolute values equal to 0.5 J/K. Positive (negative) value contours are continuous (dashed); zero-valued contours are omitted.

In the latter case, the gradient field is one order of magnitude weaker than the adiabatic gradients. The gradients derived with the adiabatic adjoint model are not realistic in the sense that they contain non-meteorological fast growing structures confined only to the first model levels. Their time evolution must be similar to an error field evolution, and this is more realistically described when using reduced physics. It is known, that in the absence of any planetary boundary layer parameterization, the adiabatic model develops strong wind anomalies near the surface due to the lack of friction (*Buizza*, 1993). The importance of the physical description of the processes in the planetary boundary layer is highlighted by the results derived using the dissipative part of simplified physics as shown in *Fig. 4c*. Examination of *Fig. 4c* points out that the magnitude of the gradient has the same order than with reduced physics.

The sensitivity forecasts were performed using initial data perturbations following the procedure described in the previous section. The gradients of the forecast error cost function, computed adiabatically with reduced physics and dissipative part of the simplified physics, were normalized with a scaling factor $\alpha=0.1$ and added to the initial conditions. In this way, three new initial model states have been created, a priori each of them being "better" than the original one. The results of the sensitivity forecasts are presented in *Figs. 5a–c*. If compared with *Fig. 1b*, the general feature is that all sensitivity forecasts have improved the precipitation forecast. The introduction of a scaled gradient of the forecast error in the initial conditions has led to the reduction of the 6 hours precipitation amount with a maximum of about 7 mm in the case when the dissipative scheme has been used (*Fig. 5c*).

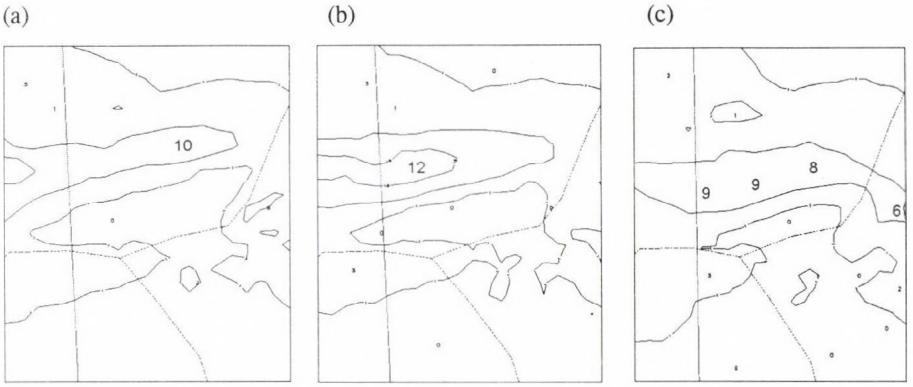

Fig. 5. Sensitivity precipitation forecasts – zoomed over the region of interest (target area) – performed starting from modified initial conditions with scaled gradients computed (*a*) adiabatically, (*b*) with reduced physics, and (*c*) with the dissipative part of the simplified physical parameterization. Contour values are 1, 5, and 10, respectively, with units mm/6h.

In *Figs. 5a* and *5b*, the precipitation fields from the sensitivity forecast run with the scaled gradients computed adiabatically, and with reduced physics, respectively, have been plotted. Surprisingly, the scaled gradients computed adiabatically have corrected the precipitation field as well (*Fig. 5a*). However, the perturbations introduced in the initial temperature field are relatively large in the first model levels. For example, at model level 29, the maximum value of the perturbation added was 3.5 K, while when gradients were computed with reduced physics, the magnitude was –0.6 K. For comparison, at the same level, when the gradients were calculated using dissipative physics, the maximum value of the perturbation was –0.5 K. These corrections of the initial dynamical model fields lead to a better match of the forecast with the verifying analysis. For example, *Figs. 6a–b* shows the difference of 500 hPa zonal wind and temperature, between the modified 6h forecast and verifying analysis. This experiment was run using the gradient computed with the reduced physics. Results obtained with the adiabatic adjoint model were very similar (not shown). *Fig. 6* has to be compared with *Fig. 2*. It can be seen that, in absolute values, the 500 hPa zonal wind difference between the sensitivity forecast and analysis has diminished by 2 m/s in the area of main concern, and by 4 m/s in the western part of Hungary. For other levels (not shown), it was noticed that the whole vertical structure of the wind field was changed. To be specific, there is a significant decrease of the vertical wind shear. Since this vertical shear is one crucial element to trigger convection,

this modification can at least partially explain the reduction of the activity of the system. Furthermore, the temperature has decreased as illustrated in *Fig. 6b*.

Since no moist parameterization was used in the adjoint model, the adjoint computation can be considered as dry. However, the correction of the precipitation field was substantial, so we do believe that, for this case, the evolution of the physical processes were partially driven by the dynamical forcing of precipitation.

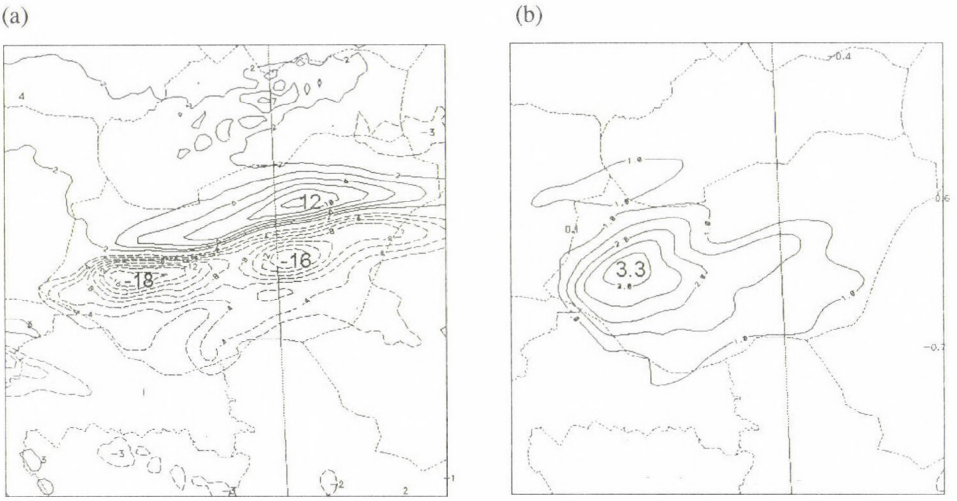

Fig. 6. (*a*) 500 hPa zonal wind difference between the +6 hours reference forecast and the verifying analysis valid at 18 UTC June 22, 2001. Contour intervals are at every 2 m/s. Positive (negative) value contours are continuous (dashed), and zero-valued contours are omitted. The sensitivity was computed with the adjoint model with reduced physics (*Buizza,* 1993). (*b*) As in Fig. 6a, except for the temperature. Contour intervals are at every 0.5 K. (Contour for values less than 1 K were omitted.)

5. Concluding remarks

In this paper, the adjoint model has served as a tool for calculating the sensitivity of 6 hours forecast errors to the initial conditions as measured by a dry total energy norm.

After describing briefly the mathematical basis of the adjoint method, results obtained for sensitivity experiments were presented. Special attention was devoted to the use of linearized physics such as vertical diffusion and surface drag during the adjoint integration.

The gradients computed with an adiabatic adjoint model, without any vertical diffusion and surface drag applied to the momentum equation, produce non-meteorological structures in the lowest model levels. For a 6 hours adjoint integration, their values can be one order of magnitude greater than if dissipative processes are taken into account. Including vertical diffusion and surface drag, the gradients are realistically improved.

In this study, when using the small domain, the sensitivity fields were located in the proximity of the western lateral boundary. This suggests the necessity of a larger integration domain, which may allow the enlargement of the sensitive area.

When computing mesoscale sensitivities using a high resolution adjoint model, their 6 hours amplification rate have the same order of magnitude as for the large scale gradients calculated by a low resolution adjoint model for larger time ranges (*Gustafsson* and *Huang*, 1996; *Rabier et al.,* 1996). This is why a scaling factor, $\alpha=0.1$, has proved to be optimal for the June 22, 2001 case study. Thus, it may suggest that there are mesoscale situations in which errors in the initial conditions may grow faster for a high resolution limited area model than for a low resolution one. For one selected case study, the sensitivity integration substantially improved the 6 hours precipitation forecast. However, this result should be carefully interpreted. Yet it does not allow to claim, that using a dry energy norm and a simplified physical parameterization without moist diabatic processes in the sensitivity computation, will always lead to a dramatic improvement of the precipitation field. Indeed, in other cases, the initial state modification based on dry gradients did not produce equivalently "desired" corrections in precipitation. An example is presented in *Fig. 7*, where the difference between the operational and sensitivity precipitation forecasts was plotted. This is a spring case, covering the period between 00–06 UTC, March 5, 2001, which was selected due to the fact that the operational precipitation forecast was overestimated by about 20 mm/6h. As one may see in *Fig. 7a*, the sensitivity forecast performed starting from the "improved" initial conditions (gradients computed with reduced physics and $\alpha=0.1$) was rather neutral, since the amount of precipitation was slightly increased by about 1 mm/6h in the area of main interest, i.e., the centre of the domain. For bigger α, the sensitivity precipitation forecast shows a degradation, when compared to the operational one (*Fig. 7b*), while for smaller values the gradient is negligible. Similar results were obtained using gradients computed adiabatically or with dissipative physics. Hence, the forecast failure cannot be attributed to errors in the initial conditions, but it has to be explained by some other reasons.

It is very likely that the good result obtained in the summer case is due to the fact, that the sensitive area was mainly over the Alps, a data-sparse

region, especially for vertical soundings. In this respect, however, detailed studies are to be performed with the goal of a better understanding of mesoscale gradients.

This study is understood as a first step for the evaluation of the benefit of adjoint computations in the frame of small scale and mesoscale numerical weather prediction. Indeed, while the adjoint approach (and the associated 4D-VAR assimilation) has been very successful for the representation of synoptic and sub-synoptic atmospheric flows, much needs to be done to evaluate its potential at smaller scales. The main interest then lies in the description of the humidity distribution inside a frontal system, or fine vertical profiles of all atmospheric fields to capture the boundary layer, capping inversions, convective areas, or inertia-gravity waves.

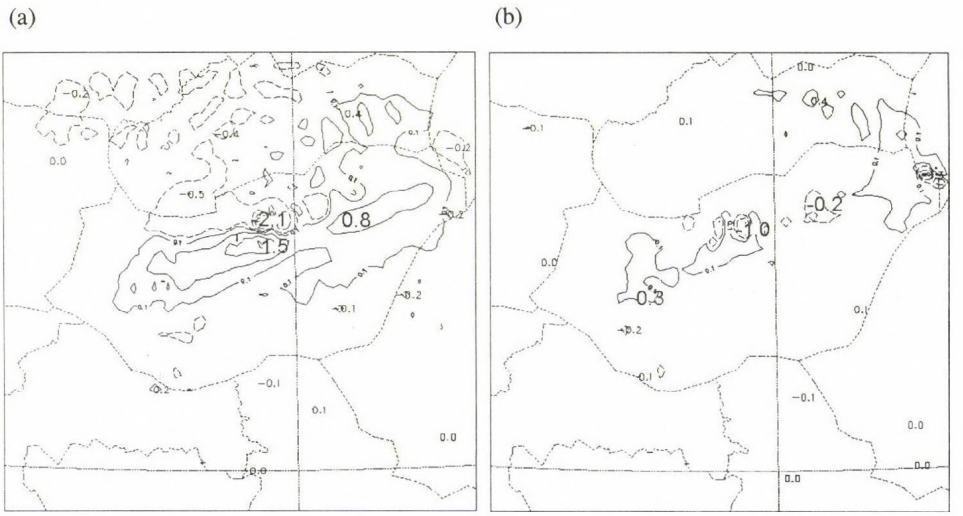

Fig. 7. (*a*) Difference between the 6 hours operational and sensitivity precipitation forecasts (valid at 06 UTC, March 5, 2001). Positive (negative) value contours are continuous (dashed), and zero-valued contours are omitted. The sensitivity was computed with the adjoint model with reduced physics. Contour values are 0.1, 0.5, 1, and 1.5, respectively, with units mm/6h. (*b*) As in Fig. 7a, except for α=0.75.

In the future work on sensitivity analysis, we will concentrate on the computation of the gradients of the forecast errors to the initial conditions by including the moist parameterization schemes in the ALADIN adjoint model. These moist linearized schemes will be useful for extracting meaningful sensitivity over the regions, where the evolution of the atmospheric flow is not only dictated by dynamical instability but also by strong local humid processes.

Acknowledgements—We thank Météo France and Hungarian Meteorological Service for scientific and technical support. This work was made possible thanks to ALATNET Grant HPRN-CT-2000-00057. ALATNET is supported by the TMR/IHP Programme of the European Community, but the information provided here is the sole responsibility of the ALATNET team and does not reflect the Community's opinion. The Community is not responsible for any use that might be made of data appearing here. *C. Soci* was on leave from the NIMH, Bucharest. ALADIN is an international NWP project (with presently 15 partner countries). We are grateful to all colleagues from the partner institutes who have contributed to maintain and develop the numerical tools used in this study. Also, we are grateful to the anonymous reviewers for their useful comments and suggestions, which resulted in a significant improvement of the paper.

References

Buizza, R., 1993: Impact of a simple vertical diffusion scheme and of the optimisation time interval on optimal unstable structures. *ECMWF Tech. Memo.* 192, 25 pp.

Courtier, Ph., Freydier, C., Geleyn, J-F., Rabier, F., and *Rochas, M.*, 1991: The ARPEGE project at Météo France. *ECMWF Seminar Proceeding, Reading*, Vol. II, 193-231.

Davies, H.C., 1983: Limitation of some common lateral boundary schemes used in NWP models. *Mon. Wea. Rev. 111*, 1002-1012.

Errico, R., 1997: What is an adjoint model ? *Bull. Amer. Meteor. Soc. 78*, 2577-2591.

Errico, R. and *Vukicevic, T.*, 1992: Sensitivity analysis using an adjoint of the PSU-NCAR mesoscale model. *Mon. Wea. Rev. 120*, 1644-1660.

Gustafsson, N. and *Huang, X.-Y.*, 1996: Sensitivity experiments with the spectral HIRLAM and its adjoint. *Tellus*, 48A, 501-517.

Horányi, A. and *Joly, A.*, 1996: Some aspects of the sensitivity of idealised frontal waves. *Beitr.Phys.Atmosph. 69*, 517-533.

Horányi, A., Ihász, I., and *Radnóti, G.*, 1996: ARPEGE/ALADIN: A numerical weather prediction model for Central-Europe with the participation of the Hungarian Meteorological Service. *Időjárás 100*, 277-301.

Janisková, M., Thépaut, J-N., and *Geleyn, J-F.*, 1999: Simplified and regular physical parametrizations for incremental four-dimensional variational assimilation. *Mon. Wea. Rev. 127*, 26-45.

Joly, A., 1995: The stability of steady fronts and the adjoint method: nonmodal frontal waves. *J. Atmos. Sci. 52*, 3081-3108.

Le Dimet, F-X. and *Talagrand, O.*, 1986: Variational algorithms for analysis and assimilation of meteorological observations: theoretical aspects. *Tellus 38*A, 97-110.

Rabier, F., Klinker, E., Courtier, Ph., and *Hollingsworth, A.*, 1996: Sensitivity of forecast errors to the initial conditions. *Quart. J. Roy. Meteor. Soc. 122*, 121-150.

IDŐJÁRÁS

Quarterly Journal of the Hungarian Meteorological Service
Vol. 107, No. 1, January–March 2003, pp. 67–83

Mesoscale atmospheric vortex generation over the Adriatic Sea

Branka Ivančan-Picek and **Vesna Jurčec**

Meteorological and Hydrological Service of Croatia,
Grič 3, 10000 Zagreb, Croatia; E-mail: picek@cirus.dhz.hr

(Manuscript received January 17, 2002; in final form July 3, 2002)

Astract—Circumstances under which the Adriatic mesoscale vortex was generated at the end of March, 1995 is investigated. Assuming that a mesoscale vortex can be isolated from the synoptic environment, the scale separation technique is employed. This provides the mesoscale orographic disturbances with characteristic quasi-antisymmetric dipolar structure across the Dinaric Alps. The mesoscale wind field contains a pronounced ageostrophic component with small-scale vortices of short duration and clearly marked convergence zones. Hence, the cyclonic vortex was generated over the middle Adriatic in a macroscale wind field as defined here, in which the smaller scale instabilities, as noise, are filtered out during the procedure. A very persistent mesoscale anticyclonic vortex is found in Pannonian Plain following the northerly flow around the eastern flank of Alps. This flow is responsible for the bora occurrence, but it also contributes to the Adriatic circulation, in which jugo wind in the southern and bora in the northern Adriatic lead to the vortex generation examined.

Key-words: mesoscale vortex, scale separation technique, bora, jugo, orographic pressure dipole.

1. Introduction

In recent years, mesoscale meteorology, and especially the orographic influence on mesoscale circulations and frontal deformations have received increasing attention of the scientific world. Many investigations in the Alpine area were motivated by the significant gap between very sophisticated high-resolution mesoscale models and poorly observed complex phenomena at the sea level. To provide datasets for the validation and improvement of high-resolution numerical weather prediction in mountainous terrain was one of the

main objectives of the MAP – Mesoscale Alpine Programm (*Binder* and *Schär*, 1996).

Vortex generation was observed in the western Mediterranean by *Gomis et al.* (1990) considering the composition of several lee cyclogeneses that occurred during the ALPEX SOP. Applying the scale separation method to 850 hPa level data, they isolated the subsynoptic/meso-β features from the "undisturbed" state characterizing the larger scale structure of this phenomenon. Vortices over the Adriatic Sea appeared in numerical simulation, but had never been shown by objective analysis with real surface data.

Jurčec et al. (1996) employed the same method using *the sea level observational data* in order to separate mesoscale features in the Adriatic area from the synoptic fields characterized by a cyclone in the gulf of Genoa and strong jugo wind over the Adriatic Sea. The complex structure of the mesoscale Adriatic fields with pronounced ageostrophic flow was clearly indicated, suggesting the need for further studies of this problem under different larger scale circumstances.

Our present study is dealing with objective analysis of two cases of Adriatic vortex generation at the end of March, 1995 marked by extremely strong bora wind. It was studied earlier by *Tafferner* (1995), *Brzović* and *Jurčec* (1997), *Ivančan-Picek* (1997), and *Brzović* (1999). The analyses include all available data in the Adriatic coast and islands in addition to ordinary synoptic data, aiming to separate the subsynoptic/meso-β scale features from the larger scale structures, using scale separation technique with known spatial filtering properties. We concentrate mainly on the wind field and search for cyclonic and anticyclonic vortices over the Adriatic Sea and surroundings.

Section 2 describes the Adriatic characteristics of cyclones (including low level shallow depressions by orography and thermal contrasts) and local winds, section 3 gives a synoptic overview, section 4 describes the scale separation, section 5 contains the results of macro- and mesoscale fields over the Adriatic area, and section 6 summarizes the conclusions.

2. Adriatic cyclones and wind characteristics

The Mediterranean area presents the highest concentration of real cyclogenesis (including low level shallow depressions by orography and thermal contrasts) in the world. The most famous is the Genoa cyclogenesis (*Buzzi* and *Tibaldi*, 1978). Nevertheless, there are other areas with quite frequent true cyclogenesis. One is located in the Adriatic (*Ivančan-Picek*, 1997). Mediterranean local winds (including Adriatic bora and jugo) can be seen as the results of the orographic mesoscale pressure perturbation induced by the

flow/mountain interaction. High and low pressure centres of the orographic disturbance (and/or the orographic pressure dipole as a whole) create local areas of strong pressure gradient, that provide intense local acceleration, leading to local wind generation (*Campins et al.*, 1995). The synergistic combination of intense cyclone and local wind generation can explain of the extreme violence of some of the strong wind events. Synoptic and local weather characteristics during the bora and jugo episodes are discussed in several studies, (e.g., *Ivančan-Picek* and *Tutiš*, 1996; *Jurčec et al.*, 1996, and references therein). However, there is an evidence of relationship between bora, jugo, and a cyclone in the Adriatic.

The obvious constraint on the spatial scales of an atmospheric system is the geometry of its boundaries. The Adriatic Sea is about 200 km wide and surrounded by the Alps on the north, Dinaric Alps on the eastern coast of Croatia, and the Apennines on the west in central Italy. Orographic effects are therefore essential for the Adriatic systems, particularly cyclones and wind characteristics. Northern Adriatic is frequently exposed to Alpine lee cyclogenesis. These cyclones move southeast along the Adriatic Sea, and usually deepen extending throughout the troposphere in the southern Adriatic. The first mesoscale numerical experiment in the Adriatic area, using the high-resolution ALADIN model, was performed by *Brzović* (1999) indicating the decisive role played by the Dinaric Alps on the maintenance of Adriatic cyclones and wind systems. Jugo (*jug* means *south* in Croatian), the strong southerly, warm, and humid wind appears ahead of the Adriatic cyclones or frontal zones, while the northeasterly cold bora wind is behind them.

Until recently, jugo was considered as a part of the sirocco wind family, which has the origin in the southern Mediterranean and northern Africa, characterized by dry and dusty air from the Sahara. Crossing the Mediterranean, the air picks up moisture, and reaching southern Italy it looses its force and energy, becoming a hot and humid wind (*Huschke*, 1959). However, jugo on the contrary could be very severe reaching the maximum speed over 40 m/s. Statistics and many case studies (*Jurčec et al.*, 1996) have indicated that jugo is associated mainly with Alpine lee cyclogenesis on synoptic scale in the western Mediterranean, whereas in the Adriatic Sea, subsynoptic scale analyses established the connection of jugo with mesoscale cyclones and fronts. Thus, jugo does not belong to the sirocco wind system, although, there may be some special cases of very strong southerly current ahead of the Mediterranean cyclone, which may bring a relatively dry air from the Sahara to the Adriatic area.

The best-known severe wind in the Adriatic area is the northeasterly bora wind, which is a down slope cold and gusty wind of the eastern Adriatic coast.

Until the ALPEX program in 1982, it was defined as a "falling wind", which accelerates as it moves down slope due to its low temperature and greater density. Results of the first aircraft observations of the bora in Croatia accomplished during the ALPEX project did not verify this popular idea of the bora as falling wind, since the aircraft measurements indicated an upstream acceleration too, which begins where the mountains begin to rise. This is explained by the conservation of mass flow between the rising terrain and descending isentropes toward the warm Adriatic Sea, which requires flow acceleration upstream from the mountaintop. From this analysis *Smith* (1987) introduced the internal hydraulic mechanism as a mathematical description of bora features.

For the ALPEX SOP (March–April 1982), the pressure drag exerted by the Dinaric Alps was evaluated by *Tutiš* and *Ivančan-Picek* (1991), *Ivančan-Picek* and *Tutiš* (1995), using data from mesoscale array of microbarographic stations. The pressure drag maxima were always connected with bora periods. In these cases we may compare the Dinaric Alps to the Alpine region in the drag value magnitudes. The orographic pressure dipole is a key phenomenon for the organization and intensification of the local bora wind. The pressure difference between the upstream and downstream regions during the bora periods can be greater than 10 hPa/50 km.

In our case study, we will describe some of these features in section 3. More details on this subject are presented by *Jurčec* and *Brzović* (1995, and references there), and a general description of the winds in the Adriatic area is given by *Poje* (1992).

3. Synoptic overview of the case study

Circumstances, under which the Adriatic mesoscale vortex is generated at the end of March 1995 are investigated. In a relatively short time period (March 28–30, 1995), two cold air outbreaks propagated towards Croatia, and resulted in two cyclogeneses over the northern Adriatic Sea. Abundant rain and snowfall were recorded over many parts of Croatia including Dalmatia, which is an extraordinary event for the last days of March. This situation has been chosen as an exceptional case of cold air outbreak over the Alps, which caused one of the strongest bora storms registered in the coastal region of Croatia.

The essential feature of this case study is a deep low in the Baltic area influencing the development in the Alpine region. On the first day, March 27, this low of 975 hPa was in southern Sweden with another center of the same intensity over the Barents Sea. These two lows, extending to the low troposphere, intensified the northerly flow over NW Europe and the W-SW

current over the Alpine area, Pannonian Plain, and Adriatic Sea. The frontal system from central Europe rapidly moved southward across the Alps, and a cold air outbreak influenced the pressure rise over Western Europe with a pronounced ridge to the north of the Alps. This process resulted in a strong cyclogenesis in the northern Adriatic on March 28 (*Fig. 1a*) with a front connecting this cyclone with the Baltic one, which moved to the east while deepening.

On March 29 the Baltic low decreased in size, and its influence on the Adriatic area gradually diminished (*Fig. 1b*). The cyclone from the Adriatic was already in the eastern Balkan, and a new weak low formed in northern Italy ahead of the frontal system approaching the Alpine area. This again intensified the Adriatic cyclone, which was moving toward the southern Adriatic, where it slowed down deepening and extending to the upper tropospheric levels (*Fig. 1c*). The intensification of the cyclone in this area is related to the upper level development in agreement with the conclusion by *Tafferner* (1990, 1994), who identified this process with other Alpine cyclogeneses.

Figs. 1 d–f show the 850 hPa charts for the same days. Due to the intensity of the Baltic low, the northerly current with strong winds did not encounter the Alpine region, which was, south of the front in *Fig. 1d*, under the influence of strong SW winds. This is not typical for the process of Alpine lee cyclogenesis, where the splitting current on the western Alps is missing. This was the reason why the cyclogenesis did not take place in the western Mediterranean but instead affected the north Adriatic through a very cold air outbreak circulating around the eastern flank of the Alps. This process was very fast marked by the *cross isobaric flow* over the Alpine area as a sign of increasing acceleration. On March 29 the Alpine area was again under the influence of lows (*Fig. 1e*), and on the last day (*Fig. 1f*), a deep low extended from the surface to higher tropospheric levels, and a ridge covered the western and middle Europe including the Alpine area.

Upstream conditions suitable for bora onset can be divided into two main groups (*Fig. 2*): (a) unidirectional northern flow throughout the troposphere; (b) shallow low-level bora flow below a critical level, defined either as the level of strong temperature inversion or level of flow reversal. This is demonstrated by the low and middle tropospheric changes in the sounding of Zagreb, characteristic for the upstream condition of the bora wind (see *Smith* (1987) for definition of upstream bora condition). The large temperature drop from 27th to 28th of March, with the changes of wind direction from SW to NE in the low level up to 2–3 km, covers the bora layer and explains the bora intensity in terms of hydraulic mechanism referred already in section 2.

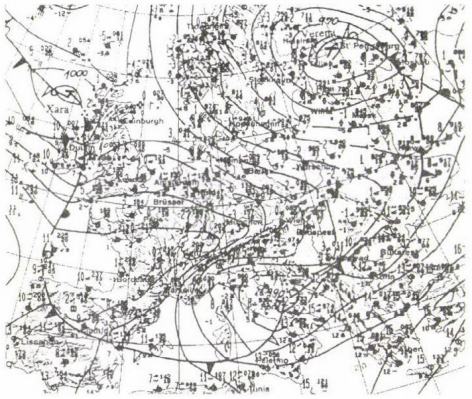

(a) March 28, 1995, 06 UTC, surface

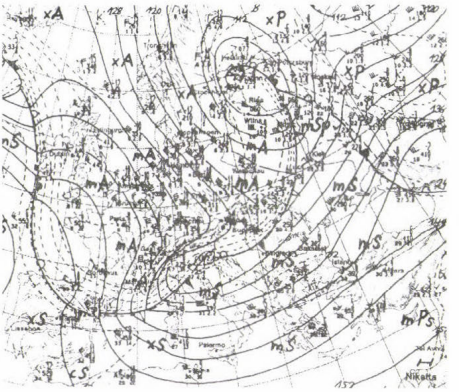

(d) March 28, 1995, 00 UTC, 850 hPa

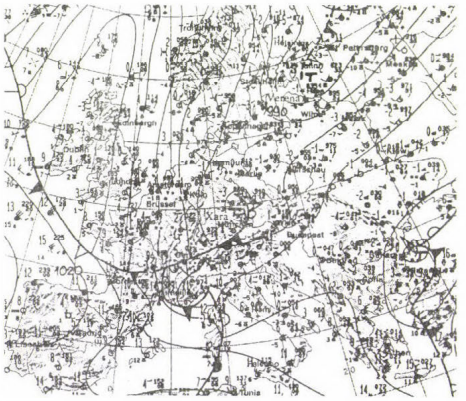

(b) March 29, 1995, 06 UTC, surface

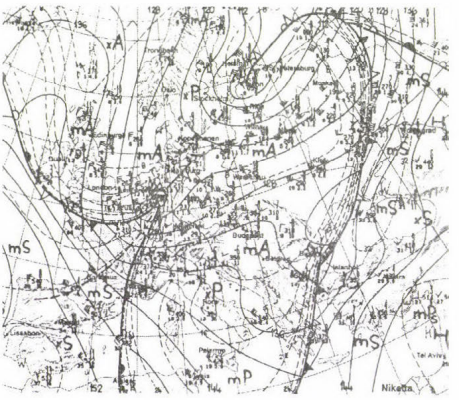

(e) March 29, 1995, 00 UTC, 850 hPa

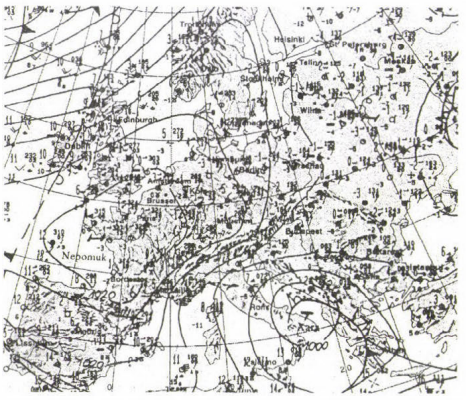

(c) March 30, 1995, 06 UTC, surface

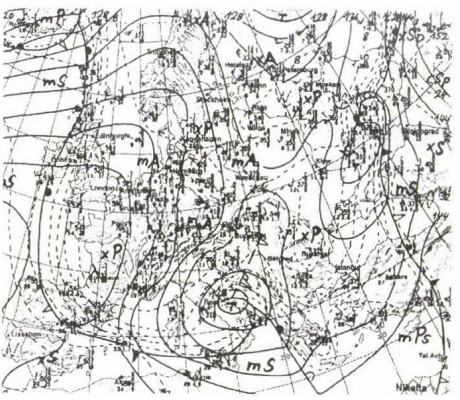

(f) March 30, 1995, 00 UTC, 850 hPa

Fig. 1. Subjective analysis of synoptic situation (from Berliner Wetterkarte).

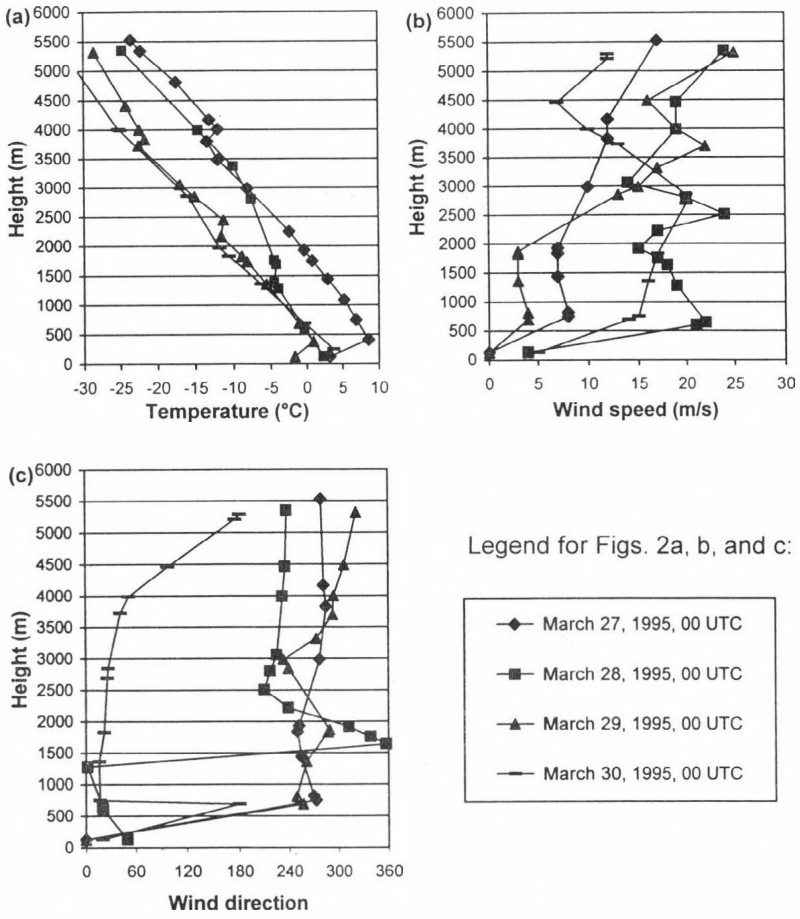

Fig. 2. Vertical profiles of temperature (*a*), wind speed (*b*), and wind direction (*c*) for Zagreb-Maksimir radiosounding station on March 27–30, 1995, 00 UTC.

Very strong bora events are illustrated in *Fig. 3* for Split in the middle Adriatic coast (see *Fig. 4*). It represents the daily courses of sea level pressure, temperature, and wind during the considered period. The striking feature is a large temperature drop following the pressure minimum on March 28, which coincides with the high increase of bora speed and gusts exceeding 45 m/s. The first bora event did not last long in comparison with the next episode of bora, which started at this location in the evening of March 29 with less variation in temperature. This is the result of both upstream and downstream influences, which is a known process under this condition in the southern Adriatic with a very deep and intense cyclonic activity (*Jurčec* and *Visković*, 1994).

(a)

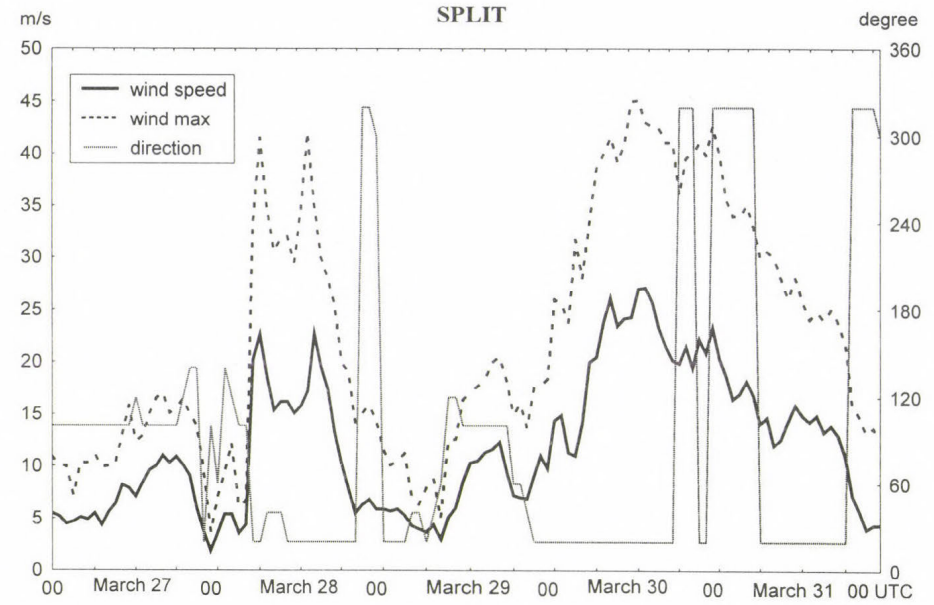

(b)

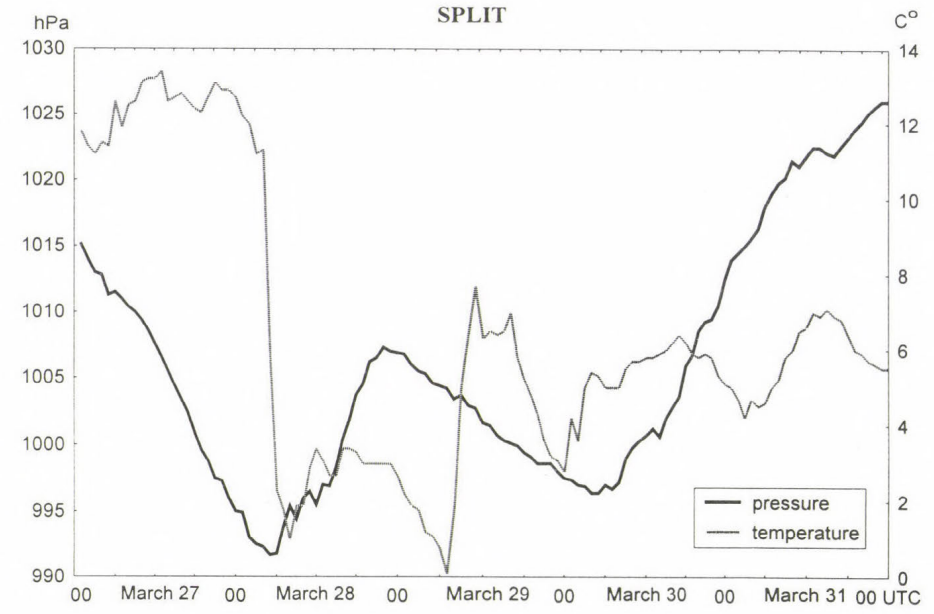

Fig. 3. Time courses of mean hourly wind speed, maximum wind gusts, wind direction (*a*), temperature and mean sea level pressure (*b*) in Split; March 27–31, 1995, 00 UTC.

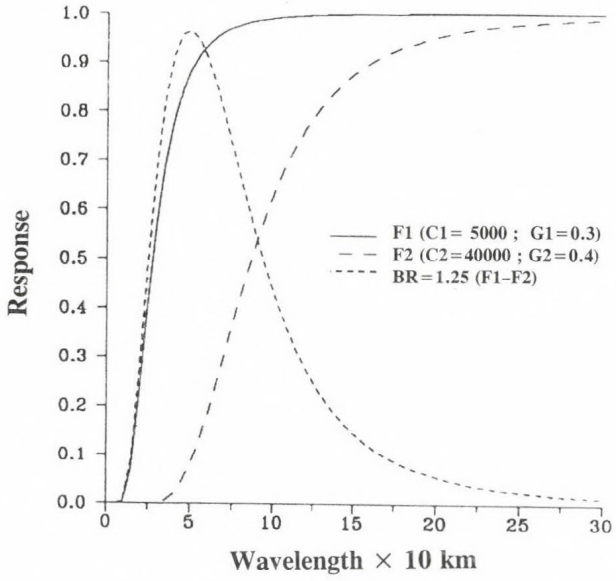

Fig. 4. Response curves for filters used in the objective scale separation technique (*Maddox*, 1980). Curves F1 and F2 are for low-pass filters used to define the bandpass (mesoscale) filter, curve BR. Response F2 also defines the macroscale field.

4. Data and computational method

The analysis technique employed here provides a scale separation successfully used by *Maddox* (1980), *Gomis* and *Alonso* (1988, 1990), *Gomis et al.* (1990), and *Jurčec et al.* (1996) in diagnosis of mesoscale structures. Briefly, the basic procedure is composed of two steps. The first step provides two macroscale fields after applying different low-pass filters. In the second step the subsynoptic (mesoscale) signal is obtained as a band pass field by subtracting those two macroscale fields. The total meteorological field is recovered as the sum of the macroscale and mesoscale fields, while the short wavelength noise is filtered out throughout the analysis.

There are two main features of the wavelength dependence of the analysis response: the cut-off wavelength for the large- and synoptic-scale contribution (hereafter referred to as "macroscale"), and the wavelenght at which the subsynoptic/meso-α contribution (hereafter referred to as "mesoscale") is centered. The response is controlled by a set of four parameters. Filtering and scale separation properties of the analysis, for the parameter values adopted in this work, are shown in Fig. 4. The mesoscale response retains the wavelengths in the range of about 500 km, and the response functions show the magnitude of damping of the shorter wavelengths, e.g., 50% damping at 250 km.

Our macroscale includes all features of wavelengths larger than approximately 900 km with damping of about 50% at 1000 km. Thus, both of our scales are much smaller than in the study of *Gomis et al.* (1990) at 850 hPa, where the mesoscale response describes wavelengths in the range of 500 –2000 km, and a macroscale response retains essentially wavelengths larger than about 2500 km. To minimize errors due to inhomogeneity of data distribution, we introduced the correction scheme as described briefly by *Gomis et al.* (1990), and in details by *Buzzi et al.* (1991).

Average data set contained 40 to 50 observations (*Fig. 5*), including data also from the climatological stations along the Adriatic coast and islands besides the conventional SYNOP observations. This data proved essential, particularly for the analysis of wind fields. To get reasonable values near the borders, stations outside the domain of the analysis were also included. The data were analyzed in a network of 25 × 25 grid points to a 0.5° longitude by 0.5° latitude grid extending from 38° to 50°N and 8° to 20°E (roughly 1100 × 900 km).

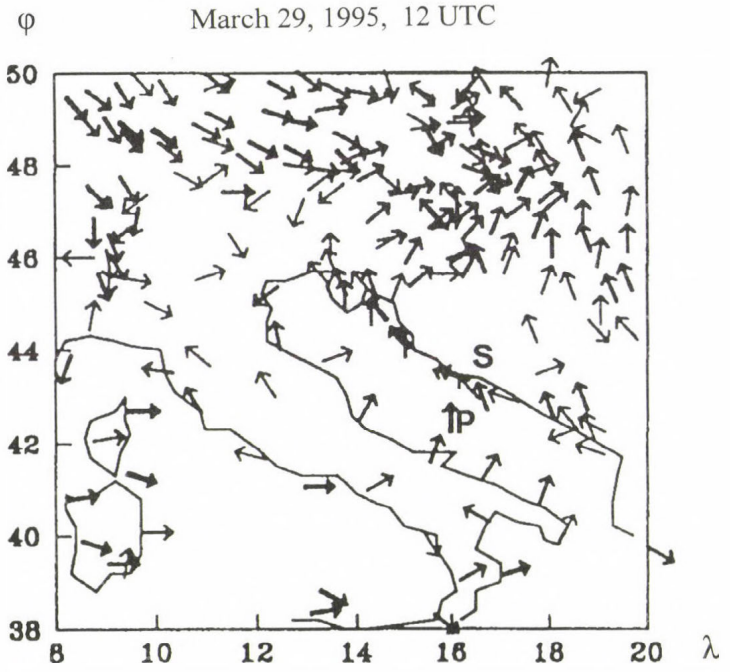

Fig. 5. Observed wind at available stations on March 29, 1995, 12 UTC. S and P indicate positions of Split and Palagruža. Thick arrows are for wind speed larger than 10 m/s, thinner arrows are for speed of 5–10 m/s, and thin arrows are for speed less than 5 m/s.

5. Results

Fig. 6a shows the total pressure field at 00 UTC on March 28 with a low center on the northern Adriatic. Across this low, the total wind field (*Fig. 6b*) indicates the convergence zone, which extends eastward and separates rather uniform N-NW winds in the north from the W-SW winds on the south. A relatively uniform wind structure at the northern (continental) and southern (Mediterranean) part of the considered area is typical for the macroscale wind field in the selected case study.

A strong dipolar structure is found in the mesoscale pressure field at that time (not shown), which is also seen across the Dinaric Alps at 06 UTC (*Fig. 6c*), when the mesoscale low extends to the middle Adriatic and central Italy toward the Tyrrhenian sea. The mesoscale wind field (*Fig. 6d*) at that time exhibits the convergence zone in the middle Adriatic and central Italy through the mesoscale low pressure. A small *cyclonic vortex* is seen in the northern Italy along the pressure trough. Notice that a cyclonic vortex is not found in the mesoscale wind field over the Adriatic sea, which is presumably the result of the warm sea intensifying the frontal zone and convergence at these zones only with possible appearance of very small and short-lived vortices.

On the contrary, the persistent vortex on this mesoscale field is the *anticyclonic vortex,* which also appears on the continent, e.g., on the eastern side of the Alps in the Pannonian Plain following the splitting current around the eastern flank of the Alps.

The mesoscale pressure field intensifies during the next 6 hours with a deep low in the southern Adriatic and a separate low in the Tyrrhenian Sea close to the Italian coast (*Fig. 6e*). The convergence zone (*Fig. 6f*) remains in the mesoscale wind field along this low pressure. The anticyclonic vortex is still seen in the Pannonian Plain, but cyclonic center in northern Italy no longer exists. Instead, there is a convergence line in this area in the direction of Genoa bay, where a small-scale cyclonic vortex is found. This vortex also disappears during the next few hours.

Fig. 7a presents the mesoscale temperature field at 12 UTC. It shows cold air behind the low centers and convergence zone in the southern Adriatic and central Italy. A very strong temperature gradient along the southern Adriatic coast is associated with the descending isentropes from the coastal mountains to the warm sea. This produces a horizontal density gradient, which hydrostatically gives rise to a pressure gradient below. This pressure gradient is directly responsible for the flow acceleration and bora intensification (*Smith*, 1987; *Tutiš* and *Ivančan-Picek*, 1991).

Fig. 7b presents the vorticity field at 850 hPa indicating a strong cyclonic vorticity over the southern Adriatic low.

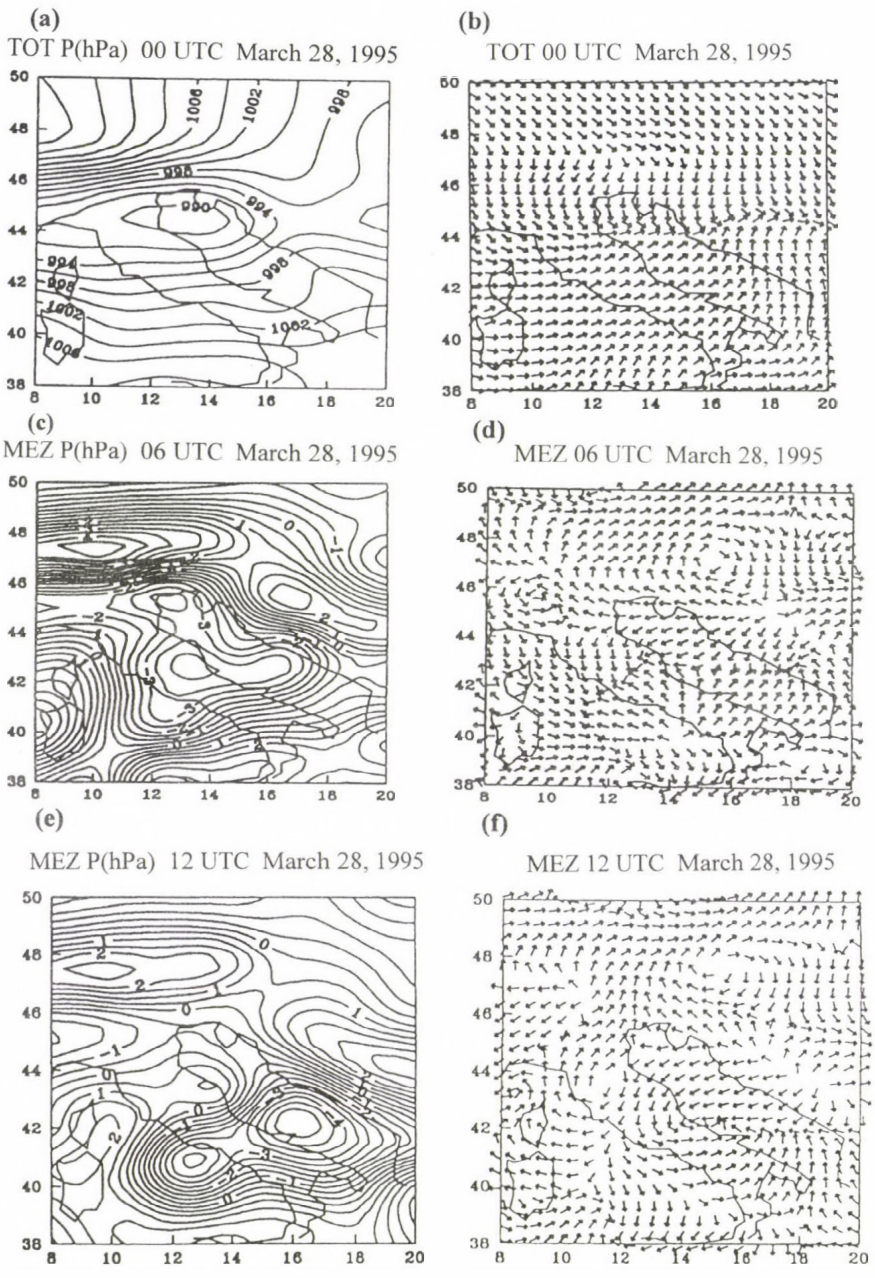

Fig. 6. Objective analysis of total pressure (*a*) and wind field (*b*) on March 28, 00 UTC; mesoscale presure (*c*) and wind field (*d*) on March 28, 06 UTC; mesoscale pressure (*e*) and wind field (*f*) on March 28, 12 UTC.

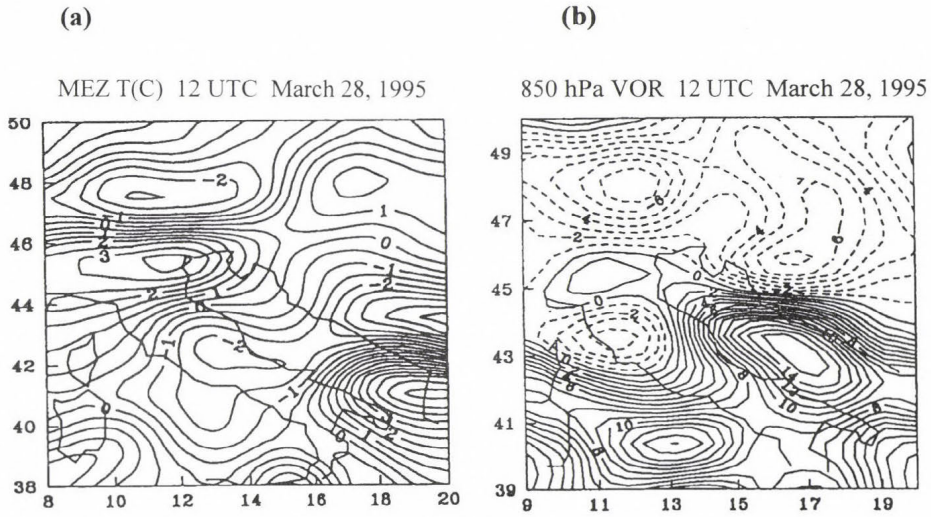

Fig. 7. Objective analysis of mesoscale temperature field (*a*) and relative vorticity (10^{-5}/s; solid lines are for positive values, dashed lines are for negative values) (*b*) on the 850 hPa level on March 28, 1995, 12 UTC.

Thus, this analysis does not indicate any vortex in the mesoscale wind field over the Adriatic area, leading to presumption that the marked fast moving front and strong bora wind along the *entire* Adriatic coast are not favorable for the vortex generation over the sea area. This is implied by the results of the second case study on the next day.

In this case we find the most essential feature of our analysis – the vortex generation in the middle Adriatic (*Fig. 8 a–d*). It is seen that this vortex is generated in the macroscale wind field to the north of macroscale pressure center. What is causing the cyclonic vortex generation in a macroscale wind field and why does it not appear on the mesoscale? The simplest answer would be that the mesoscale field is too much ageostrophic for such a process. Of course it is not surprising, that the vortex generation requires a more balanced condition similar to those found in larger scale field above the ground level as demonstrated by *Gomis et al.* (1990), where smaller scale *noise* is filtered out. Second, we noticed already more uniform currents over the middle Europe, to the north of Adriatic, as well as over the Mediterranean, with converging currents close to the Adriatic area. Third, the Adriatic basin and geometry of its boundary are convenient for the formation of *mesoscale atmospheric systems*. Finally, the specific condition for the observed Adriatic vortex is the appearance of strong bora in the northern, and jugo in the southern Adriatic. Using the same objective analysis, *Jurčec et al.* (1996) have shown that the

wind distribution in the southern Adriatic essentially changes if the strong jugo at Palagruža island (see Fig. 5) is included in the analysis. Therefore, the strong horizontal wind shear is convenient for the vortex generation, although it is not sufficient for such a process. Numerical simulation with dry and moist dynamics of this particular case study (*Brzović* and *Jurčec*, 1997) have revealed that jugo wind contains a humid air so that *diabatic effects could also contribute to the vortex formation*, although to a lesser degree that the orography.

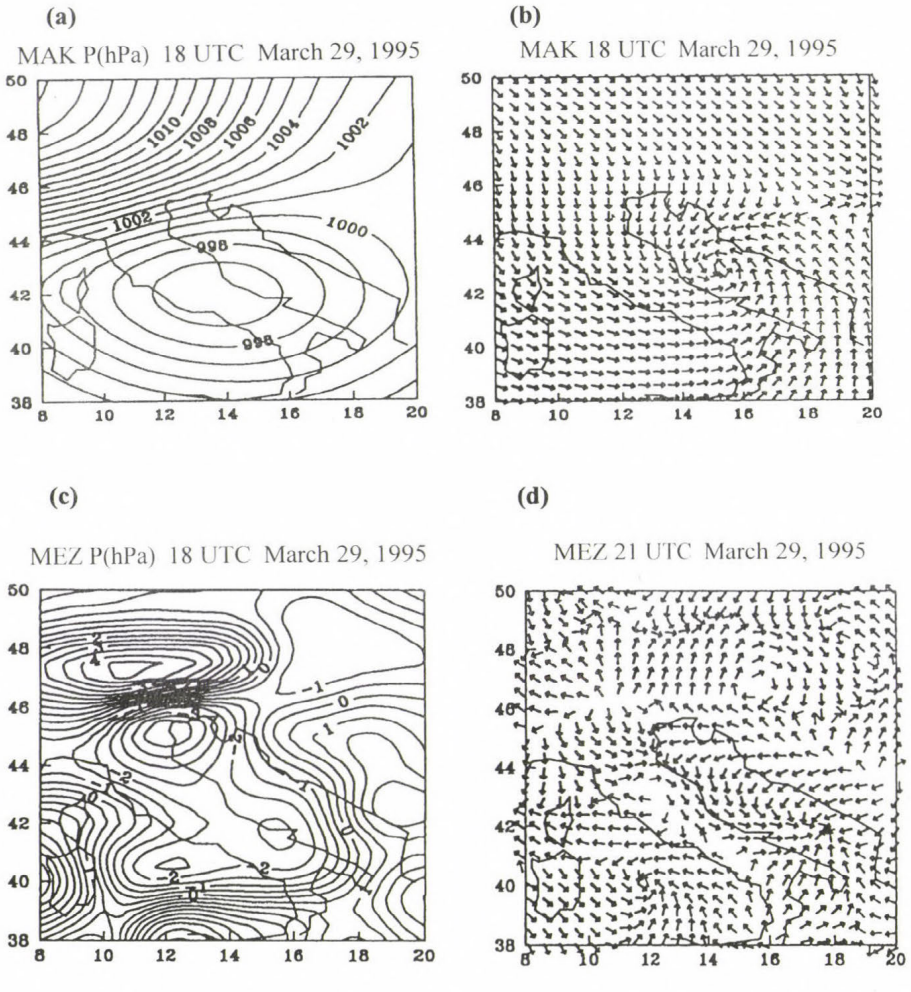

Fig. 8. Objective analysis of macroscale pressure field (*a*), macroscale wind field (*b*), mesoscale pressure field (*c*) on March 29, 1995, 18 UTC, and mesoscale wind field on March 29, 1995, 21 UTC (*d*).

On the other side, bora flow is mainly associated with the strong gravity wave breaking (*Glasnović* and *Jurčec*, 1990), and presumably the formation of Kelvin-Helmholtz instabilities influences the smaller scale motions over the sea (*Smith,* 1991). However, these instabilities as well as convective instability in a humid air occupied by jugo are filtered out as noise in our macroscale procedure. The bora intensified in the northern Adriatic at the low pressure as it can be seen in *Fig. 8c*.

The middle Adriatic vortex did not last long, since after 3 hours the bora flow occupied the entire eastern coast, and we found only a convergence zone in the southern Adriatic existing in both macro- and mesoscale wind fields (*Fig. 8d*).

6. Conclusions

- The objective sea level mesoscale analyses have shown, as expected, highly ageostrophic regime over the Adriatic Sea.
- Mesoscale fields are characterized by the dipole structure in wind, temperature, and pressure fields in the northern Adriatic. The same characteristics appear later on across the Dinaric Alps along the eastern Adriatic coast, influencing the low pressure centers, moving downstream, and intensifying together with the convergence zones in the wind field associated with these lows. Thus, these are clearly the *orogenic features mainly caused by orography*.
- This analysis intends to capture the Adriatic mesoscale vortices with wavelengths in the range of about 500 km and damping of the shorter wavelengths at 250 km, whereas the macroscale includes the features of wavelengths larger than approximately 900 km.
- Thus, no remarkable vortices were generated on selected mesoscale over the Adriatic Sea, except for temporary occurrence of very small size and short living vortices.
- Vortex centers in the mesoscale wind field over the entire area considered are displaced from the position of the corresponding pressure centers, indicating the existence of organized ageostrophic components of the flow. However, this ageostrophic flow in selected mesoscale is not solely to blame for the nonexistence of larger vortices over the Adriatic area. We find mesoscale vortices over the continent, such as cyclonic vortex over northern Italy, and especially a very persistent anticyclonic vortex in the Pannonian Plain. Therefore, warmer sea surface temperature must be responsible for the intensification of fronts and convergence lines with

frequent occurrence of very small vortices following the cold outbreaks from the north.

- The circumstance, under which the middle Adriatic vortex was generated, was the strong jugo wind in the southern and severe bora flow in the northern Adriatic. In the mesoscale, such vortex does not appear presumably for some of the following reasons: (1) due to ageostrophic condition, (2) warm sea surface increasing the frontal activities, (3) various instabilities on this scale, and (4) orographic effects leading to strong bora flow or jugo wind along the entire Adriatic coast.
- Jugo wind appears in the moist air, where convective activities are usually strong, and in this particular case the intensity of storm is accompanied by intensive rain and snow, even in the islands along Dalmatia.
- On the other side, strong and dry bora wind is well known in regions with strong turbulence ("dead regions"), and intensive gusts at the sea level are apparently caused by the Kelvin-Helmholtz instability (*Smith,* 1991). Since these instabilities, which are contained in the small wavelengths presenting the noise, are filtered out in the macroscale, this is considered as the main reason why the Adriatic vortex in this case study was generated in the macroscale and not mesoscale wind field defined in our procedure.
- This is, of course, only one case study, and more cases should be presented, particularly with numerical model simulations in order to corroborate these results. Scientific community expects significant observing efforts from the new project, MEDEX — Mediterranean Experiment on Cyclones that produce High Impact Weather in the Mediterranean (*Jansa et al.*, 2000). Thus, additional data should be focused to determine low-level distribution of wind, temperature, humidity and surface fluxes.

Acknowledgements—This study was partly supported by Ministry of Science and Technology of Croatia (project : 0004001). We appreciate very much *Prof. Werner Wehry* from Deutsche Meteorologische Gesellschaft and *Dr. Dražen Poje* for synoptic charts presented.

References

Binder, P. and *Schär, C.*, 1996: The Mesoscale Alpine Programme. Design Proposal, MeteoSwiss, 75 pp. (Available from the MAP Programme Office, MeteoSwiss, CH-8044, Zurich, Switzerland).

Brzović, N., 1999: Factors affecting the Adriatic cyclone and associated windstorms. *Contr. Atmos. Phys. 72*, No.1, 51-65.

Brzović, N. and *Jurčec, V.*, 1997: Numerical simulation of the Adriatic cyclone development. *Geofizika 14*, 29-46.

Buzzi, A. and *Tibaldi, S.*, 1978: Cyclogenesis in the lee of the Alps: a case study. *Quart. J. Roy. Meteorol. Soc. 103*, 135-150.

Buzzi, A. and *Alberoni, P.P.*, 1992: Analysis and numerical modelling of a frontal passage associated with thunderstorm development over the Po Valley and the Adriatic Sea. *Meteor. Atmos. Phys. 48*, 205-224.

Buzzi, A., Gomis, D., Pedder, M.A., and *Alonso, S.*, 1991: A method to reduce the adverse impact that inhomogeneous station distributions have on spatial interpolation. *Mon. Wea. Rev. 119*, 2465-2491.

Campins, J., Jansa, A., Benech, B., Koffi, E. and *Bessemoulin, P.*, 1995: PYREX observation and model diagnosis of the tramontane wind. *Meteorol. Atmos. Phys. 56*, 209-228.

Glasnović, D. and *Jurčec, V.*, 1990: determination of upstream bora layer depth. *Meteor. Atmos. Phys. 43*, 137-144.

Gomis, D. and *Alonso, S.*, 1988: Structure function responses in a limited area. *Mon. Wea. Rev. 116*, 2254-2264.

Gomis, D. and *Alonso, S.*, 1990: Diagnosis of a cyclogenetic event in the western Mediterranean using an objective technique for scale separation. *Mon. Wea. Rev. 118*, 723-736.

Gomis, D., Buzzi, A. and *Alonso, S.*, 1990: Diagnosis of mesoscale structures in cases of lee cyclogenesis during ALPEX. *Meteor. Atmos. Phys. 43*, 49-57.

Huschke, R.E. (ed.), 1959: Glossary of Meteorology. *American Meteorological Society*, 638 pp.

Ivančan-Picek, B., 1997: Adriatic cyclogenesis - mesoscale structures. *Proc. of the Int. Symposium on Cyclones and Hazardous Weather in the Mediterranean*, 14-17 April 1997, Palma de Mallorca, 267-272.

Ivančan-Picek, B. and *Tutiš, V.*, 1995: Mesoscale bora flow and mountain pressure drag. *Meteorologische Zeitschrift 4*, No. 3, 1-10.

Ivančan-Picek, B. and *Tutiš, V.*, 1996: A case study of severe Adriatic bora on 28 December 1992. *Tellus 48A*, 357-367.

Jansa, A., Alpert, P., Arbogast, P., and *Buzzi, A.*, 2000: Cyclones that produce high impact weather in the Mediterranean - MEDEX. *Preliminary research proposal to the WWRP*, http://www.inm.es/MEDEX/.

Jurčec, V. and *Visković, S.*, 1994: Mesoscale characteristics of southern Adriatic bora storms. *Geofizika 11*, 33-46.

Jurčec, V. and *Brzović, N.*, 1995: The Adriatic bora: Special case studies. *Geofizika 12*, 15-32.

Jurčec, V., Ivančan-Picek, B., Tutiš, V., and *Vukičević, V.*, 1996: Severe Adriatic jugo wind. *Meteorologische Zeitschrift*, N. F. 5, 67-75.

Maddox, R.A., 1980: An objective technique for separation macroscale and mesoscale features in meteorological data. *Mon. Wea. Rev. 108*, 1108-1121.

Poje, D., 1992: Wind persistence in Croatia. *Int. J. Climat. 12*, 569-586.

Smith, R.B., 1987: Aerial observations of the Yugoslavian bora. *J. Atmos. Sci.* 44, 269-297.

Smith, R.B., 1991: Kelvin-Helmholtz Instability in severe downslope wind flow. *J. Atmos. Sci. 48*, 1319-1328.

Tafferner, A., 1990: Lee cyclogenesis resulting from the combined outbreak of cold air and potential vorticity against the Alps. *Meteor. Atmos. Phys. 43*, 31-47.

Tafferner, A., 1994: Life cycle of the mountain generated Adriatic cyclone. *Proc. of Int. Symposium on the Life Cycles of Extratropical Cyclones. 27 June-1July 1994, Bergen, Norway*, 101-106.

Tafferner, A., 1995: The passage of the cold front of 27 March 1995 over the Alps: upper and lower-level flow features. *MAP-newsletter*, No. 3, October 1995, 75.

Tutiš, V. and *Ivančan-Picek, B.*, 1991: Pressure drag on the Dinaric Alps during the ALPEX SOP. *Meteor. Atmos. Phys. 47*, 73-81.

GUIDE FOR AUTHORS OF *IDŐJÁRÁS*

The purpose of the journal is to publish papers in any field of meteorology and atmosphere related scientific areas. These may be

- research papers on new results of scientific investigations,
- critical review articles summarizing the current state of art of a certain topic,
- short contributions dealing with a particular question.

Some issues contain "News" and "Book review", therefore, such contributions are also welcome. The papers must be in American English and should be checked by a native speaker if necessary.

Authors are requested to send their manuscripts to

Editor-in Chief of IDŐJÁRÁS

P.O. Box 39, H-1675 Budapest, Hungary

in three identical printed copies including all illustrations. Papers will then be reviewed normally by two independent referees, who remain unidentified for the author(s). The Editor-in-Chief will inform the author(s) whether or not the paper is acceptable for publication, and what modifications, if any, are necessary.

Please, follow the order given below when typing manuscripts.

Title part: should consist of the title, the name(s) of the author(s), their affiliation(s) including full postal and E-mail address(es). In case of more than one author, the corresponding author must be identified.

Abstract: should contain the purpose, the applied data and methods as well as the basic conclusion(s) of the paper.

Key-words: must be included (from 5 to 10) to help to classify the topic.

Text: has to be typed in double spacing with wide margins on one side of an A4 size white paper. Use of S.I. units are expected, and the use of negative exponent is preferred to fractional sign. Mathematical formulae are expected to be as simple as possible and numbered in parentheses at the right margin.

All publications cited in the text should be presented in a *list of references*, arranged in alphabetical order. For an article: name(s) of author(s) in Italics, year, title of article, name of journal, volume, number (the latter two in Italics) and pages. E.g., *Nathan, K.K.,* 1986: A note on the relationship between photo-synthetically active radiation and cloud amount. *Időjárás 90,* 10-13. For a book: name(s) of author(s), year, title of the book (all in Italics except the year), publisher and place of publication. E.g., *Junge, C. E.,* 1963: *Air Chemistry and Radioactivity*. Academic Press, New York and London. Reference in the text should contain the name(s) of the author(s) in Italics and year of publication. E.g., in the case of one author: *Miller* (1989); in the case of two authors: *Gamov* and *Cleveland* (1973); and if there are more than two authors: *Smith et al.* (1990). If the name of the author cannot be fitted into the text: *(Miller,* 1989); etc. When referring papers published in the same year by the same author, letters a, b, c, etc. should follow the year of publication.

Tables should be marked by Arabic numbers and printed in separate sheets with their numbers and legends given below them. Avoid too lengthy or complicated tables, or tables duplicating results given in other form in the manuscript (e.g., graphs)

Figures should also be marked with Arabic numbers and printed in black and white in camera-ready form in separate sheets with their numbers and captions given below them. Good quality laser printings are preferred.

The text should be submitted both in manuscript and in electronic form, the latter on diskette or in E-mail. Use standard 3.5" MS-DOS formatted diskette or CD for this purpose. MS Word format is preferred.

Reprints: authors receive 30 reprints free of charge. Additional reprints may be ordered at the authors' expense when sending back the proofs to the Editorial Office.

More information for authors is available: antal.e@met.hu

Information on the last issues: http://omsz.met.hu/irodalom/firat_ido/ido_hu.html

Published by the Hungarian Meteorological Service

Budapest, Hungary

INDEX: 26 361

HU ISSN 0324-6329